AN ABSTRACT OF THE THESIS OF

A. Rodrigo Iriarte I. for the degree of Master of Science in Geology Presented on May 22, 2012

Title: The Cerro Guacha Caldera Complex: An Upper Miocene-Pliocene Polycyclic Volcano-Tectonic Structure in the Altiplano Puna Volcanic Complex of the Central Andes of Bolivia

Abstract approved:

Shanaka L. de Silva

Four multicyclic complex calderas and smaller ignimbrite shields located within the Altiplano Puna Volcanic Complex of the Central Andes (APVC) erupted 13000 km^3 of magma within the last 11 Ma. One of the largest and most complex of these is the Cerro Guacha Caldera. Ar-Ar age determinations and paleomagnetic directions suggest that the Cerro Guacha Caldera was formed by two major eruptions, caldera collapse, resurgence cycles and several smaller eruptions. Two major ignimbrites (> 600 km^3) are found with ^{40}Ar-^{39}Ar from biotites and sanidines of 5.65 ± 0.01Ma for the 1300 km^3 (magma volume) Guacha ignimbrite and 3.49 ± 0.01Ma for the 800 km^3 Tara Ignimbrite. The last major eruption occurred on the western flank producing the 1.72 ± 0.02 Ma Puripica Chico Ignimbrite with a volume of approximately 10 km^3. Characteristic remanent magnetization data (ChRM) for these ignimbrites show that the Guacha has reverse polarity, while the Tara is normally polarized and the magnetic fingerprints have allowed their current full extents to be identified. A conspicuous lineament of volcanic structures

in the eastern part of the caldera, bordering a caldera moat, filled out welded ignimbrites and sedimentary lacustrine sequences suggest an earlier 60x40 km outer collapse associated with the Guacha explosive episode. A central graben formed on the Guacha welded ignimbrite is related to a first episode of resurgence. Evidence of a second 30 x15 km inner collapse includes offset of welded Guacha ignimbrites and alignment of lava domes associated with the Tara ignimbrite. A second resurgence episode is suggested by the presence of an uplifted central block consisting primarily of welded Tara ignimbrite.

As a whole the three ignimbrites (Guacha, Tara and Puripica Chico) share the same petrological and geochemical characteristics: high-K series, compositional ranges from dacite to rhyolite, with andesitic members present as lavas (for the Guacha and Puripica Chico Ignimbrites) and as pumices (for the Tara Ignimbrite). Highest silica content is found in the Chajnantor dome. Rayleigh modeling for Ba, Rb and Sr suggests at least 60% of crystal fractionation to account for the compositional variation between the Guacha andesite and the Chajnantor dome. Dy/Hb ratio increases with time from the Guacha andesite to the Negreal andesite suggesting stabilization of garnet owing to crustal thickening. Fe-Ti exchange geothermometry for the Tara Ignimbrite yielded log fO_2 values ranging from -13.06 to -13.38 and temperatures of 714˚ to 801˚C. Amphibole geobarometry yielded pressures ranging from 150 to 180 MPa equivalent to 5.3 and 6.4 km depth respectively for the Tara Ignimbrite; the pressures range between 133 to 242 MPa, equivalent to 5.0 to 9.2 km depth for the Guacha Ignimbrite. The zircon saturation method yielded saturation temperatures of 716˚ and 705˚C for the Guacha and Chajnantor dome respectively and 784˚C for the Tara Ignimbrite.

The zircon crystallization range for the magmas of the Cerro Guacha Caldera is 1.25 Ma for the Guacha Ignimbrite; 1.09 Ma for the Puripica Chico Ignimbrite and 0.95 Ma for the Tara Ignimbrite. Recycling of antecrystic zircons within the caldera magmas is continuos through time.

The Cerro Guacha Caldera Complex: An Upper Miocene-Pliocene Polycyclic Volcano-Tectonic Structure in the Altiplano Puna Volcanic Complex of the Central Andes of Bolivia

by

Rodrigo Iriarte

A THESIS

submitted to

Oregon State University

in partial fulfillment of

the requirement for the degree of

Master of Science

Presented May 22, 2012

Commencement June 2012

Master of Science thesis of A.Rodrigo Iriarte I. presented on May 22, 2012

APPROVED:

Major Professor, representing Geology

Dean of the College of Earth, Ocean and Atmospheric Sciences

Dean of the Graduate School

I understand that my thesis will become part of the permanent collection of Oregon State University libraries. My signature below authorizes release of my thesis to any reader upon request

---

A. Rodrigo Iriarte I., Author

ACKNOWLEDGEMENTS

I would like to sincerely thank everyone who has helped me out to finish my thesis. First and foremost, I would like to express my appreciation to my advisor, Shan de Silva, for the opportunity to come to Oregon State University and be part of this exciting experience. Shan's support, patience, guidance and encouragement were very important to the successful completion of this project.

Thanks to John Dilles, Adam Kent and Brian Haley for accepting to be part of my committee and being supportive and knowledgeable whenever I needed their advice.

Special thanks to Axel K. Schmitt, Rita Economos, Michael H. Ort, Anita Grunder, Charles Knaack and the lab team from University of Washington, Jose Viramonte, professors and staff of the Universidad Nacional de Salta for the help through lab work, collaboration and advice when required.

A very important part of the completion of this project was the feedback and support from my research group mates, Dale Burns, Stephanie Grocke, Jason Kaiser, Bob Peckyno, Jamie Kern, Trish Gregg, Zakk Carter and Augustin Ortiz, who were always available to help me without hesitation.

Thanks sincerely to the VIPER group, Wilkinson Hall students, Geosciences and Grad School staff and OSU professors who served as a great resource, support and excellent friendship during my time in Corvallis.

Special thanks to the friendship and collaboration of Morgan Salisbury, Federico Cernuschi, Joss Cuzzone, Terry Frueh and my roommates John, Nick and Mikel

Thanks to my family, professors of the Universidad Mayor de San Andres, my former advisor Nestor Jimenez and friends from Bolivia who were supportive through the distance and always made me feel as if they were close to me.

TABLE OF CONTENTS

LIST OF FIGURES

Page

LIST OF FIGURES (continued)

Page

LIST OF TABLES

1.0 Introduction

Calderas are large volcanic depressions produced by roof collapse into magma chambers from which large volumes of magma are explosively evacuated (William, 1941; Smith and Bailey, 1968). The most common product are large ignimbrites and associated deposits that are the surface output of magmatic system that is thought to extend to a deeper major intrusive complex (Lipman, 1984; de Silva et al., 2006). The largest calderas, such as La Garita from the San Juan volcanic field, Colorado (Lipman, 1984), Yellowstone, Wyoming (Christiansen, 2001), Toba, Indonesia (Chesner, 2012), and La Pacana from the Altiplano Puna Volcanic Complex (Lindsay et al., 2001), are multicyclic and long-lived and are often the focus of activity for several millions of years and several eruption cycles. Volumes of several thousands of cubic kilometers of magma are erupted during their lifetimes that are thought to record the growth of a composite batholith underneath (e.g. de Silva and Gosnold, 2007; Lipman, 2007). Understanding these systems is therefore essential for the study of the development of large continental magmatic system and the magma fluxes associated with them. Their association with economically and strategically significant mineral resources (Smith & Bailey, 1964; Lipman, 1984; Bethke, 1988) and geothermal energy (Cole et al., 2004) also makes them important to study.

Each eruption leaves a volcanic and structural record that can be deciphered to rebuild the history of the system, such as the Valles (Smith and Bailey, 1968; Self et al., 1986), Yellowstone (Hamilton, 1959; Christiansen, 2001), Galan (Francis et al., 1978; Lindsay et al., 2001), La Garita (Steven and Lipman, 1976; Lipman 2007), and Toba (van Bemmelen, 1939; Chesner, 2011). These efforts involve application of the methods of stratigraphy, volcanology, petrology, and geochemistry coupled with structural geology and geochronology to establish the history of these systems.

One of the best-preserved records of caldera volcanism on Earth, is the Altiplano Puna Volcanic Complex (APVC; de Silva et al., 1989b) located at the shared border between Argentina, Bolivia, and Chile (Fig 1). The Altiplano is one of highest plateaus in the world (following Tibet) averaging 4000 m height (13,100 ft). In this region about ~15,000 km^3 of magma was erupted from four, multicyclic calderas and smaller ignimbrite shields from ~11 Ma to present. Detailed volcanology and petrology studies of individual centers in the APVC have been made in the smaller centers of Panizos (Ort, 1993; Ort et al., 1995) and Purico (Schmitt et al., 2001). Only the

large calderas of La Pacana (Gardeweg and Ramirez, 1987; Lindsay, 2001) and Vilama Caldera (Soler et al., 2007) have been studied in detail. These two large calderas have a different structural expression than the other two major complexes in the APVC, the Cerro Guacha and Pastos Grandes. Reconnaissance work on the Guacha Caldera describe it as a polycyclic caldera formed by the eruption of three explosive units, trapdoor-like caldera collapse and later structural resurgence (Salisbury et al., 2010), but no detailed analysis about the nature of collapse, resurgence, and evolution of the magmatic system has been completed. The purpose of this thesis is to advance our understanding of one of the largest resurgent calderas yet discovered, the Cerro Guacha caldera complex located in southwestern Bolivia.

Figure 1 (next page) Location map showing the Altiplano Puna Volcanic Complex (APVC) in the context of the Central Volcanic Zone (CVZ). Black lines and circles within the APVC represent caldera scarps, ignimbrite shields and Pleistocene lava domes and volcanoes. 1 Vilama Caldera, 2 Cerro Panizos, 3 Cerro Guacha Caldera, 4 Pastos Grandes Caldera, 5 La Pacana Caldera, 6 Laguna Colorada Ignimbrite shield, 7 Purico complex, 8 Pleistocene lava domes and 9 Uturuncu Volcano. Northern Volcanic Zone NVZ extends from 5˚ N to 2˚ S, and Southern Volcanic Zone SVZ from 30˚ S to 42˚ S.

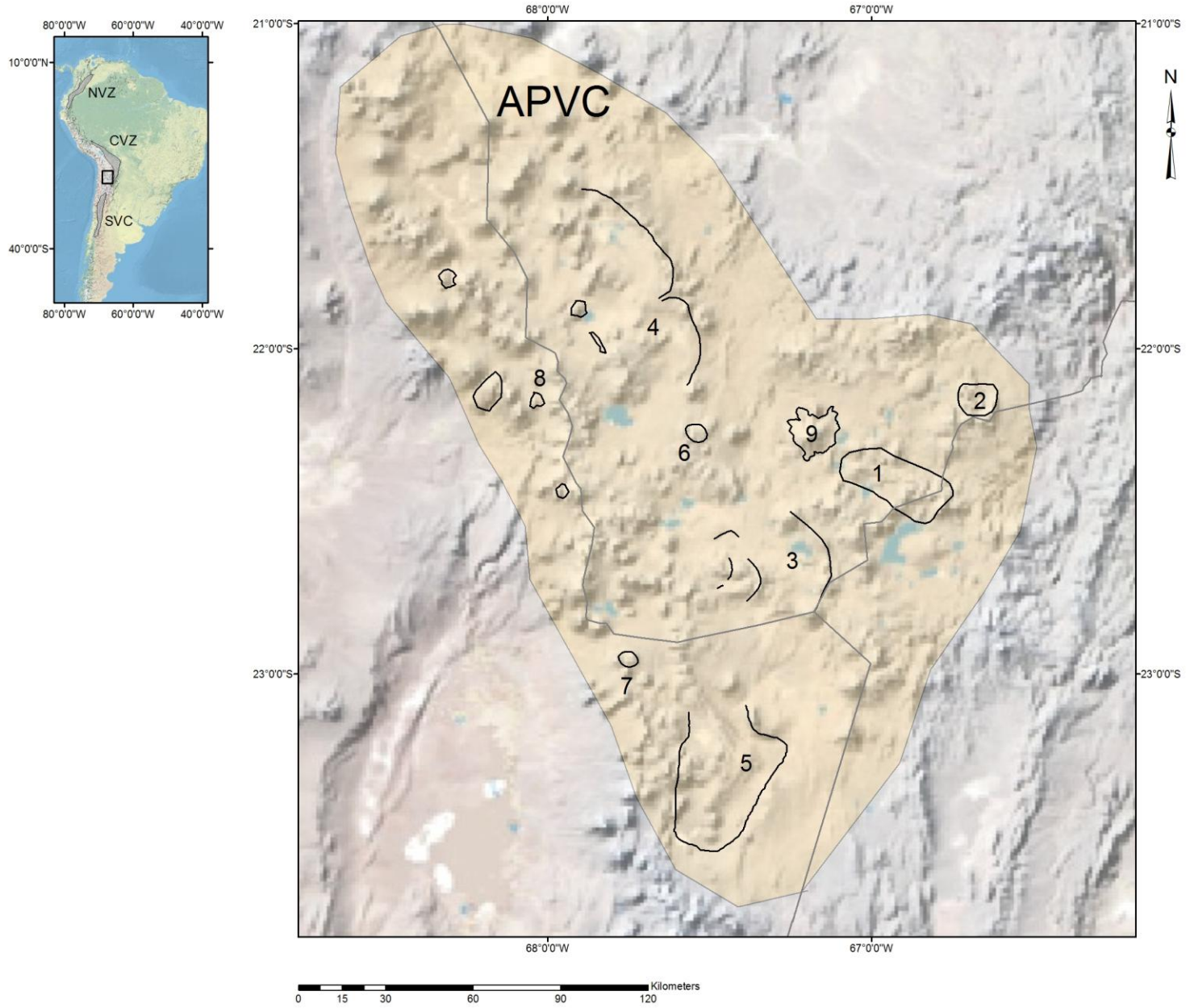
80°0'0"W
60°0'0"W
40°0'0"W
10°0'0"N
40°0'0"S
NVZ
CVZ
SVC
68°0'0"W
67°0'0"W
21°0'0"S
22°0'0"S
23°0'0"S
APVC
N
1
2
3
4
5
6
7
8
9
Kilometers
0
15
30
60
90
120

1.1 Purpose and scope of this thesis

This study,was funded by the NSF to investigate the Guacha system. The goal is to establish the timing and development of the caldera and its magmatic system and understand its context within the APVC and relationship with new ongoing activity at the Uturuncu volcano on its north flank (Pritchard and Simmons, 2002; 2004). The following hypothesis is tested:

The Cerro Guacha Caldera is a polycyclic caldera with at least two large super-eruptions that triggered successive confocal collapse and resurgence resulting in the current nested volcano-tectonic depression

Three objectives address this hypothesis and form the science in this thesis (Table 2):

1) **Revise and update the geochronology and stratigraphy of all components of the Guacha caldera**:

   The various spatially-temporally and genetically related components of the system will be identified through field mapping and correlations supplemented by new ^{40}Ar-^{39}Ar new ages, ^{206}U-^{238}Pb zircon ages and paleomagnetic determinations. All data will be compiled in a Geographic Information System.

2) **Relate the volcanic stratigraphy to the structural elements to constrain the structural development of the caldera**:

   No prior work has focused on the structural development of the caldera, both regionally and locally. Remote sensing, field mapping and unit correlations are combined with new age determinations to link the structural elements to the volcanic stratigraphy. Particular focus is placed on understanding the stratigraphy and structure of the intra-caldera elements (resurgent blocks and graben) and the two major collapse scarps.

3) **Link the volcanological evolution to the magmatic evolution of the system**

   Zircon U-Pb ages are used to link the eruptive to the magmatic chronology, yielding zircon crystallization ranges for the three different magmatic suites along with constraints about the magmatic input. Petrology and geochemistry will characterize the system in pressure, temperature and geochemical composition**.**

1.2 Geologic Background

1.2.1 Overview of the Andes

Evolution of the Central Andes can be distinguished in two stages: stage one is constrained to early Paleozoic and characterized by transfer of sedimentary mass in the upper crust; and stage two beginning during the late Cretaceous is associated with recycling of crustal mass (Jimenez et al., 2009). In the Early Paleozoic, an intra-cratonic marine basin was formed and interacted with restricted episodes of deformation including: Ocloyic phase (Ordovician-Silurian); Eohercinic phase (Devonian-Carboniferous); and Hercinian phase (Late Carboniferous). However early subduction related magmatism observed in Chile (26°15'N and 69° 30'W), yielded Permian-Triassic ages (Halpern, 1978). In the Mesozoic, an overall extentional regime along with brief marine incursions occurred before major compressional Andean Orogeny. and Early subduction-related uplifting initiated approximately 70 Ma. It was followed by episodic eastward fold-thrust, that resulted in shortening and thickening of the lithosphere (McQuarry et al., 2005; Isacks, 1988). At about 26 Ma shallowing of the subducting slab due to initiation of fast, nearly orthogonal convergence resulted in readjustment of the overall setting, including eastward migration of the arc (de Silva and Gosnold, 2007).This process along with tectonic erosion, hydration and mechanical instability, probably triggered lithospheric delamination, (Isacks 1988; Ruetter 2001 in de Silva et al., 2006).

1.2.2 Central Volcanic Zone evolution

Located between 14˚-28˚S, the Central Volcanic Zone is one of four volcanic zones along the Andean margin (Fig. 1). It lies above an exceptionally thick crust (~70 km) resulted from tectonic shortening beginning about 12 Ma (James, 1971; Isacks, 1988; in de Silva, 1991)_). Backarc volcanic activity is almost continuous from Paleozoic to present (Jimenez et al., 2009), meanwhile arc-related volcanism initiated during Late Oligocene.

From 25 Ma to nearly 10 Ma the region between 21˚-24˚S lay above a lithosphere that was "pre-heated" by subduction and delamination driven basaltic fluxes, which hybridized the upper crust base, favoring the formation of a batholithic proportions magmatic body (Altiplano Puna Magma Body, de Silva et al., 2006) from which approximately 15,000km^3 of imagma was erupted. Caldera collapse is associated with these eruptions.

1.2.3 The Altiplano Puna Volcanic Complex

High resolution geochronology, volume, and spatial estimations done by Salisbury et al., 2010 allowed them to define the onset and timing of magmatic activity within the APVC. Approximately at 11 Ma, earliest activity is recorded through small volume (280 km^3) and widespread volcanism located in Northern Chile and Argentina. Major ignimbrite volcanism began 2 million year later (9-7.5 Ma) with the eruptions of the Sifon and Vilama Ignimbrites (2400 km^3). Between 7.5-6.0 Ma a smaller pulse (1900 km^3) is represented by the Panizos, Toconce and Coranzuli Ignimbrites. The period between 6.0-4.5 Ma is characterized by the eruption of the Pelon, Pujsa, Guacha, Chuhuilla and Alota ignimbrites, recording an estimated volume of 3120 km^3. This period corresponds to the first and major eruption of the Cerro Guacha Caldera, CGC (the homonymous Guacha Ignimbrite) at 5.6 Ma with an estimated volume of 1300 km^3. The period of 4.5-3.0 Ma is characterized by the eruption of the Toconao, Puripicar, Atana and Tara ignimbrites with a volume of 4000 km^3. Belonging to this period, the second major eruption of the CGC is recorded by the eruption of the Tara Ignimbrite at about 3.49 Ma and with an estimated volume of 900 km^3. From 3.0 to 1.5 Ma the Pastos Grandes, Laguna Colorada and Puripica Chico Ignimbrites were erupted from distinctive sources to produce a volume of about 1570 km^3. Belonging to this period the Puripica Chico Ignimbrite marks the last eruption related to the CGC at 1.7 Ma and with a volume of 10 km^3. Finally, the last period of volcanism at the APVC (dated at 1.5 Ma to present) is characterized by the eruption of the Purico, Tatio and Filo Delgado ignimbrites with an estimated volume of 150 km^3. Overall the APVC shows an estimated volume of > 12,800 km^3 of magma erupted through 11 Ma to present, with an average output rate of of 1.11 km^3/k.y.

1.2.4. Introduction to Cerro Guacha Caldera (CGC)

Early remote sensing and reconnaissance done by Francis and Baker (1978) first identified the Cerro Guacha Caldera as a complex collapse caldera with two overlapping uplifted blocks with an apical graben. They suggested that the caldera was the source of the Guatiquina ignimbrite (now known to be a combination of the Guacha, Tara and Atana ignimbrites, de Silva and Francis 1989; 1991). They also suggested that the Puripica ignimbrite was erupted from the Guacha Caldera, and they identified two periods of resurgence with the westerly being the younger. Field mapping and K-Ar dating by the Geological Service of Bolivia (Almendras et al, 1996; Pacheco

and Ramirez, 1997b,c) at the resurgent dome distinguished three welded tuffs whose ages range from 6.6±0.5 to 5.9±0.4 Ma however, no further interpretation about the caldera collapse or resurgence was made. While these early studies were important in establishing a base knowledge for the Guacha caldera, they were regional reconnaissance and suffered from a lack of the detailed chronological framework that was developing to the west and south in Chile (Gardeweg and Ramirez, 1987; de Silva, 1989; de Silva and Francis, 1989).

A key piece of work in unraveling the Guacha stratigraphy was the work of Lindsay et al. (2001) who reinterpreted the work of Gardeweg and Ramirez, 1987 and showed that the eastern side of the La Pacana caldera had a section with three ignimbrites. The ~4.0 Ma Atana ignimbrite from La Pacana was underlain by the 5.6 Ma Lower Tara and overlain by the 4.0 Ma Upper Tara ignimbrite, and both were sourced from Cerro Guacha. An earlier interpretation for the Guacha caldera tectonic evolution was made by Mobarec C., (1994), that suggested a polycyclic caldera with trap door collapse, however no systematic dating supported his interpretation.

In 2006, an NSF-funded project to establish a coherent geochronological and stratigraphic framework (Salisbury et al., 2010) established the current stratigraphy and distribution of the outflow, obtaining new ^{40}Ar-^{39}Ar ages (Table 1) and new volumes of extra- and intra-caldera ignimbrites. Lindsay's Lower Tara was renamed as the Guacha Ignimbrite and their Upper Tara was renamed the Tara ignimbrite and the extents of the ignimbrites were mapped from La Pacana northward forming mostly the southern and eastern side of the Guacha resurgent dome (Fig. 2). Ages for two of the post resurgent domes, Chajnantor and Rio Guacha were also determined.

Salisbury et al., (2010) established that the Guacha Ignimbrite is a crystal-rich, dacite with an intracaldera thickness of at least 700 m. The outflows extend northward almost 60 km towards Soniquera in the north of the Quetena Valley. An estimated DRE volume of 1300 km^3 was proposed. ^{40}Ar-^{39}Ar dating obtained from 26 sanidines of distal outflows yielded the preferred weighted mean age of 5.65±0.01Ma. The overlying Tara ignimbrite was shown to range in composition from andesite to rhyolite with outflows of more than 200 m thick and an overall volume of 800 km^3. 40 sanidines from outflow pumices yielded a weighted mean age of 3.49±0.01 Ma. To the northwestern edge of the caldera the Puripica Chico Ignimbrite apparently corresponds to the younger caldera event. This ignimbrite is dacitic in composition and new ^{40}Ar-^{39}Ar dating yielded an age of 1.70±0.02 Ma.

Figure 2 (next page) Reconnaissance geologic map of the Cerro Guacha Caldera showing the main resurgent block, the three main caldera related ignimbrites, scarps, post collapse lava domes, lake deposits (located within the caldera moat) and younger stratovolcanoes. Observed collapse scarps are located to the east of the main block; two consecutive scarps (black lines) are associated to collapse and resurgence associated to the Tara Ignimbrite. Further to the East the outer scarp (dashed line) is associated to the Guacha Ignimbrite. Both scarps were interpreted following lava domes alignment, cross cutting relationships, Ar-Ar ages and location of sedimentary lake-sequences. A larger format version is provided in the appendix.

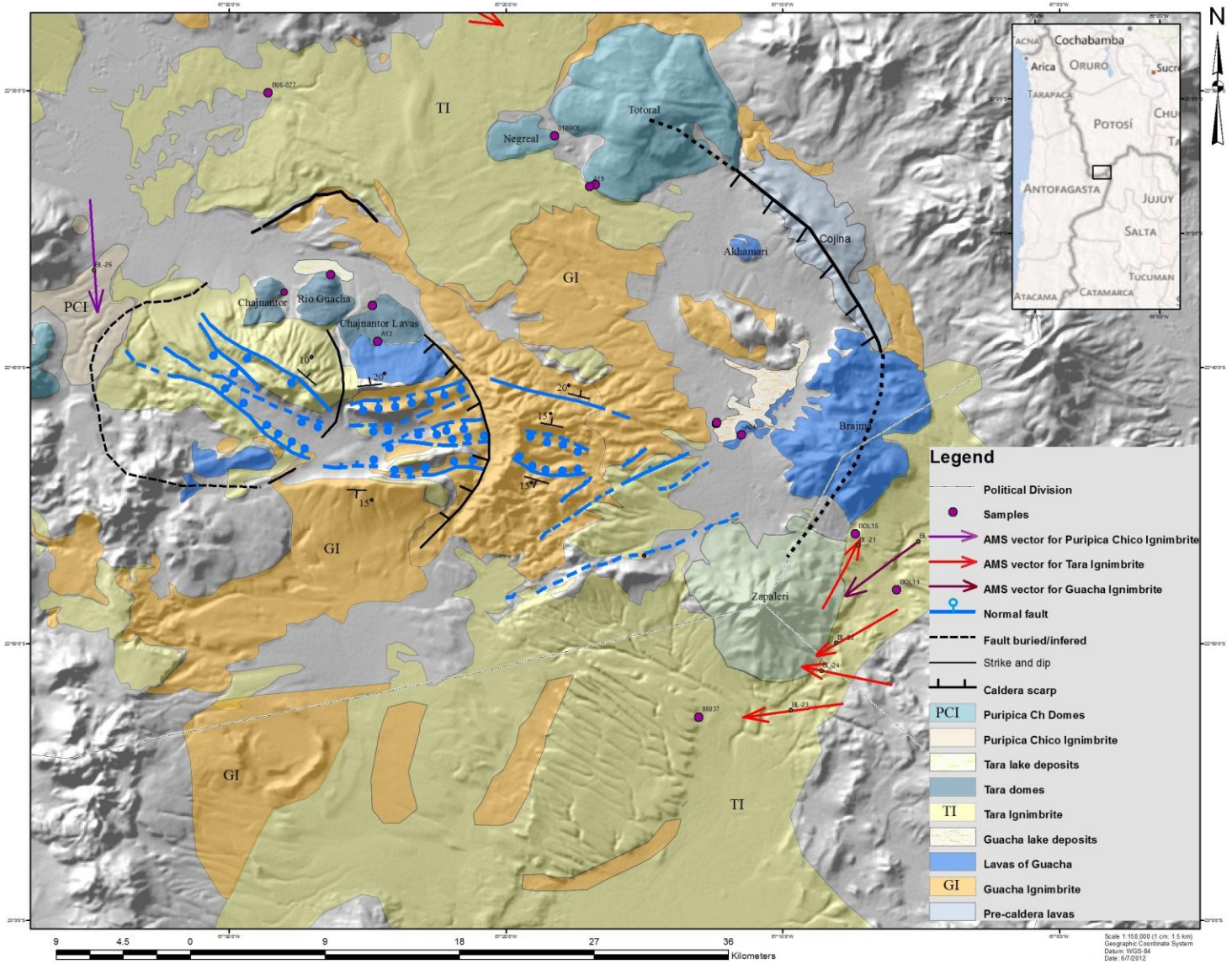
N
TI
GI
PCI
Totoral
Negreal
Cojina
Akhamarri
Chajnantor
Rio Guacha
Chajnantor Lavas
Brajma
Zapaleri
Cochabamba
Arica
ORURO
Sucre
TARAPACA
Potosí
ANTOFAGASTA
JUJUY
SALTA
TUCUMAN
ATACAMA
CATAMARCA
Legend
Political Division
Samples
AMS vector for Puripica Chico Ignimbrite
AMS vector for Tara Ignimbrite
AMS vector for Guacha Ignimbrite
Normal fault
Fault buried/infered
Strike and dip
Caldera scarp
PCI Puripica Ch Domes
Puripica Chico Ignimbrite
Tara lake deposits
Tara domes
TI Tara Ignimbrite
Guacha lake deposits
Lavas of Guacha
GI Guacha Ignimbrite
Pre-caldera lavas
9 4.5 0 9 18 27 36
Kilometers

					Age Spectrum			Isochron Analysis		
Sample ID	Rock type	Lat	Long	Mineral	Age (Ma±2σ)	MSWD	N	40Ar/36Ar (±2σ)	Age (Ma±2σ)	MSWD
Guacha Ignimbrite										
B06-002	mat	-21.84	-67.34	biotite	5.71 ± 0.05	0.62	12 of 12	290.3 ± 6.4	5.80 ± 0.13	0.41
B06-022	mat	-22.61	-67.4	biotite	5.77 ± 0.04	0.61	10 of 12	294.6 ± 2.8	5.78 ± 0.07	0.91
B06-080	pum	-22.44	-67.37	biotite	5.80 ± 0.00	1.04	13 of 13	293.6 ± 3.7	5.81 ± 0.04	1.9
B06-030	mat	-22.38	-67.15	biotite	5.84 ± 0.02	0.5	12 of 12	297.0 ± 10.0	5.82 ± 0.07	0.8
		Biotite Weighted Mean Age			5.81 ± 0.01	1.3	47			
B06-002	mat	-21.84	-67.34	sanidine	**5.65 ± 0.01**	0.52	26 of 26	306.0 ± 45	5.65 ± 0.04	0.02
Tara Ignimbrite										
B06-072	mat	-22.76	-67.64	biotite	3.48 ± 0.03	0.52	13 of 13	300.0 ± 12.0	3.44 ± 0.10	0.53
B06-025	mat	-22.63	-67.5	biotite	3.56 ± 0.02	0.4	13 of 13	296.1 ± 30	3.55 ± 0.05	0.48
B06-018	mat	-22.78	-67.25	biotite	3.56 ± 0.07	0.13	6 of 6	301.0 ± 16.0	3.51 ± 0.17	0.04
B06-013	pum	-22.45	-67.28	biotite	3.63 ± 0.04	0.24	6 of 6	253.0 ± 76.0	3.69 ± 0.11	0.18
		Biotite Weighted Mean Age			3.55 ± 0.02	1.5	38			
B06-018	mat	-22.78	-67.25	sanidine	3.51 ± 0.01	0.56	32 of 32	291 ± 14	3.51 ± 0.04	0.81
89002	pum	-22.51	-67.64	sanidine	3.46 ± 0.02	1.18	8 of 8	295.0 ± 4.7	3.46 ± 0.03	1.37
		Sanidine Weighted Mean Age			**3.49 ± 0.01**	1.17	40			
Puripica Chico Ignimbrite										
B06-074	pum	-22.63	-67.68	biotite	**1.70 ± 0.02**	0.6	10 of 10	297.1 ± 5.5	1.69 ± 0.06	0.67
Effusive lava domes										
Rio Guacha Dome										
B06-023	lava	-22.61	-67.44	biotite	**3.61 ± 0.02**	1.01	9 of 10	308.0 ± 12.0	3.57 ± 0.04	1.17
Chajnantor dome										
B06-024	lava	-22.62	-67.47	biotite	3.59 ± 0.02	1.2	13 of 13	301.0 ± 30.0	3.56 ± 0.16	1.6
B06-024	lava	-22.62	-67.47	sanidine	**3.51 ± 0.02**	0.63	22 of 22	309 ± 16	3.50 ± 0.03	0.58
Chajnantor Lavas dome										
BOL-07-021	lava	-22.629	-67.41	sanidine	3.67 ± 0.13	1.2	7 of 7	295.7 ± 2.9	3.67 ± 0.1	1.5
Negreal andesite*										
A-01	lava	-22.5	-67.3	plagioclase	**1.54 ± 0.04**	0.08	11 of 11	297.3 ± 16.1	1.52 ± 0.22	0.08

Table 1 $^{40}Ar/^{39}Ar$ ages for the Cerro Guacha Caldera from Salisbury et al., (2010) and during this study (*); pum = pumice; mat = matrix; dis = discordant ages not used in weighted mean ages

2.2. Description of methods

Field work

Field work and mapping was done during Fall of 2010 providing new data about the Eastern scarp of the caldera, the resurgent dome and the outcrops of the Puripica Chico ignimbrite. These data where evaluated and compared with paleomagnetism measurements done by Michael Ort (in review) and Ar-Ar ages available from Salisbury et al., 2010.Geologic map was done using ArcGIS, uploading georeferenced sampling and logging locations, along with updated geochronology of the components of the caldera

Geochemistry

20 Rock powders of samples of 2007-2010 field seasons were prepared and analyzed at Washington State University to obtain major and trace elements compositions. Fresh chips of the samples were grounded in a swing mill with tungsten carbide surfaces for 2 minutes. Three and a half grams (3.5 g) of the sample powder were weighted into a plastic mixing jar with 7.0 g of spec pure dilithium tetraborate (LiB_4O_7) and mechanically mixed for two or three minutes. The mixed powders were emptied into graphic crucibles, placed on a silica tray and loaded into muffle furnace. Fusion takes 5 minutes from the time the preheated furnace returns to its normal 1000° C after loading. The silica plate and the graphite crucibles are then removed from the oven and allowed to cool. Each bead is reground in the swingmill for 35 seconds, the glass then replaced in the graphite crucibles and refused for 5 minutes. Following the second fussion, the cooled beads are labeled with an engraver, their lower flat surface is ground on 600 silicon carbide grit, washed and cleaned out. The glass beads are then ready to be loaded into the XRF-ICP spectrometer (details of method can be found at http://www.sees.wsu.edu/Geolab/note/icpms.html.)

Ar-Ar age determintaions

^{40}Ar-^{39}Ar ages were obtained from 100 mg groundmass of lava flows (A-1, 13) from the Eastern scarp and resurgent dome respectively. These samples have been handpicked under binocular and washed with acetone, DI water and left on the oven to dry off. Then were analyzed at the OSU Marine Geology Noble Gas Mass Spectrometry Lab

Pressure-temperature (intensive parameters)

Pressure-Temperature (intensive parameters) were determined using published data from Lindsay et al., (2001) and Grocke et al., (in prep) both for the Tara and Guacha Ignimbrite, including use of Fe-Ti exchange geothermometry following the method of Andersen & Lindsley, (1985) and

Ghiorso & Bernard, (2008). Amphibole thermometry was estimated using the method of Ridolfi et al., (2010) and zircon saturation thermometry was estimated following the method of Watson & Harrison (1980).

Zircon U-Pb geochronology

Zircons from pumices of the main ignimbrites along with associated lava domes were analyzed at the Secondary Ion Mass Spectometer (SIMS) at UCLA during summer, 2011 to obtain $^{206}U/^{238}Pb$ zircon crystallization ages and residence times. All samples used for the U-Pb work were pumice or lava samples. Samples of the Guacha Ignimbrite were collected in three locations: at 19 km SSW of the Quetena Chico Village (Fig.4c, Chaper 3), from a pumice (sample A-6) of the northern outflow; at the NW side of the Totoral dome (pumice sample 07BOL-11, see Fig. 8 geologic map) and the Kalina lava flow that outcrops at the western margin of the Brajma complex (geologic map and reference on map). For the Tara Ignimbrite, samples were taken at three locations: at the NW side of the Totoral dome, (pumice sample B06-013), at the inner caldera scarp, Rio Guacha (B06-023) and Chajnantor Lavas domes (BOL-21). Samples of the Puripica Chico Ignimbrite were collected at the NW side of the Puripica Chico lava dome (sample BOLPD-23, see ref on geologic map) and one for the Totoral dome (sample A-019). Zircons were difficult to indentify in the vesiculated groundmass glass, but since petrographic examination revealed no zircon inclusions in phenocrysts it is assumed they are mainly from the matrix.

At least two samples from each ignimbrite and one lava sample were selected for extraction of zircon crystals. Bulk pumice samples were crushed gently to produce rock chips no bigger than 1 cm in diameter. These were then transferred to a mortar and pestle to create a fine sand-sized aggregate. These sand-sized fractions were then placed in glass beakers and repeatedly washed with water to remove the ash sized particles. After washing, each sample was placed in an oven set at 80°C overnight to dry. When dry, the samples were inspected for their coarseness; if significant amounts of large particles remained (>1 mm diameter), the sample was further processed in the mortar and pestle again.

The highly magnetic minerals (e.g. magnetite) in each size fraction were extracted by repeatedly passing a hand magnet over the samples. The residue was then run through a Franz Isodynamic Magnetic Separator (after Rosenblum, 1958; Flinter 1959) set at 0.8 A, with a 25° forward and 20° side angle to the chute. This separated the magnetic heavy minerals (ilmenite, titanite,

monazite and any remaining biotite) from the non-magnetic heavy minerals (zircon, and minor proportions of apatite). Two different heavy liquids were used to separate minerals of varying densities. The sample aggregates were first placed in a separating column containing Tetrabromoethane (TBE; density - 2.96 g/cm^3), whereby the lightest minerals floated to the top of the separating column (quartz, feldspars, glass, some biotite). The heavy residue was then thoroughly cleaned with acetone, left to dry and placed in a second separating column containing Diiodomethane (DIM; density - 3.32 g/ cm^3). This removed apatite and any remaining biotite crystals, leaving only the densest minerals at the base of the separating column (>3.32 g/cm^3). The <250 μm fractions were then examined using a binocular microscope and at least twenty zircon crystals per sample were selected with preference given to the largest, euhedral phenocrysts visibly free of cracks and large inclusions. Selected zircon phenocrysts were cleaned with acetone and mounted in epoxy resin, sectioned to expose grain interiors and polished with 1 μm Al_2O_3. After ultrasonic cleaning, grains were surveyed for internal compositional zonations and/or inclusions via cathodoluminescence (CL) imaging using a Leo 1430VP scanning electron microscope at UCLA (e.g., Fig. 5.2).

$^{238}U/^{206}Pb$ ages were obtained using the UCLA CAMECA SIMS 1270 ion probe. Samples that had been coated with ~10 nm of Au were typically probed with a mass-filtered, 10–20 nA $^{16}O^-$ beam focused to a ~30–35 μm diameter spot. Secondary ions were extracted at 10 kV with an energy band-pass of 50 eV. The mass spectrometer was tuned to a mass resolution of ~5000 to resolve molecular interferences in the mass range analysed ($^{94}Zr_2O^+$, $^{204}Pb^+$, $^{206}Pb^+$, $^{207}Pb^+$, $^{208}Pb^+$, $^{238}Pb^+$, $^{232}Th^{16}O^+$, $^{238}U^{16}O^+$). Pb^+ yields were increased by a factor of ~2 by flooding the analysis surface with O_2 at a pressure of ~4x10^{-3} Pa. The relative sensitivities for Pb and U were determined on reference zircon AS-3 (Paces and Miller, 1993) using a calibration technique similar to Compston et al. (1984). Th and U contents were estimated by multiplying measured $^{232}Th^{16}O^+/^{94}Zr_2O^+$ and $^{238}U^{16}O^+/^{94}Zr_2O^+$ ratios on the unknowns with corresponding relative sensitivity values determined on reference zircon 91500 (Th = 28.6 ppm; U = 81.2 ppm; Wiedenbeck et al. 1995). Analysis surfaces were pre-sputtered for 4 min before analysis to minimize surficial Pb contamination. Current results show that the smallest uncertainties (for high radiogenic yields) are ~5% (i.e., ±0.01 Ma for the youngest ignimbrites in the Guacha system). Spot analyses on low uranium zircons, or those that accidentally overlap with common Pb bearing phases such as glass or apatite, have higher uncertainties. Care was taken to avoid such situations and analyses eliminated if necessary. Common Pb was corrected using $^{207}Pb/^{206}Pb$

proxy instead of traditional $^{204}Pb/^{206}Pb$, which allows also correction for the $^{206}Pb/^{238}U$ initial desiquilibrium (Schmitt et al., 2003). $^{206}Pb/^{238}U$ ages within ± 1 sigma error are shown in Table 9.

Objective	Strategy	Methods
1) Revise and update the geochronology and stratigraphy of all components of the Guacha caldera	• Within a GIS, collate and synthesize previous data • Field logging and correlation of new sections • Obtain new Ar-Ar ages on previously undated units • Obtain new U-Pb ages on previously undated units	• Elaboration of a GIS geologic map with georeferenced field data, paleomagnetism and geochemistry • Data field analysis of pre-existent logged sections and correlation with newer descriptions • ^{40}Ar-^{39}Ar geochronology of the andesites associated to the main resurgent centers • Sampling and analysis of main ignimbrites and post resurgence lava domes
2) Relate the volcanic stratigraphy to the structural elements to constrain the structural development of the caldera	• Constrain and dating of pre-syn and post-collapse units	• Field mapping and geochronology of suspected pre-sync and post collapse units
3) Link the volcanological evolution to the magmatic evolution of the system	• Geochemistry of major and trace elements all the caldera geologic units • Determination of intensive parameters and zircon saturation temperatures • U-Pb ages and crystallization dates for main caldera components	• Whole rock XRF-ICP analysis • Major and trace elements Glasses will be obtained through published data from Lindsay et al., 2001 and Grocke et al., (in prep) • $^{206}U/^{238}Pb$ dates determined at UCLA using SIMS

Table 2 Objectives, strategy, and methods to achieve the goal of this study.

3.0 Stratigraphy of the Guacha Caldera and characteristics of the ignimbrites and lavas

3.1 Previous work

The Cerro Guacha Caldera was first identified by Francis and Baker (1978) as a complex collapse caldera with two overlapping uplifted blocks oriented obliquely to one another forming the central complex. Gardeweg and Ramirez (1987) described an ignimbrite outcropping to the northeastern side of La Pacana Caldera formerly known as part of the the Atana ignimbrite. Mobarec C. (1993) made an early interpretation of the Guacha Caldera, suggesting a polycyclic caldera with trap door collapse, however no systematic dating supported his interpretation. Field mapping and K-Ar dating of the resurgent dome by the Geological Service of Bolivia (Almendras et al, 1996; Pacheco and Ramirez, 1997b,c) led to the distinction of 3 welded tuffs whose ages range from 6.6±0.5 to 5.9±0.4 Ma (Table 1). However, no further interpretation about the caldera collapse or resurgence was made.

Based on differences on welding, pumice abundance and geochemistry, Lindsay et al. (2001) distinguished between the Atana Ignimbrite from the La Pacana Caldera and suggested a probable source toward the Northeast in the Cerro Guacha. Recently, Salisbury et al. (2010) mapped two units erupted from the Guacha caldera, the Upper and Lower Tara Ignimbrite, obtaining new ^{40}Ar-^{39}Ar ages and new volumes. Salisbury et al. (2010) renamed what Lindsay had called the Lower Tara Ignimbrite as the Guacha Ignimbrite and mapped the unit from La Pacana northward forming most of the southern and eastern side of the Guacha resurgent dome (Fig. 1).

The Guacha Ignimbrite is a crystal-rich, rhyolite grading to dacite (SiO_2 = 64-76 wt.%) with an minimum estimated intracaldera thickness of ~700 m. The outflows extend northward almost 60 km toward the Quetena Valley. Based on these observations and the area of collapse, an estimated volume of 1300 km^3 has been proposed for the Guacha Ignimbrite, Salisbury et al., (2010). ^{40}Ar-^{39}Ar dating of sanidine from distal outflows yielded a weighted mean age of 5.65 ± 0.01 Ma. What Lindsay called the Upper Tara Ignimbrite, renamed by Salisbury et al. (2010) as the Tara Ignimbrite was mapped from La Pacana, northward into the Pampa Totoral plateau. This ignimbrite ranges in composition from andesite to rhyolite (SiO_2 = 62-77 wt %) with outflows >200 m thick and an overall volume of 800 km^3. Sanidine from outflow pumices yielded a weighted age of 3.49±0.01 Ma. Post collapse lava domes of rhyolitic to dacitic composition emplaced on the central resurgent dome yielded ages of 3.51±0.02 and 3.67±0.13 Ma.

To the northwestern edge of the caldera, the Puripica Chico Ignimbrite (Fig. 1) outcrops and corresponds to the youngest caldera event. This ignimbrite is a dacite (SiO_2 = 66-69 wt.%) and dating by Fernandez and Thompson (1996) of a lava flow overlying the ignimbrite yielded a K-Ar age of 2.3 ±0.5 Ma, however more recent ^{40}Ar-^{39}Ar dating has yielded an age of 1.70±0.02 Ma Salibury et al., (2010) (Table 1 and 3).

3.2 New stratigraphic and field observations

3.2.1 Guacha Ignimbrite Outflow

Outcrops of Guacha Ignimbrite outflow can be followed towards the north of the caldera along the Quetena Valley. The outflow sequence is "confined" between the Vilama and the Laguna Colorada Ignimbrites, although locally it overlays lava flows of porphyrytic dacite (Fig. 4, Photo a). A section located 19 km SSW of the Quetena Chico Village was measured, showing the following sequence from the base to the top:

- 6.0-9.0m: Massive ash-rich uniform tuff with 5-8 cm long pumices and coarser lithics at the base showing flattened pumice up section. Groundmass and pumice increase upward, along with the presence of discoidal pumices.
- 3.0-6.0m: Matrix supported tuff with flattened pumices (pumice:matrix ratio 4:6). Pumices increase in abundance but decrease in size (<3 cm) up section and lithic abundance becomes <1%. The top completely lacks pumices and is a 1-5 cm thick laminated tuff.
- 0.1-3.0m: Matrix supported tuff with rounded pumices (pumice:matrix ratio 1:4) and accidental clasts of dacitic lava. Pumice abundance increases up section, meanwhile lava clasts decrease up section. 2 cm long pumices show some sorting. At 1.5 m from the base, pumices are larger (<10 cm; Fig. 4, Photo c) and more abundant. From 1.5-3.0 m, grain size and pumice abundance decrease.
- 0-0.1m: 10 cm thick fine grained laminated ash overlaying a red paleosoil with weathered lava clasts from the unit below

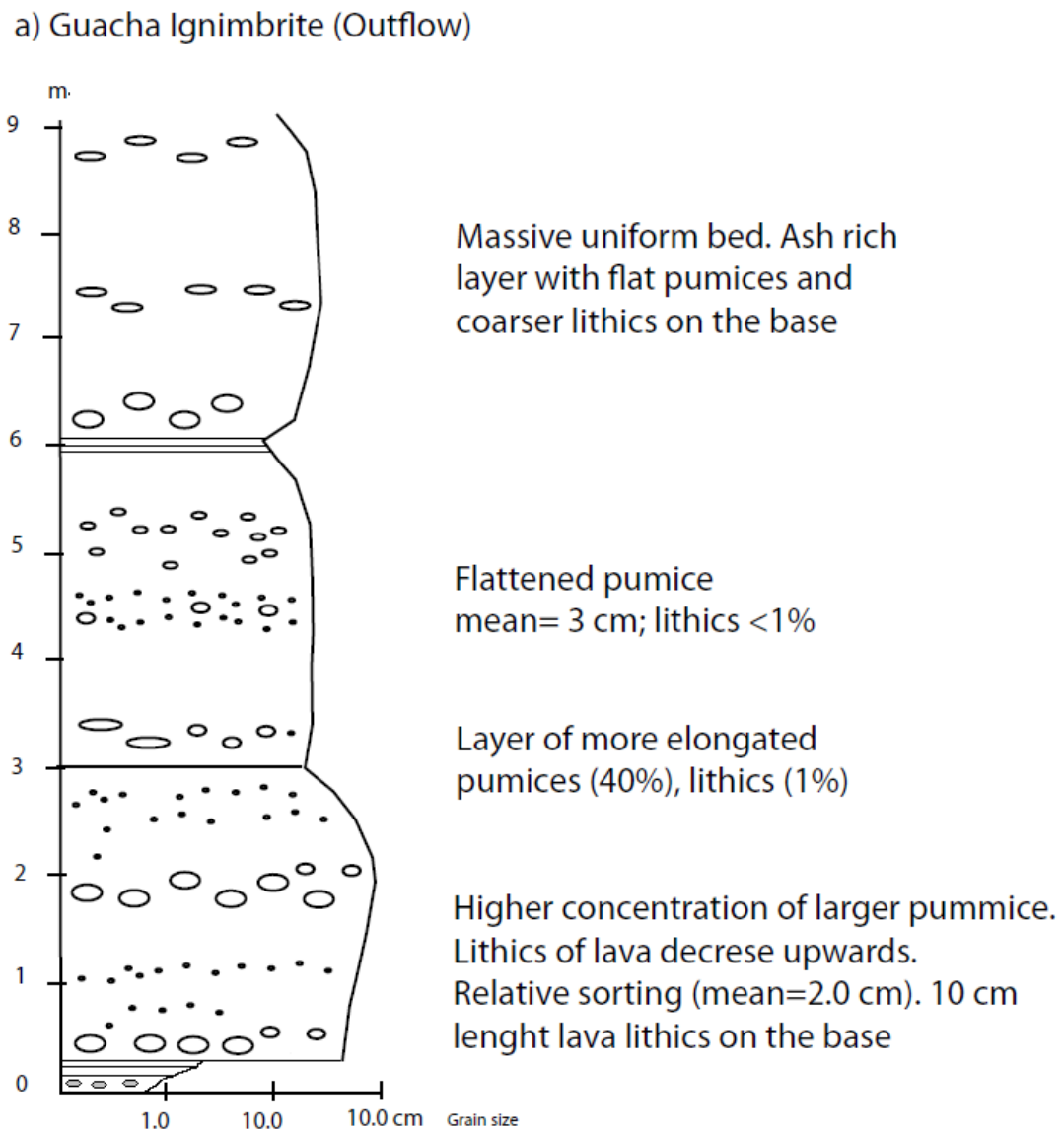

Figure 3 Stratigraphic column of ash-rich Guacha outflow located 19 km SSW of Quetena Chico Village. Vertical scale is in meters; horizontal scale refers to grain size.

Another outcrop, exposing the top of the Guacha Ignimbrite and the base of the Laguna Colorada was observed 22 km NE of the section described above (67°22'36.42"W, 22°19'38.46"S) there this contact is transitional. Two kinds of pumices, tubular and vesicular, were observed.

Figure 4a Outflow outcrops of the Guacha Ignimbrite South of Quetena Chico Village. Porhyrytic lava flows underlying main Guacha outflow. Outcrop shows flow bandig of this unit

Figure 4b Outflow outcrops of the Guacha Ignimbrite South of Quetena Chico Village. Paleosoil at base of the Guacha outflow with weathered blocks of lava from below, overlaid by fine grain ash

Figure 4c Outflow outcrops of the Guacha Ignimbrite South of Quetena Chico Village. Pumice rich tuff 2.0 m above the base; sample A-07 was taken here for geochemistry and U-Pb zircon dating.

Figure 4d Outflow outcrops of the Guacha Ignimbrite South of Quetena Chico Village. Ash-rich tuff lacking large pumices, 4.5 m above the base.

3.2.2 Tara Ignimbrite Outflow

Outcropping 25 km SE of the Rio Guacha scarp, a 70 m thick sequence of Tara Ignimbrite outflow (Fig. 5) overlays older volcanic flows and is in turn overlain by lavas of the Zapaleri volcano (Fig. 6a).

- 35.0-55.0m: Flattened pumices decrease (2-6% vol) and lithics increase to 15% vol. From 40.0 to 55.0 m, a lithic-rich, ashy groundmass-supported tuff is comprised of dark grey andesite rounded lithics (40%) and pumices 3 to 10 cm long (30%).
- 20.0-30.0m: Pumice to groundmass ratio is 1:4 (groundmass 70-75%). Andesite and/or lithics are less abundant than pumices. We move from East to West of the gulley to measure the top of the sequence
- 1.0-20.0m: Lithic-rich groundmass supported tuff. Within the basal 5.0 m the pumice to ash groundmass ratio is 2:5; tubular pumices are abundant and lighter andesite lava clasts (1-2 cm long) make up 1%. Up section the lithics (<1 cm) increase to <40%. From 15.0 to 20.0 m, pumices progressively increase in size (< 65 cm; mean 15 cm) and are more flattened. A defined cooling surface dips approximately 10-15˚ WNW (Fig. 6b).
- The sequence initiates with a 1.0 m thick layer of ash plinian deposit

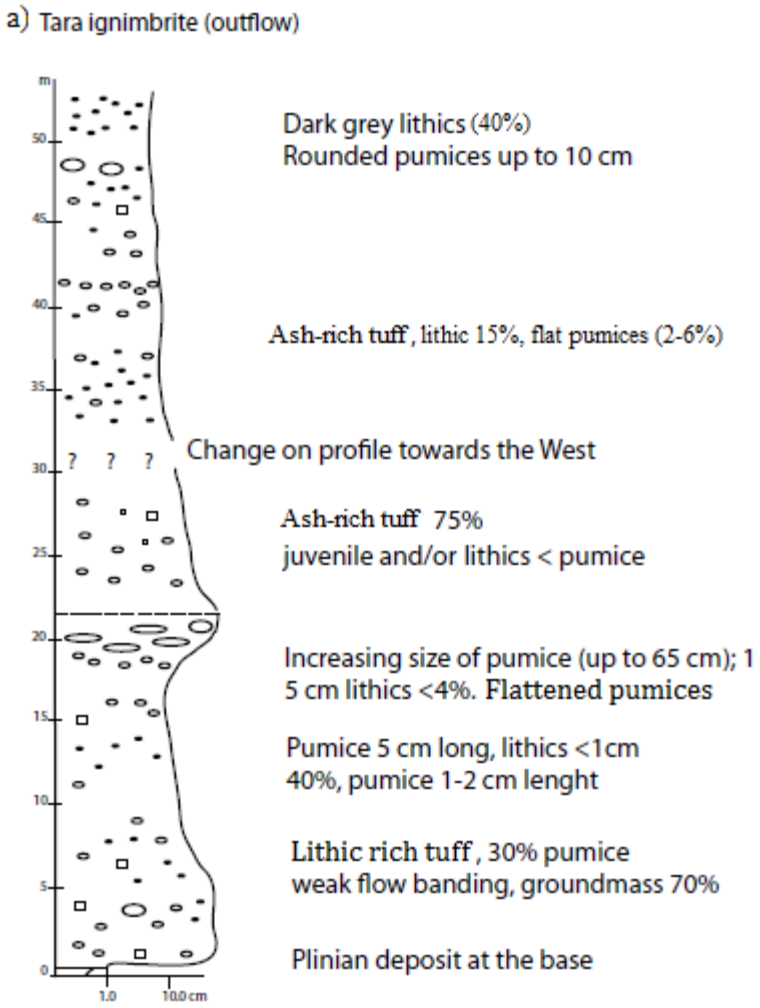

Figure 5 Stratigraphic column of the Tara Ignimbrite outflow showing plinian, pumice and lithic-rich facies, located 25 km SE of Rio Guacha scarp. Vertical and horizontal scale as in Figure 4.

From west to east three lava domes located at the inner caldera scarp are correlated with the Tara Ignimbrite. Figures on the SERGEOMIN maps refer to these domes as the Chajnantor, Rio Guacha, and Chajnantor Lavas domes.

Figure 6a Outcrops of Tara Ignimbrite outflow, 25 km from the Cerro Guacha Caldera. Top of the lithic-rich sequence overlaying by lavas from the Zapaleri volcano.

Figure 6b Outcrops of Tara Ignimbrite outflow, 25 km from the Cerro Guacha Caldera. 10-15˚ WNW dip cooling surface separating upper 65 cm long pumice-rich tuff from 75% ash-rich tuff.

Figure 6c Outcrops of Tara Ignimbrite outflow, 25 km from the Cerro Guacha Caldera. Ash-rich layers with dark andesite lithics and at least one pumice rich layer, located below cooling surface.

Figure 6d Outcrops of Tara Ignimbrite outflow, 25 km from the Cerro Guacha Caldera. Detail of flow showing predominantly rounded dark andesite and fewer (<40%) pumices.

3.2.3 Puripica Chico Ignimbrite

Located at the west edge of the Caldera, a 23m thick section of the Puripica Chico Ignimbrite is overlain by lava flows of the Puripica Grande lava dome (Fig. 7b)

1. 0-2.0m: Crystal rich tuff with 0.5 cm long quartz crystals and fewer 2.0 cm long grey pumices, <3% dark lava and lithics. Up section the grey glassy dark lavas increase in size (<0.15 m), and there is an increase in groundmass phenocrysts up to 1.0 cm long quartz crystals
2. 2.0-5.5m: Decrease in glassy grey dark lavas toward the top and increase of pumice.
3. 5.5-13.0m: Pumice-poor layer. Small pumices in coarse grain groundmass. 7.5 m above the base, tuff is poor in lithics and dark lavas.
4. 13.0-23.0m: Groundmass rich flows with at least one pumice rich layer. This sequence is overlain by lavas of the Amargo stratovolcano.

a)

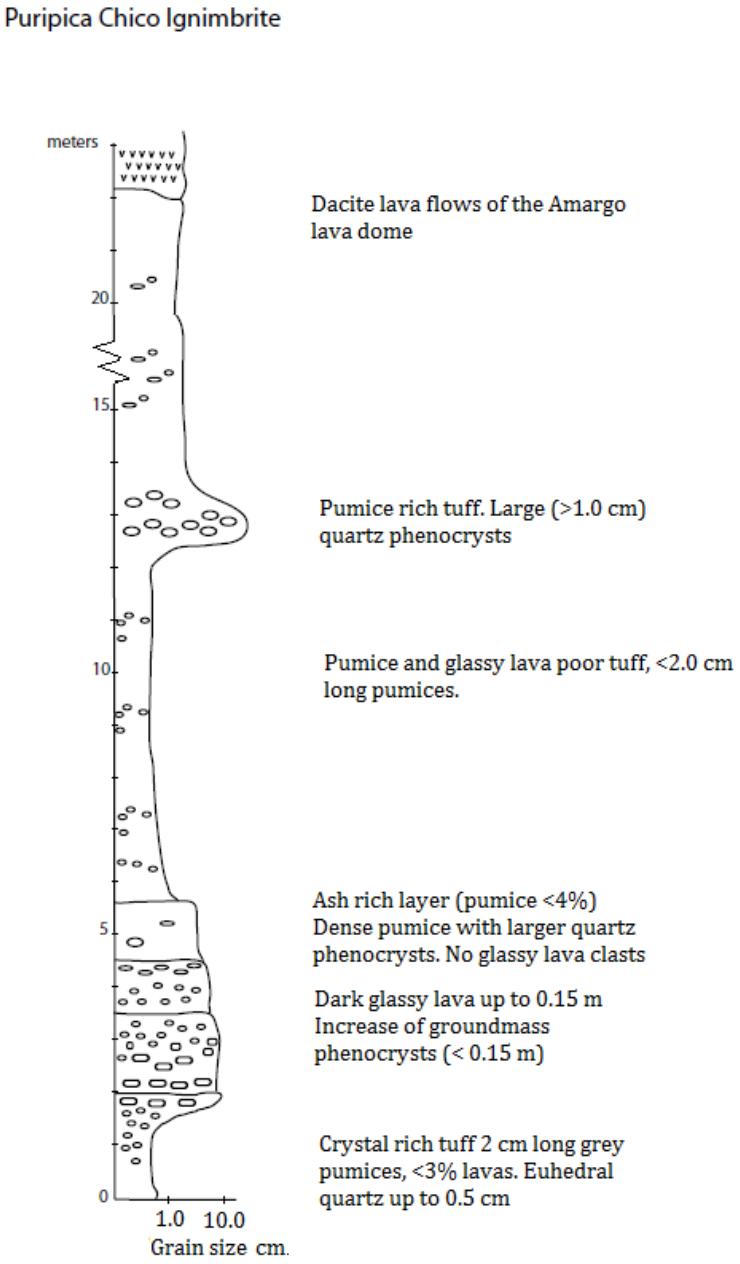

Figure 7a) 23 m thick stratigraphic column of Puripica Chico Ignimbrite measured at the West edge of the Cerro Guacha Caldera

Figure 7b Top of the Puripica Chico sequence (23 m above the base). The crystal rich tuff is poor in pumices or lithics. Top of the ignimbrite is overlayed by lavas of the Amargo lava dome.

Figure 7c) Basal part of Puripica Chico Ignimbrite, showing 15.0 m of crystal rich tuff with subordinate to none layers rich in pumices

Figure 7d) Well exposed base of the Puripica Chico Ignimbrite 4.4 km northeast of the outcrop shown in figure 7c. Glassy and rounded dacite blocks pumice and lithics forms the base of the sequence. 30 cm long hammer used as scale

Figure 8 Reconnaissance Geologic Map of the Guacha Caldera Complex (GCC) of SW Bolivia. Provided as a fold out map at the end of this document. Location of samples, stratigraphic columns, paleomagnetism data, ignimbrite distribution, caldera collapse related structures, location of the Orsu Mine (sulfur), Quetena Chico Village and Sol de Mañana hot springs are also shown

3.3. Correlations and distribution

Regional work aimed to distinguish and correlate the ignimbrites of the APVC was done by de Silva (1989), Salisbury et al. (2010), and Ort et al., (in press) and set the basis for this thesis. Two major problems in this area are the lack of correlations between ignimbrites and their sources and precise age dating. In addition, the Bolivian Geological Service (SERGEOMIN) mapped the area and recognized structures associated with the calderas, minor volcanic centers and sedimentary sequences. However large error in K-Ar ages and lack of distinction between outflow and

intracaldera tuffs makes mapping and unit revision difficult in this area. K-Ar ages displayed in Table 3 contrasts with newer Ar-Ar ages.

Salisbury et al. (2010) sampled and re-evaluated the ignimbrites and their sources, linking them spatial and temporally to calderas and minor shield volcanoes. Because of accessibility and pumice occurrence, sampling was done mainly in outflows of the Guacha and Tara ignimbrites. Finding sanidine, which is more suitable for Ar-Ar dating, is an additional challenge for accurate interpretation. Ar-Ar ages obtained from sanidine are preferred over biotite because its lower closure temperature (230 ˚C for K-feldspar versus 373 ˚C for biotite; Berger and York, 1981; Faure, 2005) and reported erroneously older ages compared to data given by sanidine (Hora et al., 2010).

Complementary to Ar-Ar dating, characteristic remanent magnetization data (ChRM) was used to correlate ignimbrites. Statistical evaluation of paleomagnetic data done by Michael Ort, distinguished two larger ignimbrites associated to the Cerro Guacha Caldera. Declination and inclination values are given in Table 4 and represent statistical values below 2-sigma error (α_{95} notation). Values are shown on stereograms (Fig. 9).

Units	Age (Ma)	Mineral	Method	Reference
		Guacha ignimbrite		
Intracaldera				
Pampa Guayaques 1,2 Tuffs	5.9 ± 0.4	biotite	K-Ar	Almendras et al., 1996
Chajnantor Tuffs	6.6 ± 0.5	biotite	K-Ar	Almendras et al., 1996
Kalina Tuffs	6.6 ± 0.4	biotite	K-Ar	Almendras et al., 1996
Ouflows				
Inca Tuffs	5.6 ± 0.5	biotite	K-Ar	Almendras et al., 1996
Tullitayoj Tuffs	5.8 ± 0.4	biotite	K-Ar	Pacheco and Ramírez, 1997c
	6.2 ± 0.4	biotite	K-Ar	Pacheco and Ramírez, 1997b
Lower Tara (Chile)	5.47 ± 0.33	biotite	K-Ar	Lindsay et al., 2001a
	5.62 ± 0.98	biotite	K-Ar	Lindsay et al., 2001a
	5.68 ± 0.14	biotite	K-Ar	Lindsay et al., 2001a
Quetena Tuffs	6.5 ± 0.4	biotite	K-Ar	Pacheco and Ramírez, 1997b
Delgada Tuffs	6.9 ± 0.7	biotite	K-Ar	Choque et al., 1996
Aguadita 1 Tuffs	6.2 ± 0.5	biotite	K-Ar	Almendras et al., 1996
	6.3 ± 0.4	biotite	K-Ar	Pacheco and Ramírez, 1997
Aguadita 2 Tuffs	4.5 ± 0.5	biotite	K-Ar	Pacheco and Ramírez, 1997b
		Tara ignimbrite		
Intracaldera				
Chajnantor Tuffs	6.6 ± 0.5	biotite	K-Ar	Almendras et al., 1996
Outflows				
Upper Tara (Chile)	3.42 ± 0.15	biotite	K-Ar	Lindsay et al., 2001a
	3.77 ± 0.15	biotite	K-Ar	Lindsay et al., 2001a
	3.65 ± 0.12	biotite	K-Ar	Lindsay et al., 2001a
	3.82 ± 0.13	biotite	K-Ar	Lindsay et al., 2001a
	3.81 ± 0.12	biotite	K-Ar	Lindsay et al., 2001a
	3.83 ± 0.21	biotite	K-Ar	Lindsay et al., 2001a
Aguiita Brava Tuffs	~ 1.0			Carta Geologica de Bolivia, Hoja Volcan Putana
Atana Tuffs	4.0 ± 0.3	biotite	K-Ar	Gardewig and Ramirez, 1985
Pampa Totoral Tuffs	~ 2.8			Carta Geologica de Bolivia, Hoja Laguna Busch
		Puripica Chico ignimbrite		
Puripica Chico Lavas	2.1 ± 0.5	biotite	K-Ar	Fernandez and Thompson, 1996

Table 3 Ignimbrites dated by K-Ar method and described in previous studies correlated with the Guacha and Tara Ignimbrites (Modified after Salisbury, et al., 2010).

Ignimbrite Characteristic Remnant Data						
Ignimbrite	Dec	Inc	α_{95}	K	n/N	Sites used
Puripica Chico	141.5	41.9	4.9	189.7	1/1	BL-26
Tara	339.3	25.7	11.6	113.1	3/7	BL-21, BL-22, BL-24
Guacha	178.9	68.8	9.0	56.6	6/6	BL-15, BL-16, BL-20, BL-25, BL-30, BL-31
Puripica Chico	141.5	41.9	4.9	189.7	1/1	26

Table 4 Paleomagnetism data showing weighted means (2σ) for declinations, inclinations, paleo flow directions (K's), number of analyses (n) and sites (N) used for statistical processed data (values of K's and location shown in Fig. 9, Ort et al., in press).

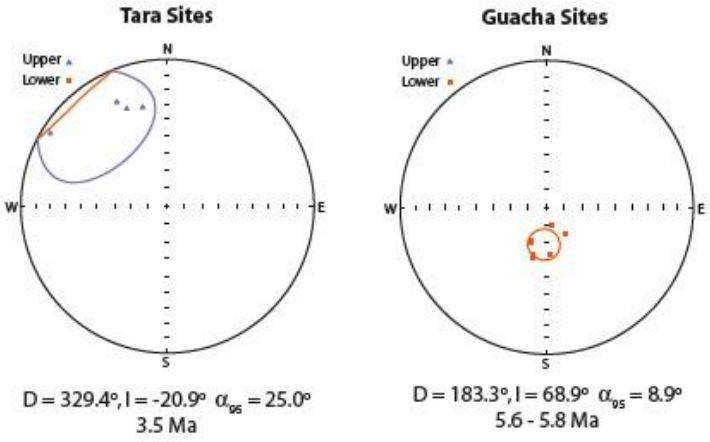

Figure 9 Stereonets showing mean declination and inclinations for Tara and Guacha Ignimbrites (Data from M. Ort, in press).

3.4 Updated stratigraphy

3.4.1 Guacha Ignimbrite

Guacha Ignimbrite outflow deposits are well exposed to the north and south of the caldera, and are most extensive to the north along the Quetena Valley (Fig. 8). Older volcanism (Loromayu lavas ~6 Ma) probably restricted the flows from flowing to the west. To the south, the Tara and Atana ignimbrites extensively overlies the Guacha Ignimbrite, obscuring stratigraphic relations of the Guacha ignimbrite.

Ar-Ar biotite dating from outflow pumices to the North side of the caldera yield ages of 5.71 ± 0.05, 5.8 ± 0.01 and 5.84 ± 0.02 Ma, Salisbury et al., (2010) (Table 1). At the inner scarp (North of Rio Guacha dome) biotite yields ages of 5.77 ± 0.04 Ma. The sanidine preferred age for the Guacha Ignimbrite was obtained from a distal outcrop at the northern side of the Quetena Valley yielding a weighted mean age of 5.65 ± 0.01 Ma (B06-002, Table 1).

ChRM declination and inclination values for the Guacha Ignimbrite (Ort et al., in press) yield an average value of 179˚ and 69˚(reverse polarity), respectively over 6 sites each with 30 individual measurements (Table 4, Fig. 4). Paleo flow directions (K_1) for sample BL-15, 16 and 20 (located at the NNE side of the caldera) yield mean azimuths of 11.3˚, 49˚ and 42˚ (Fig. 8) implying infill of a paleo valley of NE trend and a source located to the south. Sample BL-25 yields a mean K_1 value of 62˚ suggesting infill of another paleo valley of NE trend (Fig. 8)

The Guacha andesite outcrops within the main resurgent block of the caldera lying above welded Guacha intracaldera tuffs and apparently underneath the Chajnantor Lavas (3.67 Ma). It is offset to the East and West by the inner scarps associated with the eruption of the Tara Ignimbrite, indicating it that was erupted before the Tara collapse. This unit shows the same uplifted tilt as the Guacha welded tuffs, suggesting it was emplaced shortly after the eruption of the Guacha Ignimbrite. These field evidences suggests that the Guacha andesite was formed after the eruption of the Guacha Ignimbrite.

3.4.1 Tara Ignimbrite

Ar-Ar biotite ages for outflows of the Tara ignimbrite range between 3.58±0.03 to 3.89 ±0.03 Ma and include an age of 3.56 ±0.02 Ma for a sample collected close to the collapsed area (B06-025, Table 1). The preferred sanidine age is from a sample of outflow located to the northwest and southeast sides of the main resurgent block (B06-018 and 89002) that yield a weighted age of 3.49±0.01 Ma.

The Tara ignimbrite contrasts with the Guacha Ignimbrite by the fact that Tara outflows are mainly exposed to the South (Fig. 8), rather than to the North (e.g. Quetena Valley). This suggests that there was a topographic barrier to the North when the Tara ignimbrite formed or that the eruption had a direct component to the south.

ChRM declination and inclination values for the Tara Ignimbrite yielded means of 329.4˚ and -26˚(normal polarity) respectively over 3 sites each with 30 individual measurements (Table 4, Fig. 4). Paleomagnetic measurements taken on the SE side of the caldera yielded weighted paleoflow mean azimuths (K_1) of 27.2˚, 263˚ and 124˚ (Fig. 8). The 27.2˚ azimuth is coherent with the northeastern trend of the Tara outcrops at this location; the 263˚ and 124˚ azimuths suggest that the outflow moved from the west and roughly converged with the set of 27.2˚azimuth.

3.4.1.1 Pre and post collapse Tara Domes

The Chajnantor dome yielded a biotite age of 3.59±0.02 Ma which is older than the sanidine age (3.51±0.02 Ma) obtained from this same dome (Table 1); this later sanidine age overlaps within error with the Ar-Ar age of the Tara ignimbrite (3.49 ± 0.01 Ma). The Rio Guacha dome yielded a biotite age of 3.61+0.02 Ma, however the stratigraphy clearly show the domes overlying the Tara ignimbrite in the resurgent dome and the youngest U-Pb zircon age for this dome (3.15 ± 0.23 Ma, see section 6.22). The Chajnantor Lavas dome yielded a sanidine age of 3.67 ± 0.13 Ma which is older than the Ar-Ar sanidine age of the Tara Ignimbrite (3.49 ± 0.01 Ma).

The distribution of these domes along the inner scarp of the caldera (Fig 2), suggests that the Chajnantor Lavas was emplaced before the other domes along a preexistent structure coincident with the present day inner scarp of the caldera (approximately 40 ka before the eruption of the

Tara Ignimbrite). After resurgence of the Tara Ignimbrite, the Chajnator domes and the Rio Guacha and were emplaced respectively along the preexistent structure.

3.4.1.2 Puripica Chico Ignimbrite

The only available age for the Puripica Chico Ignimbrite was taken from a pumice sample (B06-073) yielding a biotite age of 1.70±0.02 Ma (Table 1). 26 K_1 paleo-flow measurements (site BL-26) yielded an azimuth of 190˚, indicating the source was located towards the south.

4.0 Caldera structure, geometry, and volcanological development

4.1 Overall structural context and main structural features

The locations and architecture of the calderas of the APVC seem to be largely controlled by regional tectonic structures. As shown in figures 1 and 2 resurgent domes of La Pacana, Vilama and Guacha Calderas strikes generally to the northwest. Folkes (2010) suggests that this configuration is parallel to the Lipez Fault Zone, a similar northwestern-southeast strike parallel to with the southern Calama-Olacapato-El Toro Fault zone (Salfity et al., 1985). Both northwest-southeast structural alignments are oblique to the regional north-south orogenic and general belt.

4.2. Main structural features

4.2.1. Eastern (outer) scarp and moat

One of the more conspicuous features of the Cerro Guacha Caldera is the Eastern arcuate rim (Fig. 2). This 40 km long scarp makes up Eastern margin of the caldera and several effusive lava domes and flows have been emplaced along and on top of other strata above this structure. No volcanic features associated with this rim are visible the north, south or western sides of the caldera; however, these areas are largely covered by younger volcanic deposits.

The Totoral dome, a roughly circular, ~12 by 11 km dome comprising of lava flows and welded basal ignimbrites (Mobarec, 1993), crop outs at the northernmost end of the rim (Fig. 2; 10a). The lava flows are characterized by light grey pophyritic dacite, containing phenocrysts of hornblende, biotite, feldspar (weathered) and quartz in a moderately altered matrix. K-Ar age of 1.9 ±0.5 Ma was obtained for the dacite lavas of this dome (Almendras et al., 1996). New U-Pb

zircon ages presented in Chapter 6 yielded a younger weighted mean age of 1.8 ±0.06 Ma (Fig. 23).

Southeast of the Totoral dome the Cojina lavas form an elongated outcrop made of andesitic lavas truncated by steep normal faults associated to caldera collapse (Mobarec, 1993; Almendras et al., 1996). West of the Cojina lavas a small outcrop of welded ignimbrite with abundant lithics and sub-vertical banding was described as a possible vent for the Guacha ignimbrite (Salisbury et al., 2010). This outcrop is called Alkhamari dome in the maps of SERGEOMIN that describe it as a light grey porphyritic rhyolite with biotite. The only available age for this rock is K-Ar biotite age yielding 7.1 ± 0.6 Ma (Almendras et al., 1996).

Southeast of the Cojina lavas, there is a light red, partially welded section of the Guacha ignimbrite that was previously named the Inca tuffs (Table 1). K-Ar age data from a single biotite crystal yielded an eruption age of 5.6 ± 0.5 Ma for the ignimbrite (Almendras et al., 1996). Southwest of the Cojina Lavas, there is a 6.6 ± 0.4 Ma K-Ar (biotite age) sequence of ignimbrites named the Kalina Tuffs by SERGEOMIN. This sequence consists of a 25 m thick ash flow tuff containing ~30% pumice, including 3-30 cm long fiamme, in a vesicular matrix of quartz, hornblende, biotite and feldspar. This ash flow overlies a 5 m thick, darker, welded ash flow that contains quartz, hornblende and biotite. This unit was mapped by SERGEOMIN as the Kalina dacite lavas. South of the Kalina lavas facing the caldera moat (Fig. 10e) there is a 10 m thick deposit of clastic sandstones and conglomerates containing abundant quartz, biotite, pyroxene, volcanic lithics and some sporadically layers of travertine. At the south edge of the Cojina lavas, the Brajma complex cropsout forming an 11 by 7 km dacite lava dome. A K-Ar age obtained from a single biotite crystal yielded an age of 6.8 ± 0.5 Ma (Lema et al., 1996). West of the main dome a coarse dacitic lava flow was sampled for U-Pb zircon dating, and yielded an age of 5.62 ± 0.06 Ma, which is slightly younger than the age assumed for the Guacha Ignimbrite. We interpret this as associatied with post collapse resurgence.

Figure 10a) Dacite lava flows of the Totoral dome located at north edge of the easter caldera rim

Figure 10b) 20 m thick Guacha intracaldera ignimbrite showing welded tuff at the base grading upwards to ash rich non welded tuff

Figure 10c) East view of caldera moat showing conglomerate sequence, lacustrine travertines and Kalina lavas on the background

Figure 10d) Close-up photograph of travertine on top of conglomerades

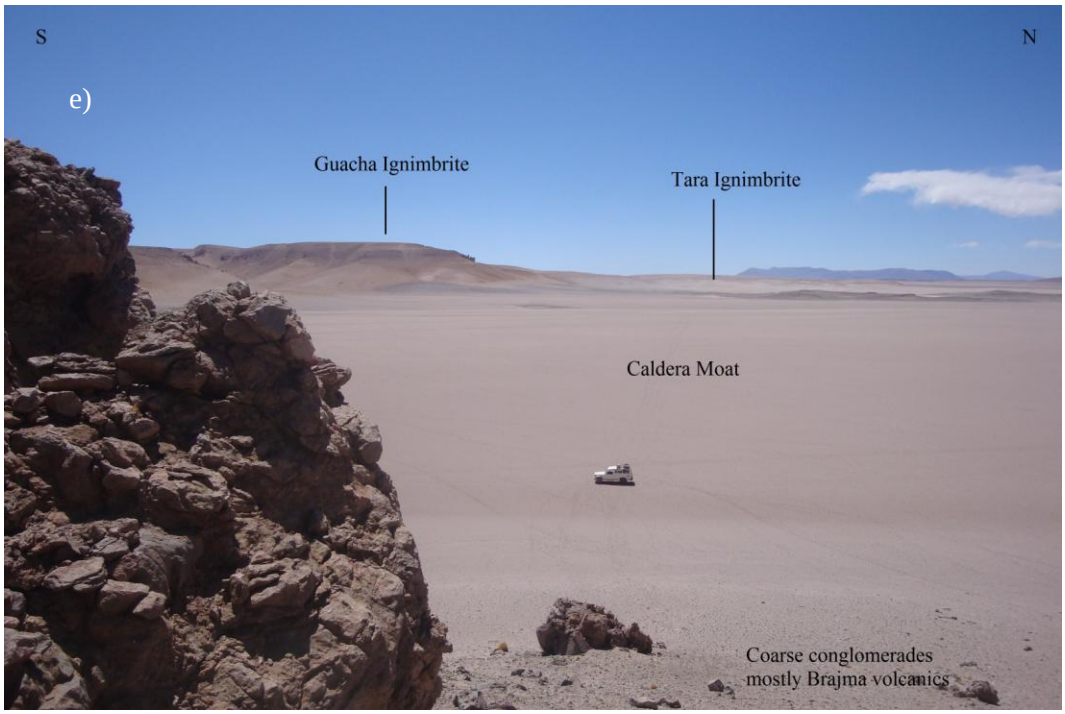

Figure 10e) West view of the caldera moat from sedimentary sequence. Resurgent post Tara dome that uplifted the welded Guacha Ignimbrite visible in the background. To the north, proximal outflows of Tara Ignimbrite (white deposits).

4.2.2. Resurgent domes

One of the main features of the Cerro Guacha Caldera is its resurgent dome (Fig. 2). This 20 x 18 Km semicircular structure is bordered to the east by concentric scarps parallel to the outer Eastern caldera rim (Fig. 11). Resurgence after the eruption of the Guacha Ignimbrite, uplifted the intracaldera tuffs which were later truncated by collapse associated to the Tara Ignimbrite.

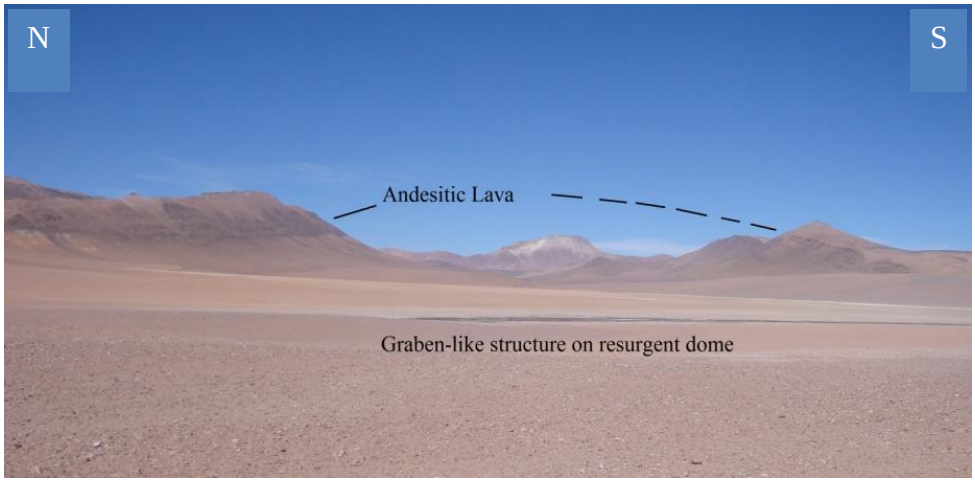

Figure 11 Apical graben of the resurgent dome: darker outcrops to the north and south correspond to Guacha andesite overlying Guacha intracaldera tuff. During caldera resurgence this sequence was uplifted producing anticline-like structure. Extension generated normal faults (showed as down thrown structures on plan view of geologic map) tilting the blocks similar to grabens on rifting zones. Picture location is shown in geologic map (Figure 8)

The resurgent dome comprises the welded intracaldera facies of the Guacha and Tara ignimbrites. The Guacha Ignimbrite crop outs mostly to the east and south, while the Tara Ignimbrite outcrops mostly in the northwest. Lying on the top of the Guacha welded tuff the Guacha andesite is a 100 m thick dark aphanitic andesite that was uplifted along the Guacha welded tuff when resurgence occurred, forming the main apical graben of the Guacha Caldera (Fig. 11). The outcrops of this andesite are offset both to the east and to the west and the scarps are associated with the Tara eruption (Figs. 8 and13). The resurgent dome consists of two distinct structural blocks divided by a complex fault system related to collapse and/or resurgence of the caldera. Although offset by the inner scarp, lateral continuity toward the east suggest that the Guacha ignimbrite was folded by doming before the Tara ignimbrite erupted.

Well exposed outcrops of intracaldera Tara tuff are observed to the northwest of the resurgent dome (Fig 8). The main block (shown in figure in 12) dips gently 10˚ to the northeast. The height difference between the highest point of the outcrop and the base of it, yielded an H value of ~350 m; the horizontal distance W is 1000 m; these values were used to calculated a thickness of ~500 m thick. This value however, is a minimum because the base of the sequence is probably deeper and therefore the W distance can be larger.

The location of the post-collapse lava domes suggests that their emplacement was structurally controlled (section 3.4.1.1)

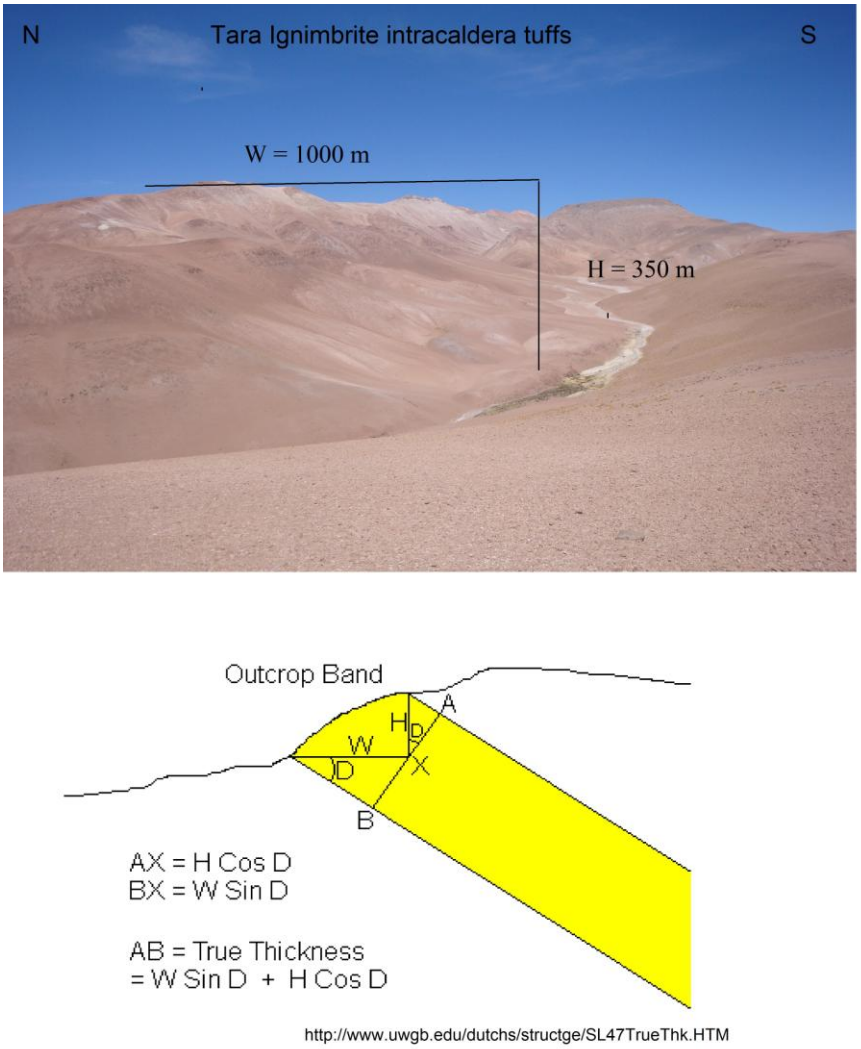

Figure 12 Welded tuff corresponding to the Tara ignimbrite located at the northwestern side of the resurgent dome. "True" thickness (~500 m) of the welded tuffs is calculated using height difference (350 m), horizontal outcrop distance (1000 m) and dip of the layers (10˚)

4.2.3 Western margin - Puripica Chico

The ~10 km^3 Puripica Chico ignimbrite crops out towards the northwestern edge of the Guacha Caldera (Fig. 7) along with lava domes and volcano vents with no caldera moat, travertines or sedimentary sequence as observed at eastern rim. The lack of surface structures towards this margin of the caldera allows suggesting that the collapse of the caldera was asymmetrical or trap-door like. This collapse style was suggested also for La Pacana caldera to the south Lindsay, (1999), Vilama to the east Soler, (2007) and seems to be also present in the Pastos Grandes caldera to the north.

4.3 A model for the surface development of the caldera

Integrating all these observations, a model for the development of the Guacha Caldera complex can be developed. A schematic evolution is shown on figure 13. The following stages are inferred:

a) 5.65 Ma Guacha Ignimbrite System (GIS): the Guacha ignimbrite erupted through vents located near the east and north edge of the structural rim (pre-caldera units mostly Cojina lavas).

b) Lack of structure to the west suggests presence of a hinge and a trap door collapse after the eruption. Andesitic lava flows flooded the caldera moat. Lake deposits and travertines were formed along the structural moat during this period.

c) Uplift of the caldera roof due to resurgence uplift and tilt the welded ignimbrites, andesitic when lavas and sedimentary lake sequence.

d) 3.49 Ma Tara Igninbrite System (TIS): eruption of the Tara ignimbrite through smaller scarp along with offsetting of Guacha Ignimbrite intracaldera units.

e) Resurgence uplifted both the Tara and Guacha intracaldera ignimbrites. Along the outer scarp, three lava domes were emplaced.

f) 1.7 Ma Puripica Chico Totoral System: Eruption of the Puripica Chicois was followed by the emplacement of lava domes along the western hinged edge of the Guacha caldera

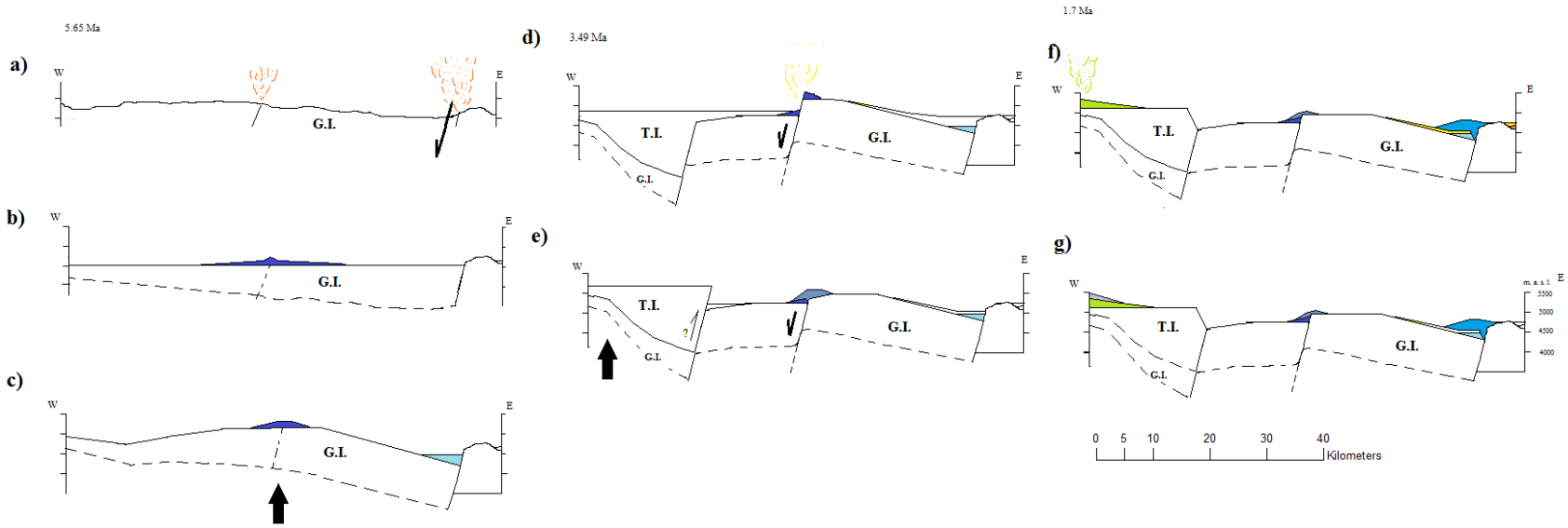

Figure 13 Structural evolution of the Cerro Guacha caldera (not magmatic system showed) a) 5.65 Ma the Guacha ignimbrite erupted through vents located near the east and north edge of the structural rim (pre-caldera units and offset Cojina lavas). Lack of structure to the west suggests presence of a hinge and a trap door collapse after the eruption. b) Guacha andesite lava flows flooded the caldera moat. Lake deposits and travertines were formed along the structural rim during this period. c) Uplift and tilting of the caldera roof due to resurgence. of intracaldera the welded tuffs and the Guacha andesite d) 3.49 Ma eruption of the Tara ignimbrite through smaller rim along with offsetting of Guacha Ignimbrite intracaldera units. e) Tara resurgence uplifted both the Tara and Guacha intracaldera ignimbrites. Along the outer scarp, three lava domes were emplaced (Chajnantor, Rio Guacha and Chajnantor Lavas dome); f) 1.7 Ma Eruption of the Puripica Chico followed by the emplacement of lava domes along the western hinged edge of the Guacha caldera.

5.0 Petrology and Geochemistry of the magmatic components of the Cerro Guacha Caldera

5.1 Introduction

On the basis of the volcanology, stratigraphy and geochronology three eruptive episodes have been identified for the Cerro Guacha Caldera Complex (CGCC). These are the 5.6 Ma Guacha Ignimbrite Stage (GIS), the 3.69 Ma Tara Ignimbrite Stage (TIS), and the 2 to 1.8 Ma Puripica Chico –Tortoral Stage (PCTS). These volcanic episodes are hypothesized to represent distinct magmatic stages during the history of the CGCC. Here the petrography and geochemistry of the three stages are described collectively as a group and as individual time constrained stages of the CGCC (Tables 5 and 6).

Whole rock analyses of 39 pumices and 7 lavas belonging to the Cerro Guacha Caldera were made using XRF-ICP techniques. Major oxides were normalized to 100% volatile free with representative analyses presented in Table 6. Samples range from andesite to high silica rhyolite and most samples belong to the high-K series, except for the Guacha andesite, the Rio Guacha and the Chajnantor Lavas domes that fall within the field of medium-K (Fig. 16a and b). Rock /chondrite normalized spider shows typical slab-related signatures (with negative Nb and Ta anomalies) with the more highly fractionated Chajnantor domes as the most evolved member of the caldera (Fig. 16c)

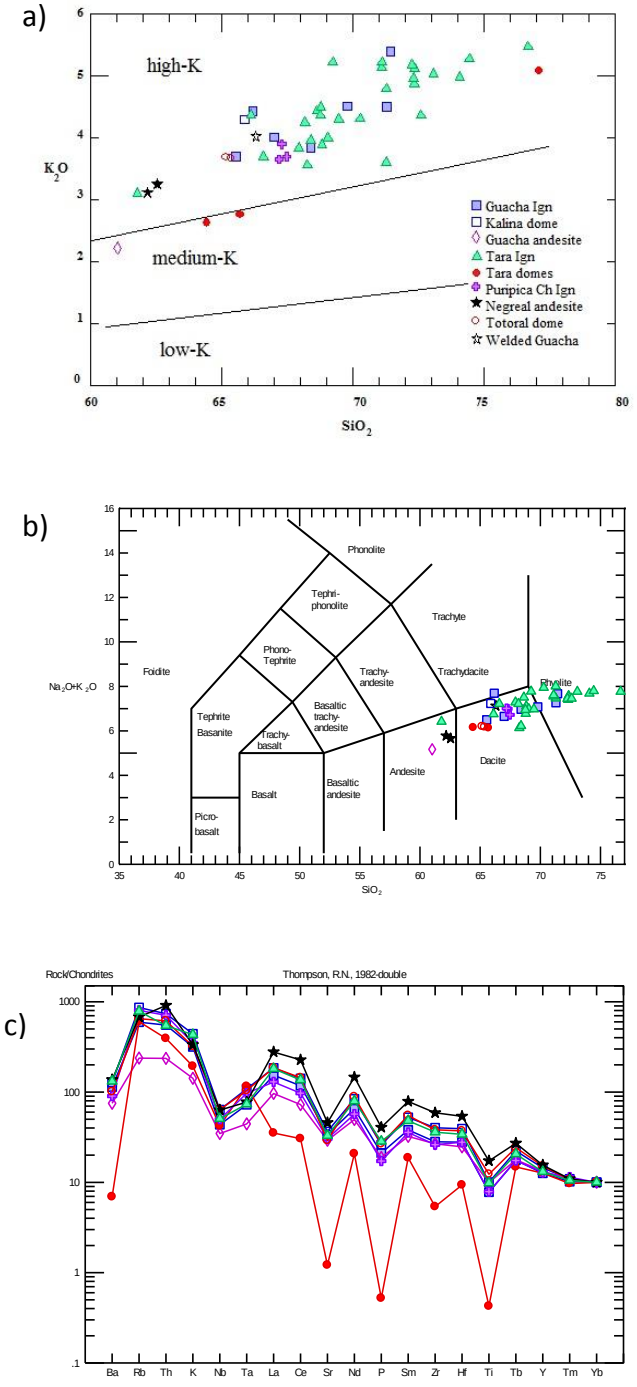

Figure 14 a) K_2O vs SiO_2 diagram showing most of the samples of the CGCC falling down the high-K field; exceptions are Tara lava domes and Guacha andesite; b) Total Alkalis Silica diagram (TAS) and c) Rock/chondrite spider of Thompson et al., (1982), showing typical slab-related arc signatures. Extreme fractionation corresponds to high silica Chajnantor dome

5.2. Petrography

Pumices of the three main ignimbrites have either tubular or rounded vesicules. Vesicular, typically dacitic rounded pumices 5.0 to 65.0 cm long, are made up of phenocrysts of quartz + hornblende + biotite + feldspar (40 vol %), along with vesicles (10-20 vol %) embedded in a silky felsic matrix; tubular pumices (up to 5 cm) are made up of finer quartz + biotite phenocrysts (5-10 vol %; 0.5 mm) in a silky matrix. Dacitic crystal rich lava flows (up to 56 vol % crystal) are made up of coarser (1 to 2 cm) phenocrysts of quartz + feldspar + hornblende + biotite in a fluidal matrix of same finer mineralogy. Porphyritic andesitic lava flows are made up of finer phenocrysts of feldspar + pyroxene (0.5-1.0 cm) in a glassy mafic matrix. The individual stages are broadly similar but have some subtle differences (Table 6).

Dacite pumices of the Guacha ignimbrite are made of phenocrysts of plagioclase > quartz > biotite > hornblende > Fe-Ti oxides (Fig. 16a). Sanidine is found occasionally. Vesicles reach up to 38 vol % and the felsic glasses ranges from 44 to 54 vol % (Table 6). Calculated vesicle-free percentage of crystals ranges from 14 to 57 vol %. Matrix is felsic, made of quartz, plagioclase and alkali feldspar (10-50 microns long). Lava flows of andesite are made of phenocrysts of subhedral and sieved plagioclase (25 vol %), cumulates and phenocrysts of subhedral opx (5.5 vol %) most with reaction rims and Fe-Ti oxides (1.75 vol %) embedded in a devitrified glass (68 vol %) of plagioclase and Fe-Ti oxides (Fig. 16b). The post collapse dacitic Kalina lava dome is made of phenocrysts of plagioclase > quartz > biotite>hornblende > sanidine > sphene > zircon (32 vol % crystals) embedded in a devitrified glass.

Rhyolite pumices of the Tara Ignimbrite System are made of phenocrysts of plagioclase > quartz > biotite > apatite, sandine. Vesicles reach up 37 vol % and glass 54 vol % (Fig. 16c). Calculated vesicle free crystals yielded 14 vol %. Dacite pumice are made of plagioclase > hornblende > biotite > clinopyroxene > Fe-Ti oxides (0.75 vol %), Vesicles reach up to 33.5 vol % and glass 47.5 vol %. Calculated vesicle free crystals yielded 29 vol %. Matrix is made of microcrystalline quartz and alkali feldspar (<30 microns). Electron microprobe analyses performed by Grocke et al., 2012 on glasses of pumices and lava domes of the Tara ignimbrite yield an overall average of 72.5 wt % SiO_2. Matrix glass composition from Post collapse Rio Guacha dacitic dome is made of plagioclase >biotite >hornblende > clinopyroxene, embedded in a devitrified glass with spherulites (73.25 vol %). Xenoliths of sandstones and gabbros (?) were also observed (1.5 vol

%). Adjacent rhyolitic Chajnantor dome is made of quartz > plagioclase > sanidine > biotite > Fe-Ti oxides > and glass (87.0 vol %) (Fig. 16d)

Crystal rich dacite pumice of the Puripica Chico Ignimbrite System is made of phenocrysts of plagioclase > biotite > hornblende > Fe-Ti oxides. Vesicles make up 10 vol % and glass 39 vol %. Calculated vesicle free crystals yielded 57 vol %. A dark inclusion on Puripica Chico Ignimbrite corresponds to welded tuff made up of fragmented phenocrysts of plagioclase > quartz > biotite > pyroxenes (?) > apatite in a welded glassy fluidal altered glass. Negreal del Totoral is an andesite with aphanitic groundmass and interbedded layers of richer in Fe-Ti oxides, showing phenocrysts of plagioclase > clinopyroxene > Fe-Ti oxides > amphibole, in a groundmass made of plagioclase and Fe-Ti oxides (Fig. 15e). Totoral Dome is a porphyrytic crystal rich dacite made up of plagioclase > clinopyroxene >biotite > Fe-Ti oxides embedded on a devitrified glass with spherulites (Fig. 15f).

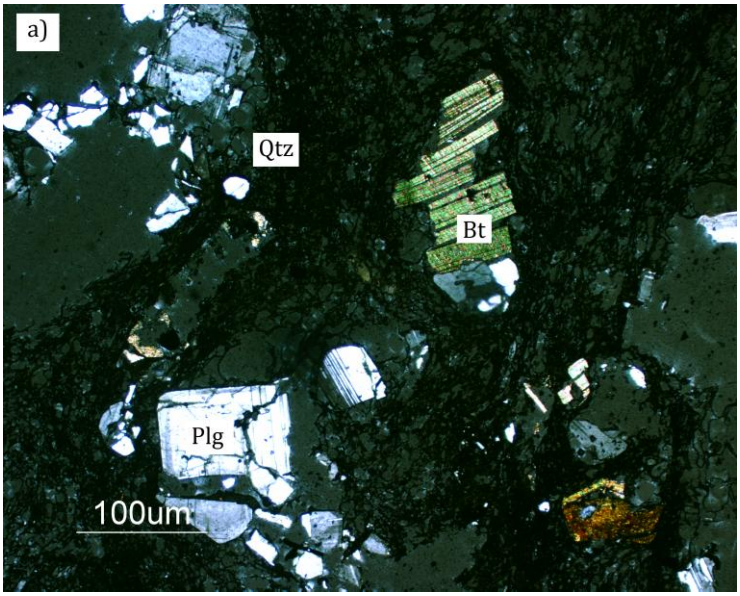

Figure 15a Polarized microphotographs of thin sections showing crystal rich dacitic pumice from Guacha Ignimbrite (B06-085) showing fractured Qz and plagioclase phenocryst along with deformed biotites

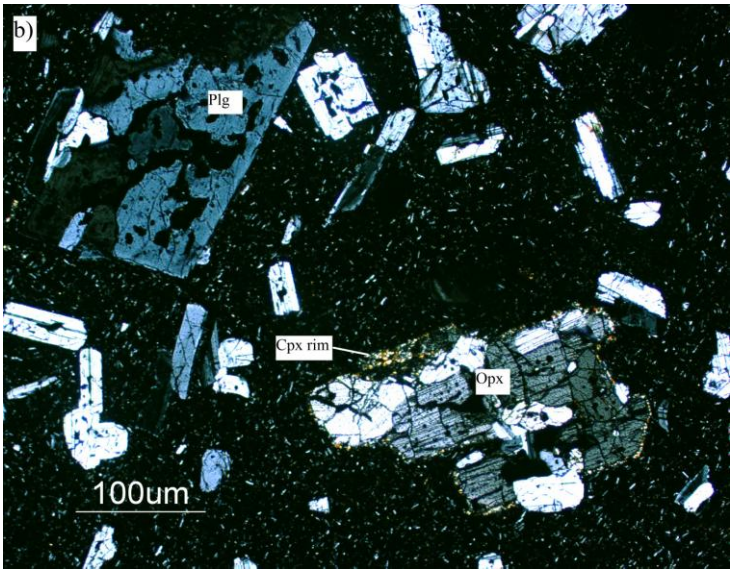

Figure 15b Polarized microphotographs of thin sections showing Guacha andesite (A-13) showing orthopyroxene and plagioclase phenocrysts in a microcrystalline groundmass made of K-feldspar and Fe-Ti oxides, orthopyroxene exhibits reaction rims of clinopyroxene

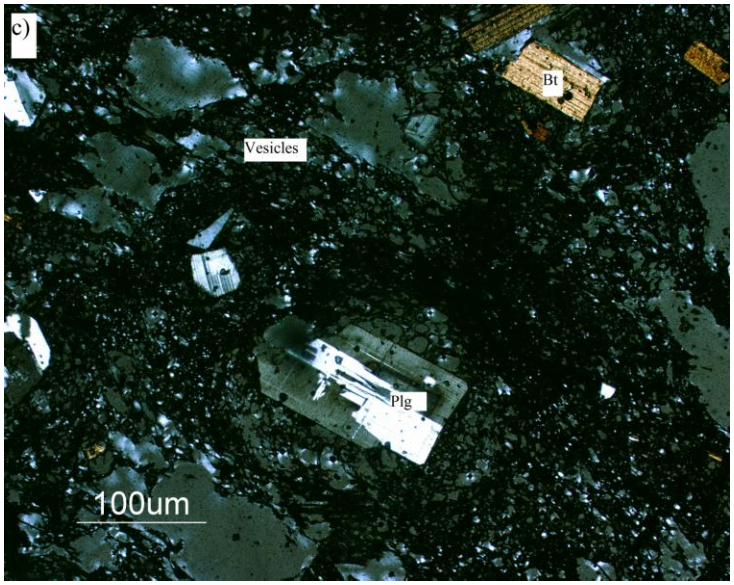

Figure 15c Polarized microphotographs of thin sections showing crystal poor rhyolitic pumice from Tara ignimbrite (B06-013) showing euhedral phenocrysts of plagioclase and biotite in a felsic groundmass with vesicles

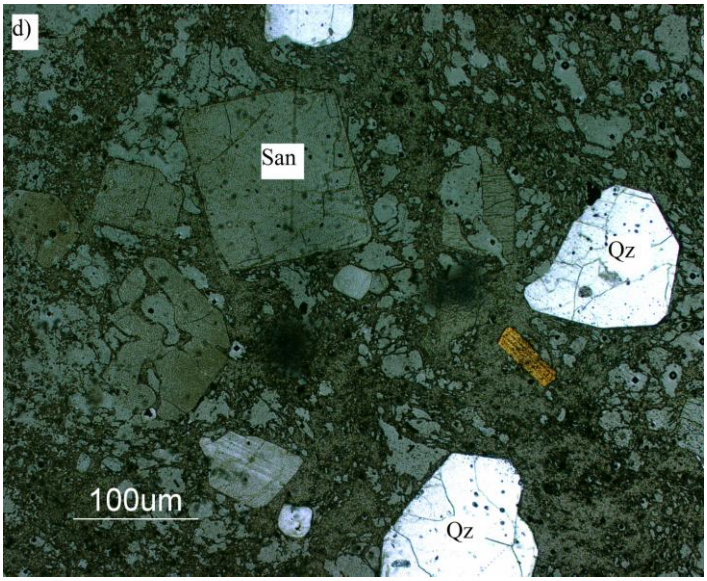

Figure 15d Polarized microphotographs of thin sections showing high-silica Chajanator dome showing phenocrysts of sanidine, quartz and biotite in a perlitic and devitrified groundmass

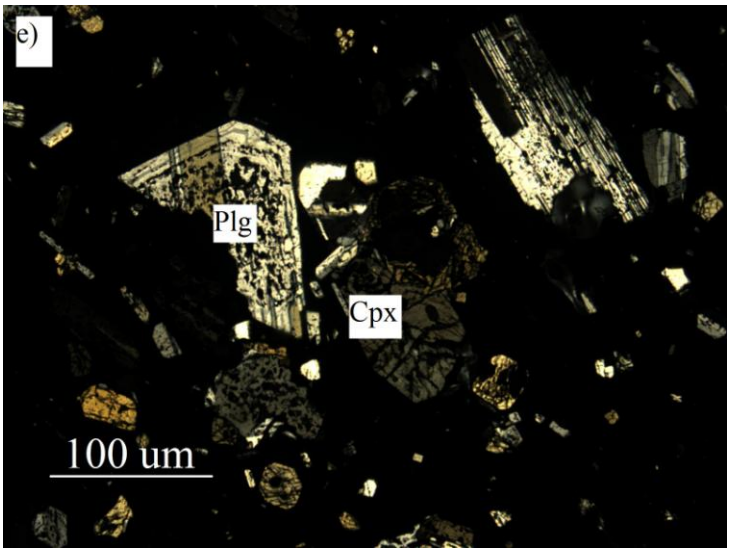

Figure 15e Polarized microphotographs of thin sections showing Negreal Andesite showing phenocrysts of clinopyroxene + plagioclase + amphibole in a glassy matrix of clinopyroxene +Fe-Ti oxides

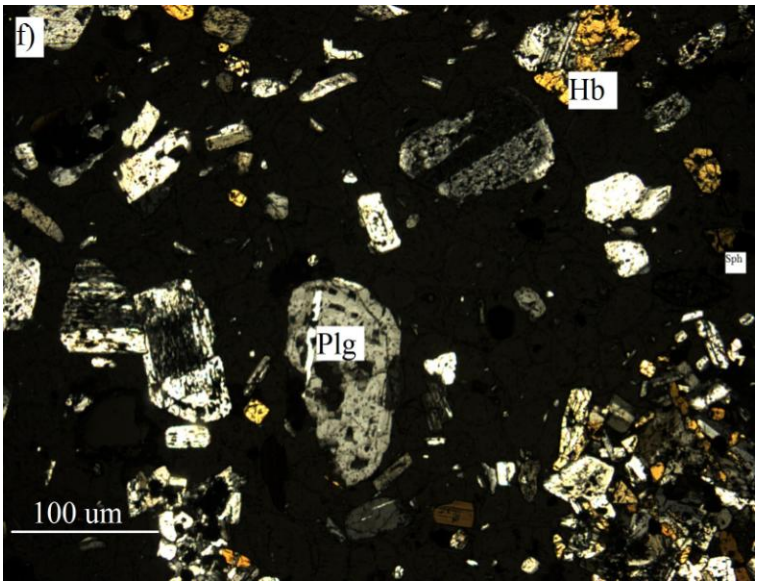

Figure 15f Polarized microphotographs of thin sections showing Totoral dome showing phenocrysts of plagioclase, quartz and hornblende in a devitrified groundmass

Table 5 Modal analyses for each individual ignimbrite, proportions are in volume percentage. Values are given after averaging four point counting. Al values were rounded up to 0

System	Guacha Ignimbrite				Tara Ignimbrite				Puripica Chico Ignimbrite		
Unit	Guacha	Guacha	Kalina dome	Guacha andesite	Tara	Tara	Río Guacha dome	Chajnantor dome	Puripica Chico	Totoral dome	Negreal
Juvenile type	pumice	pumice	lava	lava	pumice	pumice	Lava	Lava	pumice	lava	lava
Location	outflow	outflow	outer scarp collapse	resurgent dome	outflow	outflow	inner scarp collapse	inner scarp collapse	distal flow	outer scarp collapse	outer scarp collapse
Sample	B06-085	B06-030	A-04	A-13	BO6-013	BO6-027	BO6-023	BO6-024	BO6-073	A-19	A-01
Quartz	2	20	20	0	3	1	4	5	4	1	0
Biotie	3	13	12	0	2	1	5	1	6	5	0
K-feldspar	0	0	0	0	0	0	0	5	0	0	0
Plagioclase	9	9	21	25	4	14	18	2	38	28	23
Clinopyroxene	0	0	0	0	0	1	0	0	0	7	8
Ortopyroxene	0	0	0	6	0	0	2	0	0	0	0
Hornblende	2	2	0	0	0	2	2	0	0	0	0
Fe-Ti oxides	1	2	3	2	0	1	3	1	3	2	2
Sphene	0	0	0	0	0	0	0	0	0	0	0
Zircon	0	0	0	0	0	0	0	0	0	0	0
Percentage of crystal	16	46	56	32	9	19	34	13	51	42	33
Percentage of matrix	55	49	44	68	55	48	67	87	39	58	67
Percentage of vesicles	29	5	0	0	37	34	0	0	10	0	0
Percentage of crystals (vesicles free)	22.00	0.00	0.00	0.00	14.00	29.00	0.00	0.00	57.00	0	0

Table 6 XRF-ICP representative analyses for major and trace elements of the ignimbrites and lavas of the Cerro Guacha Caldera conducted at Washington State University Geo Analytical Laboratory

System	Guacha Ignimbrite Sytem			Tara Ignimbrite System				Puripica Chico Ignibrite System		
Unit	Guacha	Guacha	Kalina	Tara	Río Guacha	Chajnator lavas	Chajnantor	Puripica Chico	Totoral	Negreal
Clast ype	pumice	lava flow	lava dome	pumice	lava dome	lava dome	lava dome	pumice	lava dome	lava dome
Location	proximal outflow	resurgent dome	outer rim	distal outflow	inner rim	inner rim	inner scarp collapse	distal flow	outer rim	outer scarp collapse
Sample	BOL11	A-13	A-04	BOL15	B06-023	BOL21	B06-024	B06-073	009BOL	A-01
SiO2	66	61	66	66	66	64	77	67	65	62
TiO2	1	1	1	1	1	1	0	1	1	1
Al2O3	17	18	17	17	17	17	13	16	16	17
Fe2O3	4	5	4	4	4	5	1	4	5	6
MnO	0	0	0	0	0	0	0	0	0	0
MgO	2	3	1	2	2	2	0	2	2	3
CaO	4	7	4	3	5	5	1	4	4	5
Na2O	3	3	3	2	3	4	3	3	3	3
K2O	4	2	4	4	3	3	5	4	4	3
P2O5	0	0	0	0	0	0	0	0	0	0
Total	100	100	100	100	100	100	100	100	100	100
Ba	634	560	591	634	671	710	87	481	576	609
Cr	0	33	13	0	87	0	48	91	0	35
Ni	0	9	6	0	43	0	21	65	0	7
Rb	168	90	203	192	186	130	383	217	184	153
Sr	322	373	290	272	347	369	26	278	275	348
V	0	173	82	0	103	0	2	19	0	152
Y	20	29	19	18	29	28	46	20	24	20
Zn	0	88	85	0	103	0	29	0	0	120
Zr	156	198	185	172	288	316	67	138	211	260
Nb	12	13	15	12	17	16	27	14	18	14
Th	19	11	21	16	16	14	30	23	21	25
U	5	2	7	5	5	4	17	8	6	4
Pb	8	12	24	16	23	27	27	10	22	18

Continuation of **Table 6**

System	Guacha Ignimbrite Sytem			Tara Ignimbrite System				Puripica Chico Ignibrite System		
Unit	Guacha	Guacha	Kalina	Tara	Río Guacha	Chajnator lavas	Chajnantor	Puripica Chico	Totoral	Negreal
Clast ype	pumice	lava flow	lava dome	pumice	lava dome	lava dome	lava dome	pumice	lava	lava
Location	proximal outflow	resurgent dome	outer rim	distal outflow	inner rim	inner rim	inner rim	distal flow	outer rim	outer scarp collapse
Sample	BOL11	A-13	A-04	BOL15	B06-023	BOL21	B06-024	B06-073	009BOL	A-01
La	41	34	41	42	43	49	21	33	50	59
Ce	82	68	82	82	87	97	48	65	102	127
Pr	9	9	10	10	10	11	6	8	12	16
Nd	33	34	36	35	39	42	24	28	46	59
Sm	6	7	7	7	8	8	7	6	9	10
Eu	1	2	1	1	2	2	0	1	2	2
Gd	5	6	6	5	7	7	8	5	7	7
Tb	1	1	1	1	1	1	1	1	1	1
Dy	4	6	4	4	6	6	8	4	5	5
Ho	1	1	1	1	1	1	2	1	1	1
Er	2	3	2	2	3	3	4	2	2	2
Tm	0	0	0	0	0	0	1	0	0	0
Yb	2	2	1	2	3	2	4	2	2	1
Lu	0	0	0	0	0	0	1	0	0	0
Sc	12	18	8	11	13	14	5	9	10	12
Cu	0	12	4	0	5	0	1	67	0	7
Ga	0	20	21	0	20	0	17	20	0	21
Cs	15	5	15	10	26	13	34	15	12	4
Hf	5	5	5	5	8	8	3	4	6	7
Ta	1	1	1	1	2	1	4	2	2	1

5.3 General geochemical characteristics of the Cerro Guacha system

Samples of pumices from the Guacha Ignimbrite Stage (GIS) range from dacites (65 wt% SiO_2) to rhyolites (71.0 wt% SiO_2); for the Tara Ignimbrite Stage (TIS) range from andesites (62.0 wt% SiO_2) to high silica rhyolites (77.0 wt % SiO_2); and the Puripica Chico Totoral Stage (PTS) pumices are dacites (67.0 wt% SiO_2) (Fig. 16a). Three andesitic compositions have been found for each stage: for the GIS, the Guacha andesite (sample A-3, 61.0 wt %SiO_2); for the TIS, an andesitic pumice (sample tara-96-h29a, 61.0 wt% SiO_2) and for the PTS, the Negreal andesite (sample A-01, 62.18 wt% SiO_2, no ICP analysis available)

Harker diagrams for major oxides against SiO_2 show normal trends of differentiation. Least evolved primitive member are the andesites, showing the highest TiO_2, Fe_2O_3, Al_2O_3, MgO and CaO along with the lowest K_2O contents (Fig.16a-f). However, there are some differences between the andesites; the Guacha andesite shows rather lower P_2O_5 values compared to the other andesites of the system. The more evolved end member is the high-silica Chajnantor dome (77.0 SiO_2) showing low TiO_2, Fe_2O_3, Al_2O_3, MgO, CaO, P_2O_5 and higher K_2O (Figs 16 a-f).

Figure 16 Harker diagrams for major oxides (a-f) and trace elements (g-k) against SiO_2; g) Eu_N/Eu^* vs. Ba. Eu* expressed as the geometric mean of Sm and Gd $(Sm_N * Gd_N)^{0.5}$. Sm and Gd values taken from CI chondrite of Anders and Grevesse, 1989;j-k) Rb vs. Sr and Sr vs. Ba showing mineral vectors for plagioclase (pl), K-feldspar (Kf), hornblende (Hb) and biotite (Bt) (vectors taken from Fathy et al., 2008)

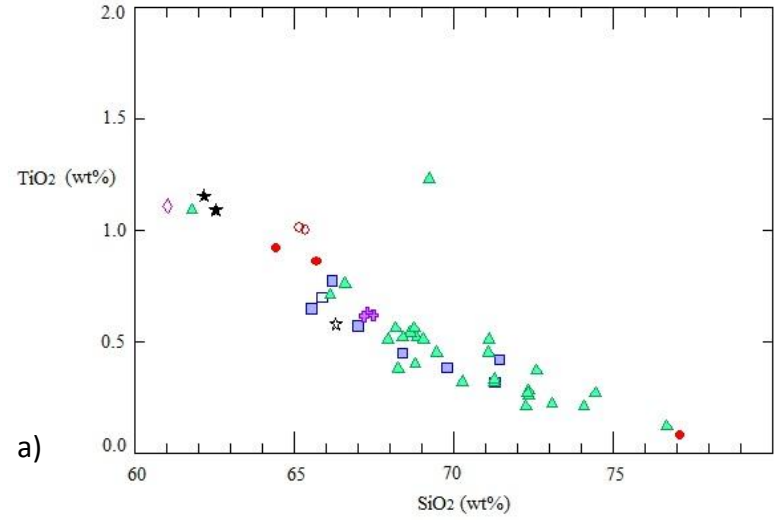
2.0
1.5
1.0
0.5
0.0
TiO2 (wt%)
60
65
70
75
SiO2 (wt%)

a)

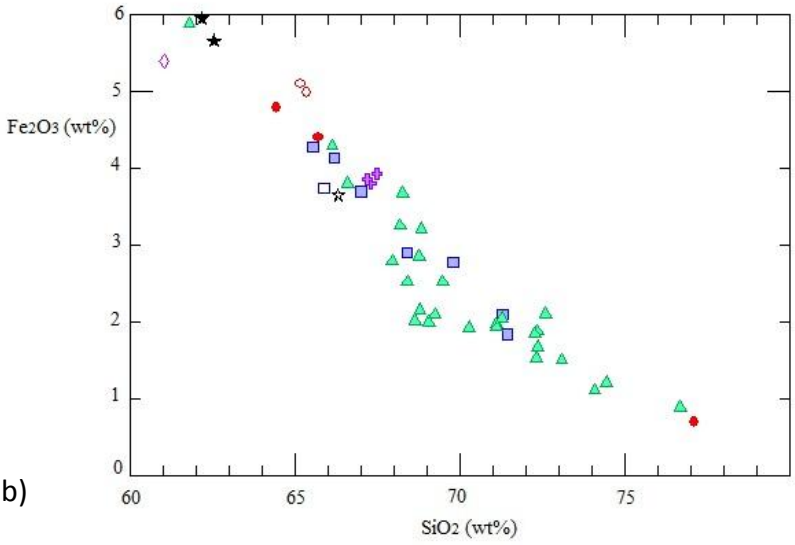
6
5
4
3
2
1
0
Fe2O3 (wt%)
60
65
70
75
SiO2 (wt%)

b)

c)

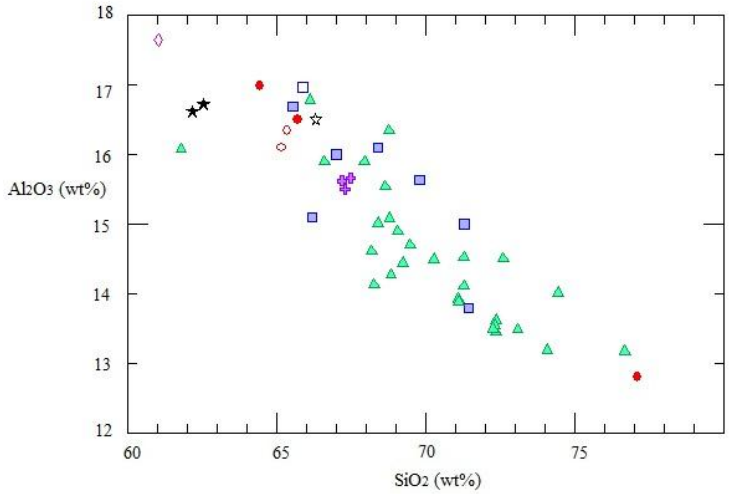
18
17
16
15
14
13
12
Al2O3 (wt%)
60
65
70
75
SiO2 (wt%)

d)

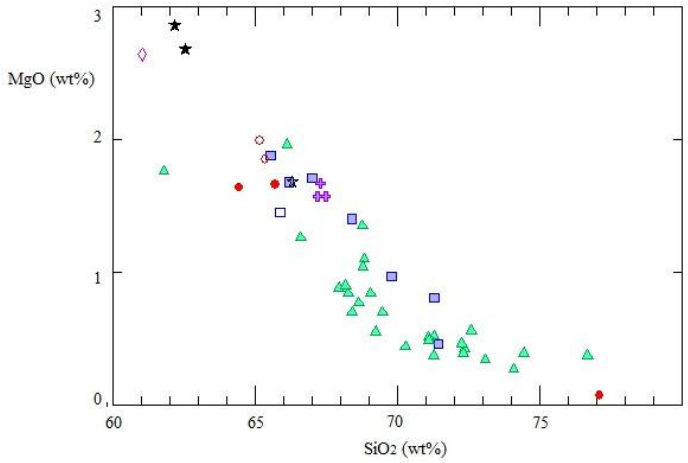
3
2
1
0
MgO (wt%)
60
65
70
75
SiO2 (wt%)

e)

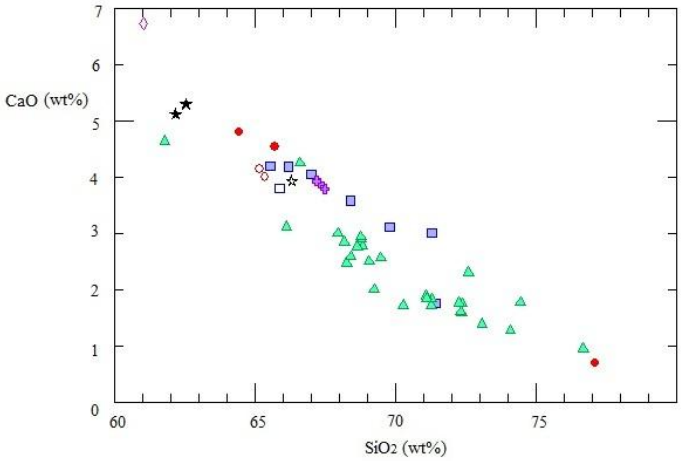
7
6
5
4
3
2
1
0
CaO (wt%)
60
65
70
75
SiO2 (wt%)

f)

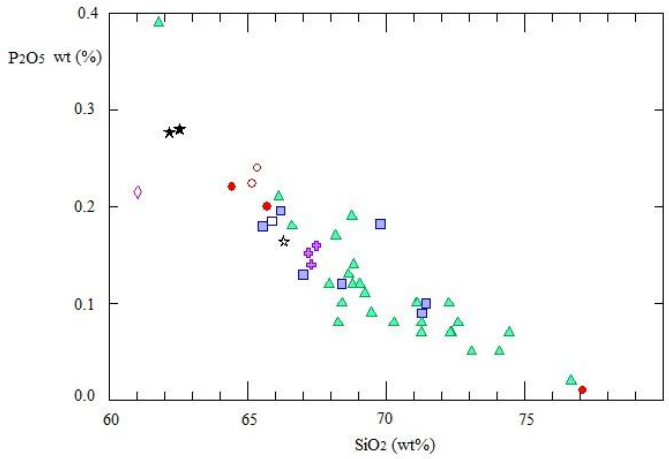
P2O5 wt (%)
0.4
0.3
0.2
0.1
0.0
60
65
70
75
SiO2 (wt%)

g)

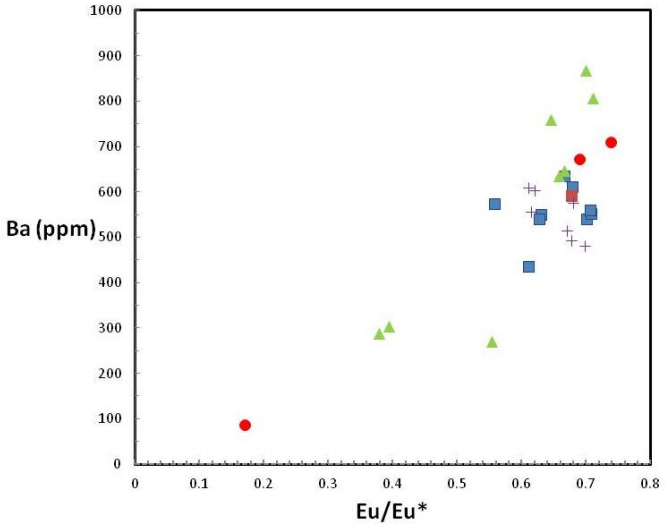
Ba (ppm)
1000
900
800
700
600
500
400
300
200
100
0
0
0.1
0.2
0.3
0.4
0.5
0.6
0.7
0.8
Eu/Eu*

h)

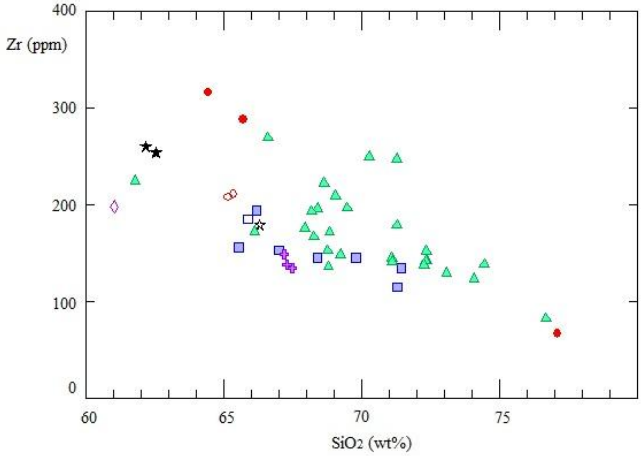
Zr (ppm)
400
300
200
100
0
60
65
70
75
SiO2 (wt%)

i)

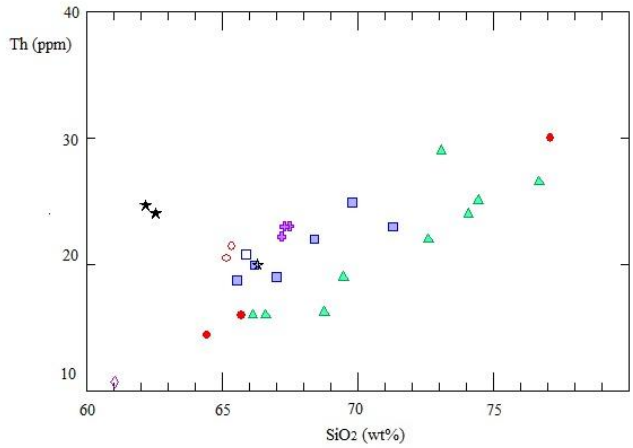
Th (ppm)
40
30
20
10
60
65
70
75
SiO2 (wt%)

j)

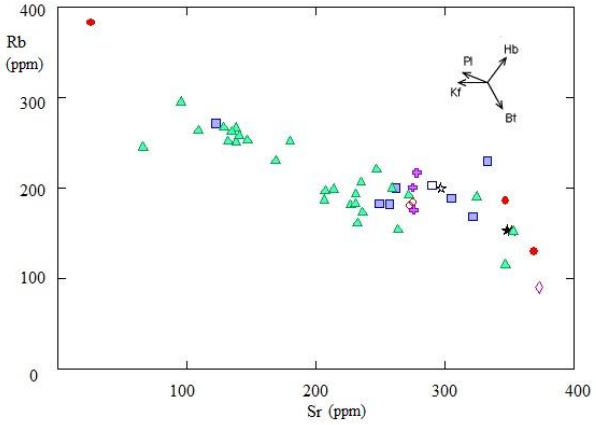
Rb
(ppm)
400
300
200
100
0
100
200
300
400
Sr (ppm)
Pl
Hb
Kf
Bt

k)

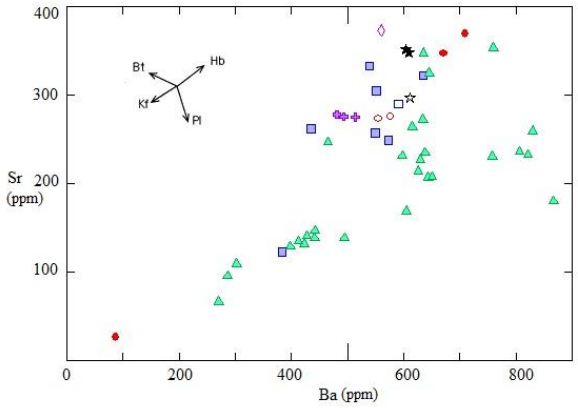
Sr
(ppm)
400
300
200
100
0
200
400
600
800
Ba (ppm)
Bt
Hb
Kf
Pl

Eu anomaly is mainly produced by fractionation of plagioclase and this is reflected by the negative value yielded in the REE rock/chondrite diagrams (Figure 18). A way to estimate the whole rock original Eu content is by calculating the Eu^* value, which is the geometric mean of the two adjacent elements between Eu, Sm and Gd. The magnitude of Eu negative anomaly observed is obtained using the following formula:

$$\frac{Eu}{Eu^*} = \frac{Eu_N}{\frac{1}{2}(Sm_N * Gd_N)}$$

where Eu_N is the ratio obtained dividing the Eu content (in ppm) from the whole rock by the Eu content (in ppm) from the Orgueil CI chondrite of Anders and Gravesse, (1989); the Sm_N was obtained dividing Sm content (in ppm) of the whole rock by the Sm content (in ppm) also from the same Orgueil CI chondrite and the Gd_N was obtained dividing Gd content (in ppm) of the whole rock by the Gd content (in ppm) also from the same Orgueil CI chondrite. Lowest values reflect higher Eu negative anomaly implying highest plagioclase fractionation.

Trace elements diagram for Ba vs. Eu_N /Eu* (Fig. 16g) show high Ba (>700 ppm) for Tara pumices outflows, suggesting sanidine accumulations; smallest Eu_N /Eu* corresponds to Chajnantor (most negative Eu anomaly, see Fig 17b) suggesting high plagioclase fractionation for this dome.

Zirconium decreases as a function of SiO_2 (as does Hf), and is higher in the Rio Guacha and Chajnantor Lavas domes (Fig. 16h), although it is relatively high in the andesites, as mafic magmas are able to bear higher amounts of Zr before saturation (Hatchar & Harrison, 2001). Chajnantor dome shows the lowest whole rock Zr contents (67 ppm) and glass (53 ppm) (Grocke et al., 2012), which is reflected in the fact that negligible zircon was found in it.

Thorium behaves incompatibly and shows the lowest values for the Guacha andesite (10.7ppm) and getting enriched towards the Chajnantor dome (30 ppm) (Fig. 16 j). High partition coefficients of Th in allanite (up to 548, Mahood & Hildreth, 1983) suggests the fractionation of this mineral in this dome magma.

Rubidium vs. Strontium (Fig. 16j) with mineral vectors shows that decrease in Sr and increase in Rb is associated to plagioclase fractionation. On the other hand, Sr vs Ba (Fig 16k), displays decreases in Ba and decreases in Sr associated with K-feldspar crystallization

Rayleigh Crystal Fractionation calculations were used to model Ba, Rb and Sr contents to show how much crystal fractionation is needed to get from the Guacha andesite (C_o) to the high silica Chajnantor dome (C_L); using a mineral assemblage of quartz + biotite + plagioclase + k-feldspar + hornblende (proportions of crystal removed shown in Table 7). The bulk partition coefficients D's values for Ba ranges between 2.8 to 2.9 for high silica rhyolite and dacite pumices respectively; D's values for Rb ranges between 0.37 to 1.0 for high silica rhyolite and dacite pumices respectively and D's values for Sr ranges between 2.9 to 3.84 0 for high silica rhyolite and dacite pumices respectively. (D's) were calculated using database from GERM (Geochemical Earth Reference Model) homepage: http://earthref.org/KDD/.

Rayleigh Crystal Fractionation $C_L/C_o = F^{(D-1)}$, considers C_o as the concentration of the element in the original magma, C_L as the concentration of the element in the residual liquid, D's as the bulk partition coefficient and *F* as the fraction of melt remaining

Theoretical values of C_L for Ba, Rb and Sr were calculated using the Rayleigh equation with 10% tic increase in *F* from 100 to 10%. C_L values for these elements correspond to crystallization fractions of 67, 59 and 68% respectively. Ratios of C_L^{Ba}/ C_o^{Rb} and C_L^{Sr}/ C_o^{Rb} were then plotted on Ba/Rb and Sr/Rb diagram (Fig. 17). Straight line representing amount of crystal fractionation is a power function instead of linear function, because of x and y axis are in logarithmic scale. This diagram shows that at least 60% of crystal fractionation of plagioclase, biotite and hornblende accounts for the compositional range from the Guacha andesite to the high silica Chajnantor dome.

Modal assemblage vol % (from pumices in CGS)

	quartz	biotite	k-felspar	plagioclase	clinopyroxene	orthopyroxene	hornblende
high Si rhyolite	73	3	19	4	0	0	0
dacite	33	18	5	30	2		10
andesite	1	1	5	64	16	2	5

KD's values (high-Si rhyo)

	quartz	biotite	k-felspar	plagioclase	clinopyroxene	orthopyroxene	hornblende
Ba		5.35	11.8	13.25			2.39
Rb		9.6	0.415	0.235			0.0335
Sr		7.2	12.1	11.8			7.735

KD's values (dacite)

	quartz	biotite	k-felspar	plagioclase	clinopyroxene	orthopyroxene	hornblende
Ba		13.9		1.05			0.28
Rb		5.27		0.24			0.18
Sr		0.31		10.7			0.6

Bulk D's

	high Si rhyolite	CHIC-96h-3A (dac pum)
Ba	2.9325	2.845
Rb	0.37625	1.0386
Sr	2.987	3.3258

Trace elements (ppm)

	Ba	Rb	Sr
high-Si rhyo	90	380	20
dacite	465	220	247
andesite	560	90	373

Table 7 Rayleigh Crystal fractionation parameters for Ba, Sr and Rb showing modal assemblages, partition coefficients (KD's) and bulk partition coefficients (D's) for high silica rhyolites and andesites.

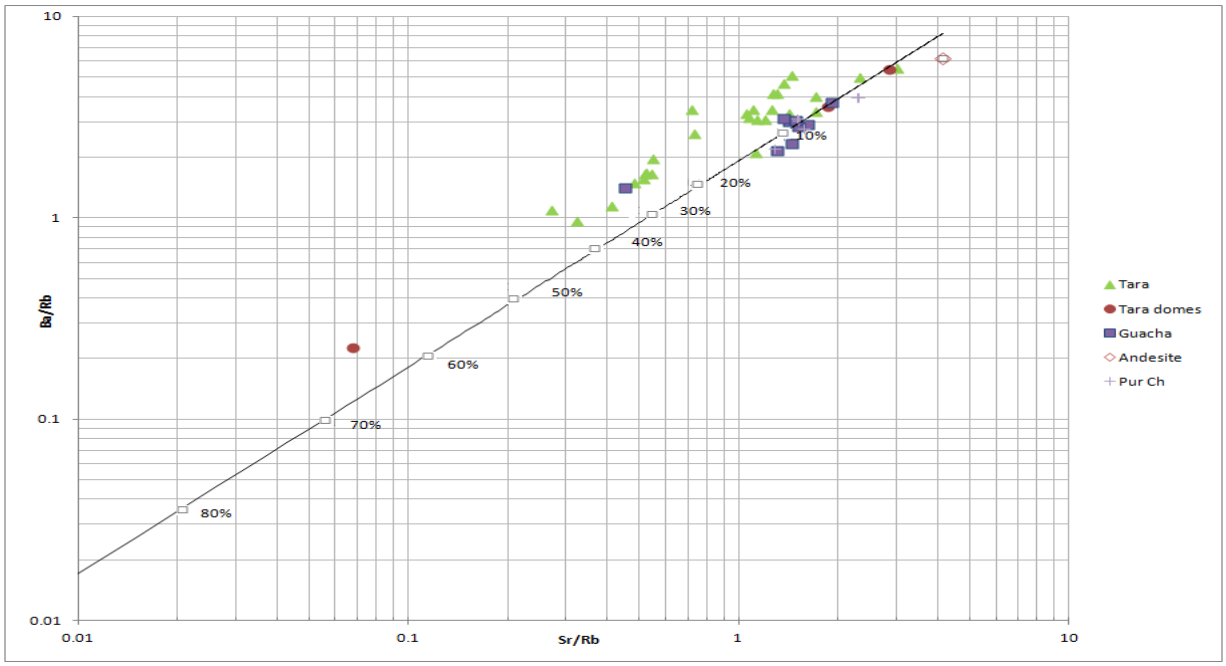

Figure 17 Amount of crystal fractionation calculated using Rayleigh equation. Straight line representing amount of crystal fractionation is a power function instead of linear function, because of x and y axis are in logarithmic scale. Model shows that at least 60% of crystal fractionation is needed to generate the high silica Chajnantor dome (filled circle) from the Guacha andesite (empty diamond)

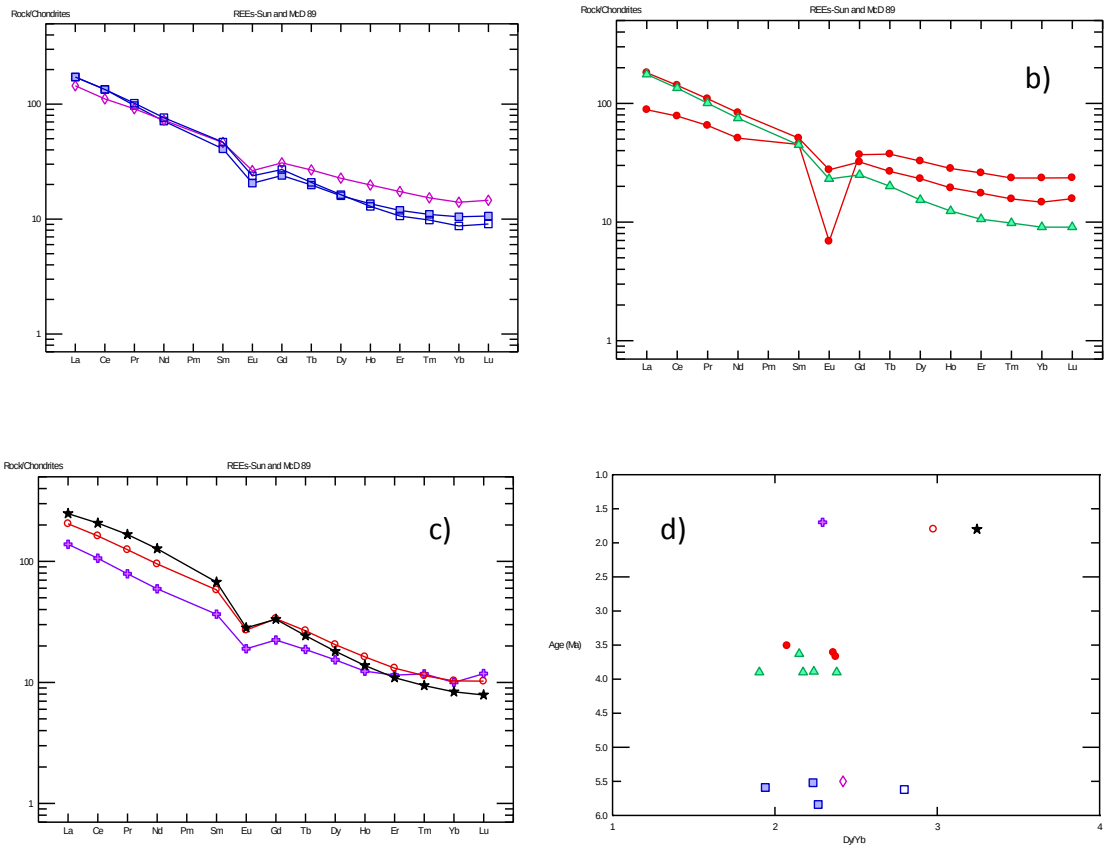

Figure 18 Rock/chondrite REE diagrams for a) the Guacha Ignimbrite Stage showing representative pumice (filled square), Kalina lava dome (empty square) and the Guacha Andesite (empty diamond); b) Tara Ignimbrite Stage showing representative pumice (filled triangle), Rio Guacha and Chajnantor post collapse lava domes (filled circle), large Eu anomaly corresponds to Chajnantor lava dome; c) Puripica Chico Stage showing representative pumice (filled "crux"), Totoral dome (empty circle) and Negreal Andesite (filled star); d) Dy/Yb ratios vs. time displaying values for andesites, ignimbrites and lava domes of the three stages of the caldera. Dy/Yb ratios increases with time as a signal related to increased garnet fractionation during mafic differentiation (Mamani et al., 2010; Walker 2011, Grunder A., pers. comm.)

Rock/Chondrites REE's element diagrams of Sun and Mc Donough (1989) are shown for the three different stages of the Cerro Guacha Caldera (Figs. 18 a-c) and Dy/Yb ratios against time are showed for the three caldera stages as well (Fig. 18d). For the GIS representative pumice, the Kalina post collapse lava dome and the Guacha andesite are plotting together (Fig 19a). The slope on a REE diagram can easily be approximated by the ratio of normalized concentration of an element on the left or Light Rare Earth Elements (LREEs) , such as La, divided by one on the right or Heavy Rare Earth Elements (HREEs) such as Yb (Winter, 2001). La/Yb ratios range from 20-30 for the pumices of the Guacha Ignimbrite and 13 for the Guacha andesite (Fig. 18a). For the TIS (Fig.18b), La/Yb ratios range from 10 to 32 for the pumices, 18-20 for the Rio Guacha and Chajnantor Lavas domes and 15 for the Chajnantor dome. Notable is the high Eu anomaly of the Chajnantor dome, associated with strong plagioclase fractionation (compare with Fig. 16h). La/Yb ratios for the PTS range between 18-21 for the pumices, 27 for the Totoral dome and 40 for the Negreal andesite (the highest values of the entire system).

Figure 18d shows Dy/Hb ratio against time for the three representative ignimbrites stages of the caldera. Ratios displaying middle REE (MREEs) such as Dy over Heavy REEs (HREEs) such as Yb were used by several authors to correlate crustal thickness and REE fractionation (Hildrteh and Moorbath, 1988; Davidson et al., 1991; Mc Millan et al., 1993; Kay et al., 1999; Haschke et al., 2002; Mamani, 2010, Walker, 2011, Grunder A. pers. comm.). Mamani and others (2010) showed that central Andean rocks have had elevated MREE/HREE (Dy/Sm and Sm/Yb) ratios since 30 Ma, corresponding to stabilization of garnet owing to crustal thickening (Walker, 2011). The model shown here for the CGC agrees with this overall systematic, and suggests establishment of consecutive magma chambers during the Guacha Ignimbrite Stage (5.65 Ma), again during the Tara Ignimbrite Stage (3.49 Ma) and finally during the Puripica Chico Ignimbrite (1.7 Ma) that modified the crust yielding to garnet stabilization. This process is represented by the slight increase in the Dy/Yb ratio (Fig. 18 d) for the Guacha (2.4) to the Negreal andesites (3.2). However further studies on andesites of the same age are need to prove this model and its application to the magmas of the APVC.

5.4 Intensive Parameters

5.4.1 Fe-Ti oxides

Samples of pumices of Tara ignimbrite were analyzed by Lindsay, (1999) in her study of La Pacana Caldera. Fe-Ti exchange reaction temperatures and oxygen fugacity were calculated following the methods of Andersen & Lindsley (1985) and Giorso & Evans 2008 and are shown in table 8. Two oxide geothermometers estimate temperature and fO_2 based in the reaction $FeTiO_3 + Fe_3O4 = Fe_2TiO_4 + Fe_2O_3$. Calculated values for the Tara Ignimbrite range from714˚ to 754˚C (Giorso and Evans, 2008) and from 783˚ to 801˚C (Andersen and Lindsley, 1985). Major oxides, recalculated values, temperatures and oxygen fugacity are shown in Table 8

Table 8 Fe-Ti oxide compositions and calculation of equilibration temperature

Sample	tara-96h-23		tara-96h-23	
crystal	1	1	1	2
mineral	magnetite	ilmenite	magnetite	ilmenite
comment	core	core	rim	rim
SiO2	0	0.02	0	0
TiO2	6.52	43.83	5.78	44.19
Al2O3	1.89	0	1.42	0
FeO	34.84	35.89	34.21	36.47
Fe2O3	51.04	14.42	53.4	13.7
MnO	0.6	2.04	0.66	1.9
MgO	0.28	0.82	0.26	0.75
CaO	0	0	0	0
Na2O	0	0	0	0
K2O	0	0	0	0
subtotal	95.17	97.02	95.73	97.01
Recalculation of Fe_{tot} using method of Stormer, 1983				
Fe2O3	50.9	14.1	53.3	13.6
FeO	34.9	35.9	34.3	36.5
Total	95.1	96.8	95.7	97
Mol % Usp	20.79		17.94	
Mol % Ilm		85.54		86.13
Calculated following Andersen & Lindsley , 1985				
T °C		801		783
log fO2		-13.06		-13.38
Calculated following Giorso & Evans, 2008				
T °C (Fe-Ti exchange)		754		714
log_{10} fO2 (NNO)		0.63		0.67

5.4.2 Amphibole Geobarometry

Amphiboles that correspond to the Guacha and Tara Ignimbrites were analyzed by Lindsay, (1999) and were used here to calculate physical-chemical conditions of crystallization of this mineral, using the AMP-TB. xls spreadsheet of Ridolfi et al., (2010). Calculated depths and oxygen fugacities for ΔNNO buffer are also shown in Table 9. Temperatures for the Tara ignimbrite yielded core-rim values of 873˚ to 905˚C; pressures range from 149 to 182 MPa equivalent to 5.3 and 6.4 km depth respectively. Temperature values for the Guacha Ignimbrite range between 835˚ to 901˚C; pressures ranges between 133 to 242 MPa, which is equivalent to 5.0 to 9.2 km depth.

5.5 Zircon Saturation

Zircon saturation temperature calculated using the algorithm of Watson & Harrison, 1983 was used to estimated temperature of which magmatic melts saturated and precipitated zircon for a giving M parameter (Na+K+2Ca)/(Al*Si). M and Zr values were used from matrix analyses of Tara pumice and the Chajnantor dome (sample L1 and B06-024 respectively) done by Grocke et al., (2012) and from matrix analysis of Guacha pumices (sample tara-96h-1) done by Lindsay et al., (1999). To calculate the $D^{zircon/melt}$ value, a ZrO_2 % in zircon value of 66.6 (for a calc-alkaline tonalite, Thomas et al., 2002), was used and then transformed to ppm.

These values are displayed in table 10and plotted in Fig. 20. Fe-Ti exchange temperature for the Tara Ignimbrite and Atana (Lindsay et a., 1995) were calculated using methods of Andersen and Lindsley, (1985) and Giorso and Evans (2008) (Table 9)

Table 9 Zr saturation temperatures using Zr (ppm) and M values calculated matrix analyzes done by Grocke et al., 2012 and Lindsay, 1999. Fe-Ti exchange temperature calculated using methods of Andersen and Lindsley, 1985 and Giorso and Evans, 2008 is also shown.

Unit	Zr (ppm)	zircon saturation T (˚C)	Fe-Ti exchange Temp	M
Guacha Ignimbrite	62	716	801-714	1.32
Tara Ignimbrite (L1)	130	784		1.20
Chajnantor dome (B06-013)	53	703		1.33
Atana (crystal rich) Ignimbrite	70	728	808-758	1.28

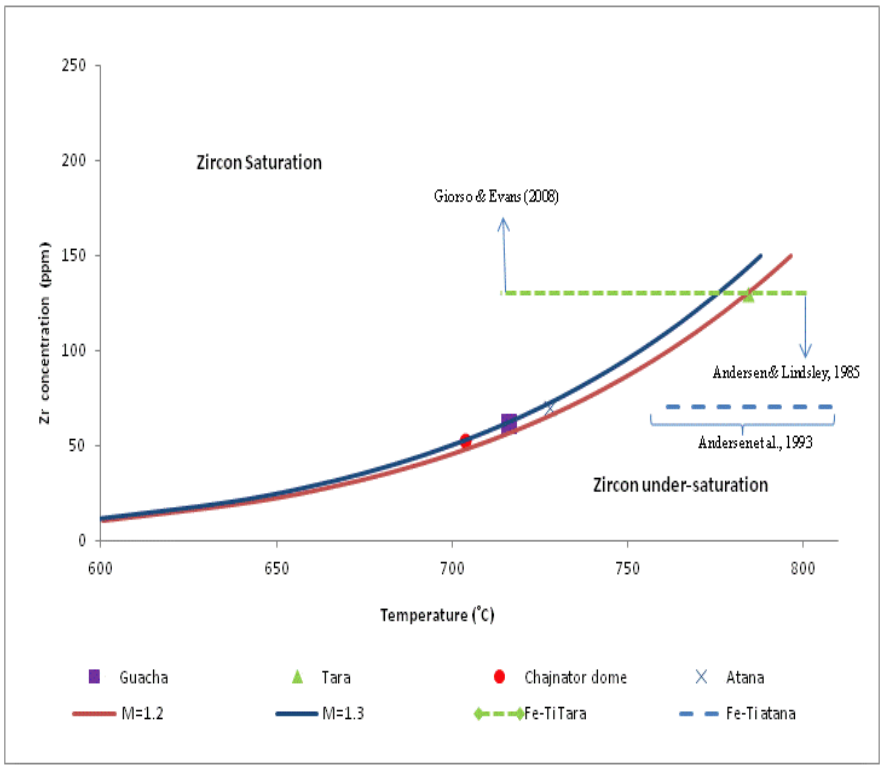

Figure 19 Zircon saturation temperature from Watson & Harrison, (1983). Temperature range showed for the Tara Ignimbrite was obtained using methods of Andersen and Lindsley, (1985) and Ghiorso and Evans, (2008), Table 8.

Fig. 19 shows zircon saturation temperatures for the Guacha Ignimbrite (sample tara 96h-1), the Tara Ignimbrite (sample L1), the Chajnantor dome (B06-013) and the Atana Ignimbrite from the La Pacana Caldera (lari-96h-5). The range of temperatures calculated for the Tara ignimbrite corresponds to the maximum and minimum temperatures obtained in Table 8. The Chajnantor dome, Guacha and Atana Ignimbrites have almost similar M values of 1.33, 1.32 and 1.28 respectively, meanwhile the Tara ignimbrite reported a lower M value (1.2). Zirconium content in the glass is high for the Tara ignimbrite (130 ppm) and rather low for the Chajnantor dome, the Guacha and the Atana Ignimbrites (53, 62 and 70 ppm respetively). Watson and Harrison, (1983) suggested that for an average peraluminous granite with M = 1.3, zircon solubilities are low and ranges from ~100 ppm of dissolved Zr at 750˚ C to 1200 ppm at 1020˚C, showing that the M value and temperature controls the solubility of zircon in the melt, and that higher Zr concentration saturates the melt at higher temperatures. They also show that the $D^{zircon/melt}$ value is temperature and M value dependent (Fig. 2 in Watson & Harrison, 1983) implying that at higher temperatures Zr will preferentially be dissolved in the melt rather than in zircon crystals. Fig. 19 shows that Tara Ignimbrite is oversaturated in Zr and saturates in zircon at higher temperatures than the Guacha or the Atana Ignimbrites.

	tara-97h-13	tara-97h-13	tara-97h-13	tara-97h-13	poq-97h-7	poq-97h-7	poq-97h-7	poq-97h-7	poq-97h-7	poq-97h-7
	4	4	5	6	1	1	2	2	4	4
	amphibole	amphibole	amphibole	amphibole	amphibole	amphibole	amphibole	amphibole	amphibole	amphibole
oxide (wt%)	core	rim	core	Rim	core	rim	core	rim	core	rim
SiO_2	46.18	44.95	45.4	45.57	46.86	45.67	44.38	46.35	44.97	44.2
TiO_2	1.76	2.16	1.93	2.07	1.19	1.29	2.62	1.98	2.04	2.07
Al_2O_3	8.59	9.34	8.54	8.97	7.94	8.67	10.44	8.84	10.02	10.2
FeO	15.59	14.09	16.66	14.41	16.94	15.06	14.44	15.74	13.9	
MnO	0.37	0.31	0.47	0.32	0.59	0.6	0.39	0.32	0.3	0.37
MgO	14.4	14.63	13.47	14.97	12.72	12.34	12.81	13.85	13.97	13.28
CaO	10.98	11.14	10.99	11.4	11.72	11.76	11.56	11.69	11.58	11.4
Na_2O	1.65	1.81	1.61	1.78	1.23	1.31	1.77	1.53	1.8	1.8
K_2O	0.67	0.8	0.68	0.74	0.75	0.93	0.77	0.74	0.7	0.64
F										
Cl										
Physical-Chemical Conditions										
T °C	873	897	881	905	818.6	843.7	901.1	856.6	893.1	896
uncertanty (σ_{est})	22	22	22	22	22	22	22	22	22	22
P (Mpa)	149	182	151	163	133.5	160.7	242.8	162.3	220.2	236.5
uncertanty (Max er	16	20	17	18	14.7	17.7	26.7	17.9	24.2	26
continental depth (I	5.3	6.4	5.3	5.8	5	6.1	9.2	6.1	8.3	8.9
ΔNNO	1.6	1.4	1.4	1.7	1	0.9	0.6	1.1	1	0.9
$logfO_2$	-10.7	-10.5	-10.8	-10.1	-12.4	-12.1	-11.3	-11.6	-11	-11.1
uncertanty (σ_{est})	0.4	0.4	0.4	0.4	0.4	0.4	0.4	0.4	0.4	0.4
H_2O_{melt} (wt.%)	4.7	4.2	5	4.4	5.2	5	5.5	4.9	5.3	5.8
uncertanty*	0.7	0.6	0.7	0.7	0.4	0.4	0.8	0.4	0.8	0.9

Table 10 Amphibole geobarometry and composition (data taken from from Lindsay, 1999)

5.5 Summary and interpretation of geochemistry

As a whole the three ignimbrites (Guacha, Tara and Puripica Chico) share the same petrological and geochemical characteristics of a high-K series, compositional ranges of pumices from dacite to rhyolites, with andesitic members present as lavas (for the Guacha and Puripica Chico Ignimbrites) and as pumices (for the Tara Ignimbrite). Highest silica content belongs to the Chajnantor dome (whole rock = 77 wt% SiO_2) , which also displays the lowest contents in Ba, Sr, P and Ti (Fig. 14c) which reflects high plagioclase fractionation.

Petrographic analysis distinguishes pumices with tubular or rounded vesicles. Vesicular pumices are usually dacitic. Vesicles in dacitic pumices reach up to 38% with felsic glasses ranges between 44 to 54 %, meanwhile rhyolite pumices vesicles reach up to 37% and glasses 54. 0%. Typical dacitic mineral assemblage is made of phenocrysts of plagioclase > quartz > biotite > hornblende > Fe-Ti oxides with minor sanidine and zircon. Rhyolite pumices exhibit phenocryst assemblage made of plagioclase > quartz > biotite > apatite > sanidine. Porphyritic Guacha andesite is made of finer phenocrysts of feldspar > pyroxene > orthopyroxene embedded in a microlithic matrix. Porphyritic Negreal andesite is made of phenocrysts of plagioclase > clinopyroxene > Fe-Ti oxides > amphibole in an aphanatic matrix of plagioclase and Fe-ti oxides.

Major oxides geochemistry shows highest TiO_2, Fe_2O_3, Al_2O_3, MgO and CaO along with the lowest K_2O contents for the andesites and lowest TiO_2, Fe_2O_3, Al_2O_3, MgO, CaO, P_2O_5 and higher K_2O (Figs 16 a-f) for the Chajnantor dome. Trace elements such as Zr behave compatibly with differentiation (Fig. 16i) meanwhile Th behaves incompatibly (Fig. 16j). Ba vs. Eu /Eu* (Fig. 16h) shows high Ba values (>700 ppm) for Tara pumices outflows, suggesting sanidine accumulations along with smallest Eu /Eu* values for Chajnantor dome suggesting high plagioclase fractionation for this dome. Rb vs. Sr and Sr vs. Ba (Figs. 16k and l) with mineral vectors show trends that suggest plagioclase and K-feldpar fractionations. Modeling Rayleigh fractionation for Ba, Rb and Sr suggests a fractionation of at least 60% of plagioclase, biotite and hornblende to account for the compositional variation between the Guacha andesite and the Chajnantor dome.

Fe-Ti exchange geothermometry for the Tara Ignimbrite yieds values ranging from 714˚ to 801˚C (Andersen and Lindsley, 1985; Giorso and Evans, 2008). Amphibole geobarometry following the Ridolfi et al, (2010) method yielded pressures ranging from 149 to 182 MPa equivalent to 5.3

and 6.4 km depth respectively for the Tara Ignimbrite; the pressures range between 133 to 242 MPa, equivalent to 5.0 to 9.2 km depth for the Guacha Ignimbrite.

Dy/Hb ratio increases with time from the Guacha andesite to the Negreal andesite (Fig. 18d) suggesting stabilization of garnet owing to crustal thickening (Hildreth and Moorbath, 1988; Kay et al., 1999; Haschke et al., 2002; Mamani, 2010, Walker, 2011). This implies that the crystal mushes were established first during the Guacha Ignimbrite Stage (5.65 Ma), secondly during the Tara Ignimbrite Stage (3.49 Ma) yielding to the modification in the Negreal andesite geochemical signature resulting in the high Dy/Hb ratio in the Negreal andesites

The zircon saturation method of Watson & Harrison (1983) yielded saturation temperatures of 716˚ and 705˚C for the Guacha and Chajnantor dome respectively and 784˚C for the Tara Ignimbrite indicating that it saturates zircon at higher temperatures than the Guacha Ignimbrite.

6.0 U-Pb Gechronology

$^{238}U/^{206}Pb$ ion microprobe data for 261 zircon crystals (30 separate interior and 231 rim analyses) analysed in this study are presented in table 11 and figure 20. In the following discussion Tera-Wasserburg diagrams ($^{207}U/^{206}Pb$ vs. $^{238}U/^{206}Pb$) are constructed for each ignimbrite with regression lines through the data points (Fig. 21-23). Concordia in these diagrams account for initial disequilibrium (^{230}Th deficit; Schmitt et al. 2003a) which requires a correction of approximately +100 ka for $^{206}Pb/^{238}U$ zircon ages. Probability density plots and histograms are shown in Figure 22-24 along with weighted mean zircon dates calculated with the Isoplot 3.0 software (Ludwig 2003). Eruption ages of the samples, where available, are shown based on $^{40}Ar/^{39}Ar$ analyses (Salisbury et al., 2010) and are shown in red in Figs. 21b-d and Figs.22 b-f.

In the following discussion, the terms autocryst, antecryst and xenolith are used. Xenocrysts are defined as those zircon crystal incorporated from the surrounding host rocks (Johnson, 1989). Antecryts refers to those zircon crystals that crystallized from an earlier pulse of magma and which are incorporated in a later pulse (Bacon and Lowenstern, 2005; Charlier et al., 2005 in Miller et al., 2010). Autocrysts are zircons that nucleate and grows directly from melt or inherited zircon crystal, also is referred as magmatic zircon (Miller et al., 2010). Autocrysts are defined here as those whose ages define the main area below the probability distribution line, some of them matching within error the Ar-Ar age. Crystal ages out of the main area are considered antecrysts.

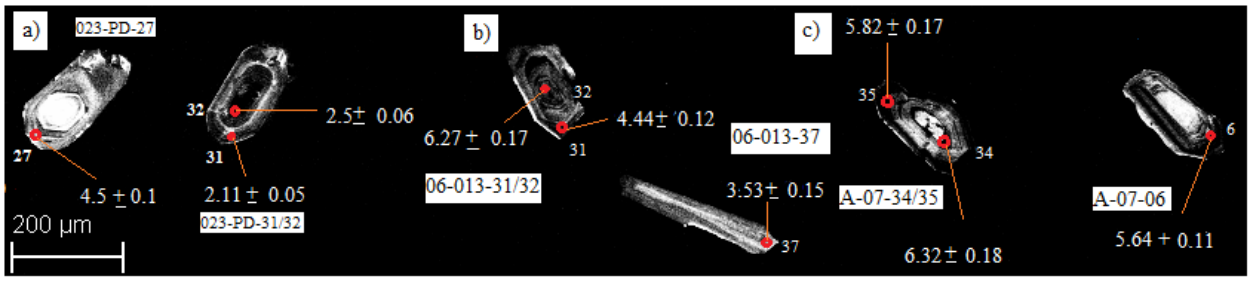

Figure 20 Ages and textures from zircons using cathodoluminescense imaging scanning Leo 1430 VP electron microscope . Spot on zircons are ^{238}U-^{206}Pb age determined using IMS 1270; numbers refers to grain analysed shown in table 9, scale bar is shown as reference. Errors in figures are ± 1 sigma a) Puripica Chico Ignimbrite pumice (sample 07BOL-023-PD); b) Tara Ignimbite (sample BOL-06-013); c) Guacha Ignimbrite pumice (sample A-07). Crystal core A-07-34 from the Guacha Ignimbrite yielded an U-Pb core age of 6.32 ±0.18 Ma, meanwhile its rims yielded 5.82±0.17; crystal rim A-07-06 yielded another younger age of 5.64 ±0.11 Ma, which overlaps with the Ar-Ar age estimated for this ignimbrite. Crystal core 06-013-32 from the Tara Ignimbrite yield an age of 6.27 ± 0.17 Ma, meanwhile its rim yielded 4.44±0.12 Ma; crystal rim 06-013-37 yielded a younger age of 3.53±0.15 Ma overlapping with Ar-Ar age for this ignimbrite. Crystal rim 023-PD-27 from the Puripica Chico Ignimbrite yield an older age of 4.5±0.1 Ma, showing clearly it is a xenocryst. Crystal core 023-PD-32 yielded an age of 2.5±0.06 Ma meanwhile the rim age is 2.11 ± 0.05 Ma. This age does not overlap with the Ar-Ar age (1.7± 0.08 Ma) estimated for this ignimbrite.

Table 11 SIMS U-Pb zircon results of the Cerro Guacha Caldera

Ignimbrite/dome $^{40}Ar/^{39}Ar$ age (Ma)	grain	rim core	238U/ 206Pb	238U/ 206Pb 1 s.e.	207Pb/ 206Pb	207Pb/ 206Pb 1 s.e.	Correlation of TW Concordia Ellipses	204Pb/ 206Pb	204Pb/ 206Pb 1 s.e.	% 206Pb*	206Pb/ 238U age [Ma]	206Pb/ 238U age [Ma] 1 s.e.	U ppm	U/ Th	UO/U
Guacha Ign	A-07-1	rim	1117.69	29.36	0.08	0.01	0.11	0.00	0.00	95.9	5.61	0.16	252	1.8	8.1
5.65 ± 0.01 Ma	A-07-2	core	1075.96	21.07	0.07	0.01	0.06	0.00	0.00	96.9	5.90	0.12	333	3.0	8.0
(sanidine)	A-07-3	rim	1043.95	31.50	0.09	0.01	0.13	0.00	0.00	94.0	5.89	0.20	222	3.2	8.0
	A-07-4	core	1044.06	28.12	0.07	0.01	-0.06	0.00	0.00	96.9	6.07	0.17	318	2.1	7.8
	A-07-06	rim	1091.46	20.25	0.09	0.00	0.01	0.00	0.00	94.1	5.64	0.11	844	2.0	8.0
	A-07-07	rim	956.94	21.70	0.09	0.01	0.10	0.00	0.00	94.5	6.44	0.16	243	1.9	7.8
	A-07-08	rim	1153.93	27.56	0.07	0.01	-0.10	0.00	0.00	96.4	5.47	0.14	331	2.2	8.1
	A-07-09	core	1090.99	28.92	0.06	0.00	-0.03	0.00	0.00	98.0	5.88	0.16	548	2.3	7.9
	A-07-10	rim	1066.21	26.83	0.07	0.01	0.14	0.00	0.00	96.7	5.93	0.16	549	2.1	7.7
	A-07-11	rim	1100.11	26.99	0.07	0.01	-0.09	0.01	0.00	96.8	5.76	0.16	355	2.2	8.1
	A-07-12	rim	1105.71	32.89	0.06	0.00	0.30	0.00	0.00	98.7	5.83	0.18	684	1.8	7.9
	A-07-13	rim	1006.44	26.03	0.07	0.01	0.17	0.00	0.00	96.4	6.26	0.17	408	3.0	7.8
	A-07-14	rim	1119.57	39.11	0.10	0.02	0.22	0.01	0.01	92.8	5.43	0.23	201	2.2	7.9
	A-07-15	rim	1048.11	35.48	0.07	0.01	-0.08	n.d.	n.d.	96.4	6.02	0.22	265	3.0	8.1
	A-07-16	rim	1104.00	31.08	0.08	0.01	-0.31	0.01	0.00	95.5	5.66	0.18	315	3.0	8.0
	A-07-17	rim	1068.83	22.05	0.07	0.01	0.02	n.d.	n.d.	97.6	5.97	0.13	414	3.3	8.0
	A-07-18	rim	1005.43	20.62	0.05	0.00	0.02	0.00	0.00	99.0	6.43	0.13	797	2.6	7.9
	A-07-19	rim	1042.75	33.38	0.05	0.01	0.45	0.01	0.00	99.0	6.21	0.20	440	2.9	7.7
	A-07-20	rim	1031.03	24.87	0.07	0.01	0.29	0.01	0.00	96.9	6.14	0.16	426	2.6	7.9
	A-07-21	rim	1005.03	27.58	0.08	0.01	0.20	0.00	0.00	95.6	6.22	0.18	289	2.3	7.9
	A-07-22	rim	1288.99	67.79	0.08	0.01	0.01	0.00	0.00	95.3	4.85	0.27	228	2.4	8.7
	A-07-23	rim	1258.18	185.21	0.06	0.00	0.12	0.00	0.00	98.2	5.12	0.76	589	2.8	8.4
	A-07-24	rim	1223.54	32.34	0.09	0.01	0.13	0.01	0.01	94.1	5.04	0.15	192	2.2	8.4
	A-07-25	rim	1038.10	40.74	0.12	0.02	-0.07	0.00	0.00	90.9	5.73	0.29	145	2.7	7.9
	A-07-26	rim	887.31	19.45	0.05	0.00	0.23	0.00	0.00	98.9	7.29	0.16	891	11.0	8.0
	A-07-27	rim	1120.32	24.98	0.06	0.01	0.46	0.00	0.00	98.7	5.77	0.14	666	2.3	8.1
	A-07-28	core	1051.41	33.83	0.09	0.01	-0.32	0.00	0.00	94.3	5.87	0.22	275	3.1	7.9

Table 11 (continuation)

Ignimbrite/dome $^{40}Ar/^{39}Ar$ age (Ma)	grain	rim core	238U/ 206Pb	238U/ 206Pb 1 s.e.	207Pb/ 206Pb	207Pb/ 206Pb 1 s.e.	Correlation of TW Concordia Ellipses	204Pb/ 206Pb	204Pb/ 206Pb 1 s.e.	% 206Pb*	206Pb/ 238U age [Ma]	206Pb/ 238U age [Ma] 1 s.e.	U ppm	U/ Th	UO/U
Tara Ign	06-013-1	core	1774.31	65.17	0.13	0.02	0.52	0.01	0.00	88.8	3.32	0.15	261	3.2	7.8
3.49 ± 0.01 Ma	06-013-2	core	1648.26	69.01	0.13	0.01	0.05	0.02	0.01	89.7	3.60	0.17	243	2.7	7.7
sanidine	06-013-3	core	1719.39	64.74	0.14	0.01	-0.02	0.03	0.01	87.5	3.36	0.15	331	1.8	7.8
	06-013-4	rim	1689.47	41.10	0.13	0.01	0.24	0.01	0.00	89.2	3.49	0.10	539	2.3	7.6
	06-013-5	rim	1546.07	38.48	0.11	0.01	0.15	0.01	0.00	91.7	3.90	0.11	542	1.8	7.5
	06-013-6	rim	1567.15	74.42	0.15	0.01	-0.06	0.02	0.01	87.2	3.66	0.21	237	1.7	7.7
	06-013-7	core	1719.10	36.94	0.08	0.00	0.16	0.00	0.00	95.2	3.67	0.08	1204	4.7	7.7
	06-013-8	rim	1610.05	47.44	0.09	0.01	-0.16	0.01	0.00	93.8	3.85	0.12	565	3.9	7.6
	06-013-9	core	1670.56	47.16	0.12	0.02	0.11	0.02	0.01	89.9	3.55	0.13	348	2.1	7.7
	06-013-10	rim	1543.45	48.12	0.15	0.01	0.26	0.02	0.01	87.1	3.71	0.15	236	1.7	7.7
	06-013-11	rim	1731.30	43.16	0.11	0.01	-0.08	0.01	0.00	92.4	3.53	0.10	473	2.6	7.7
	06-013-12	rim	646.83	14.48	0.55	0.01	0.03	0.04	0.01	35.2	3.59	0.30	398	2.4	7.6
	06-013-13	rim	1733.40	46.27	0.13	0.01	0.46	0.01	0.00	89.8	3.42	0.11	352	1.9	7.9
	06-013-14	rim	1692.05	54.97	0.12	0.01	-0.26	0.02	0.01	91.1	3.55	0.14	351	2.2	7.7
	06-013-15	rim	1625.22	81.35	0.15	0.02	-0.35	0.02	0.01	86.5	3.52	0.24	243	3.5	7.9
	06-013-16	rim	1693.48	49.33	0.11	0.01	0.15	0.00	0.00	91.4	3.57	0.12	374	2.7	7.7
	06-013-17	rim	1548.47	45.32	0.15	0.01	0.00	0.01	0.00	86.5	3.67	0.13	503	1.4	7.9
	06-013-18	rim	73.05	2.26	0.81	0.01	-0.03	0.05	0.00	2.4	2.19	3.96	246	1.5	7.8
	06-013-19	rim	1495.44	38.91	0.20	0.01	-0.08	0.02	0.01	80.5	3.56	0.13	354	3.4	7.7
	06-013-20	rim	1652.07	42.30	0.09	0.01	-0.23	0.01	0.00	94.0	3.76	0.11	507	3.5	7.7
	06-013-21	rim	1687.48	43.57	0.08	0.01	-0.39	0.01	0.00	95.2	3.73	0.10	423	2.9	7.8
	06-013-22	rim	1708.82	63.95	0.12	0.01	0.11	0.03	0.01	91.1	3.52	0.15	261	2.0	7.9
	06-013-23	rim	1774.31	48.80	0.09	0.01	0.48	0.01	0.00	94.4	3.50	0.10	476	1.4	7.8
	06-013-24	rim	1726.52	58.43	0.12	0.01	0.13	0.01	0.00	90.8	3.48	0.14	256	2.3	7.7
	06-013-25	core	1705.32	41.30	0.08	0.01	0.13	0.01	0.00	95.3	3.70	0.10	357	3.6	7.7
	06-013-26	rim	1731.90	55.79	0.10	0.01	0.69	0.00	0.00	93.7	3.57	0.13	320	2.5	7.8
	06-013-27	rim	1607.98	41.63	0.08	0.01	0.37	0.01	0.00	95.3	3.92	0.11	552	4.4	7.8
	06-013-28	rim	912.41	73.84	0.43	0.03	-0.24	0.04	0.01	50.7	3.67	0.75	280	4.3	8.0

Table 11 (continuation)

Ignimbrite/dome $^{40}Ar/^{39}Ar$ age (Ma)	grain	rim core	238U/ 206Pb	238U/ 206Pb 1 s.e.	207Pb/ 206Pb	207Pb/ 206Pb 1 s.e.	Correlation of TW Concordia Ellipses	204Pb/ 206Pb	204Pb/ 206Pb 1 s.e.	% 206Pb*	206Pb/ 238U age [Ma]	206Pb/ 238U age [Ma] 1 s.e.	U ppm	U/ Th	UO/U
Puripica Chico	023- PD-1	rim	2758.62	73.28	0.17	0.01	-0.27	0.01	0.00	83.6	2.04	0.07	1538	2.6	7.8
Ignimbrite	023- PD-2	rim	1394.70	89.09	0.51	0.02	0.04	0.04	0.00	40.6	1.96	0.35	1401	1.7	7.8
1.7 ± 0.02	023- PD-3	rim	3249.92	87.77	0.07	0.01	0.12	0.00	0.00	96.4	2.00	0.06	1300	2.7	7.8
(biotite)	023- PD-4	rim	3060.91	66.71	0.08	0.01	0.27	0.01	0.00	96.1	2.12	0.05	1177	3.2	8.0
	023- PD-5	rim	2961.21	77.34	0.08	0.01	-0.01	0.01	0.00	95.8	2.18	0.06	1055	2.9	8.1
	023- PD-6	rim	3563.79	95.76	0.08	0.01	0.04	0.00	0.00	95.0	1.81	0.05	1101	3.2	7.9
	023- PD-7	rim	3505.08	95.09	0.09	0.01	-0.24	0.01	0.00	94.2	1.83	0.06	768	3.7	7.8
	023- PD-8	core	3405.99	77.26	0.09	0.01	0.17	0.01	0.00	94.8	1.89	0.04	1199	3.1	7.8
	023- PD-9	rim	2311.60	60.92	0.13	0.02	-0.47	0.01	0.00	89.9	2.60	0.09	1147	4.0	7.8
	023- PD-10	rim	3245.70	86.49	0.10	0.01	0.11	0.00	0.00	92.9	1.94	0.06	1167	3.1	7.8
	023- PD-11	rim	3112.36	80.50	0.09	0.01	-0.03	0.00	0.00	93.8	2.04	0.06	662	4.4	8.0
	023- PD-12	rim	2992.22	76.91	0.07	0.01	-0.06	0.00	0.00	97.3	2.19	0.06	1286	3.2	7.9
	023- PD-13	rim	3572.70	90.12	0.07	0.01	0.07	0.00	0.00	96.8	1.84	0.05	1440	3.5	7.8
	023- PD-14	rim	2834.47	79.14	0.08	0.00	0.03	0.01	0.00	95.8	2.28	0.06	1645	4.6	7.8
	023- PD-15	core	2540.65	59.00	0.08	0.01	0.16	0.01	0.00	95.9	2.53	0.06	956	3.3	7.9
	023- PD-16	rim	572.41	13.96	0.73	0.02	0.10	0.04	0.01	12.6	1.52	0.41	405	4.5	7.9
	023- PD-17	rim	2572.68	76.78	0.27	0.01	0.09	0.03	0.01	72.0	1.90	0.09	911	3.1	7.8
	023- PD-18	rim	3163.56	89.07	0.08	0.01	0.05	0.00	0.00	95.1	2.03	0.06	737	3.1	7.8
	023- PD-19	rim	2933.41	63.76	0.07	0.00	0.14	0.00	0.00	97.2	2.23	0.05	1804	3.3	7.8
	023- PD-20	core	50.66	3.85	0.81	0.00	-0.01	0.05	0.00	1.9	2.57	13.65	1266	3.2	8.0
	023- PD-21	rim	2865.33	61.82	0.06	0.00	-0.07	0.00	0.00	98.2	2.29	0.05	1948	1.9	7.9
	023-PD-23	rim	3454.23	99.51	0.08	0.01	-0.17	0.01	0.00	95.7	1.87	0.06	978	2.4	7.8
	023-PD-24	rim	3159.56	84.65	0.07	0.01	0.02	0.01	0.00	96.8	2.07	0.06	1332	3.8	7.8
	023-PD-25	rim	2577.98	57.75	0.08	0.01	0.40	0.01	0.00	95.9	2.49	0.06	1057	3.3	8.0
	023-PD-26	rim	2961.21	78.04	0.08	0.01	-0.03	0.00	0.00	96.3	2.19	0.06	1212	3.4	7.8
	023-PD-27	rim	1416.23	31.49	0.06	0.01	-0.04	0.00	0.00	97.8	4.55	0.11	880	4.3	7.8
	023-PD-28	rim	3369.27	77.99	0.08	0.01	0.18	0.01	0.00	95.3	1.91	0.05	1198	2.3	7.8

6.2.1 Guacha Ignimbrite

Autocrysts ages range between 7.29 ± 0.16 (sample A-07-26) to 5.12 ± 0.76 Ma (rim of A-07-24), with error the later ones overlaps the 5.65 Ma Ar-Ar eruption age (on sanidine) measured by Salisbury et al., 2010. A weighted mean age of 6.01 ± 0.10 Ma (95% conf) (accounting for 50 individuals) was estimated, along with a MSWD (Mean Square of Weighted Deviates) of 3.9. A single older xenocryst (the only one in the entire caldera) yielded an age of 513±13 Ma.

A new U-Pb age estimated for the Kalina lava dome yield a weighted mean of 5.62 ± 0.06 Ma, with a MSWD = 0.79 measured over 24 single crystals. This age is younger than the Ar-Ar eruption age determined for the of the Guacha Ignimbrite, implying this unit postdates the collapse of the caldera (Figure 22b) Based on this, and its spatial relationship to the Guacha collapse scarp, the Kalina-Brajma massif is interpeted as Guacha post caldera volcanism. No antecrysts or xenocrysts were found.

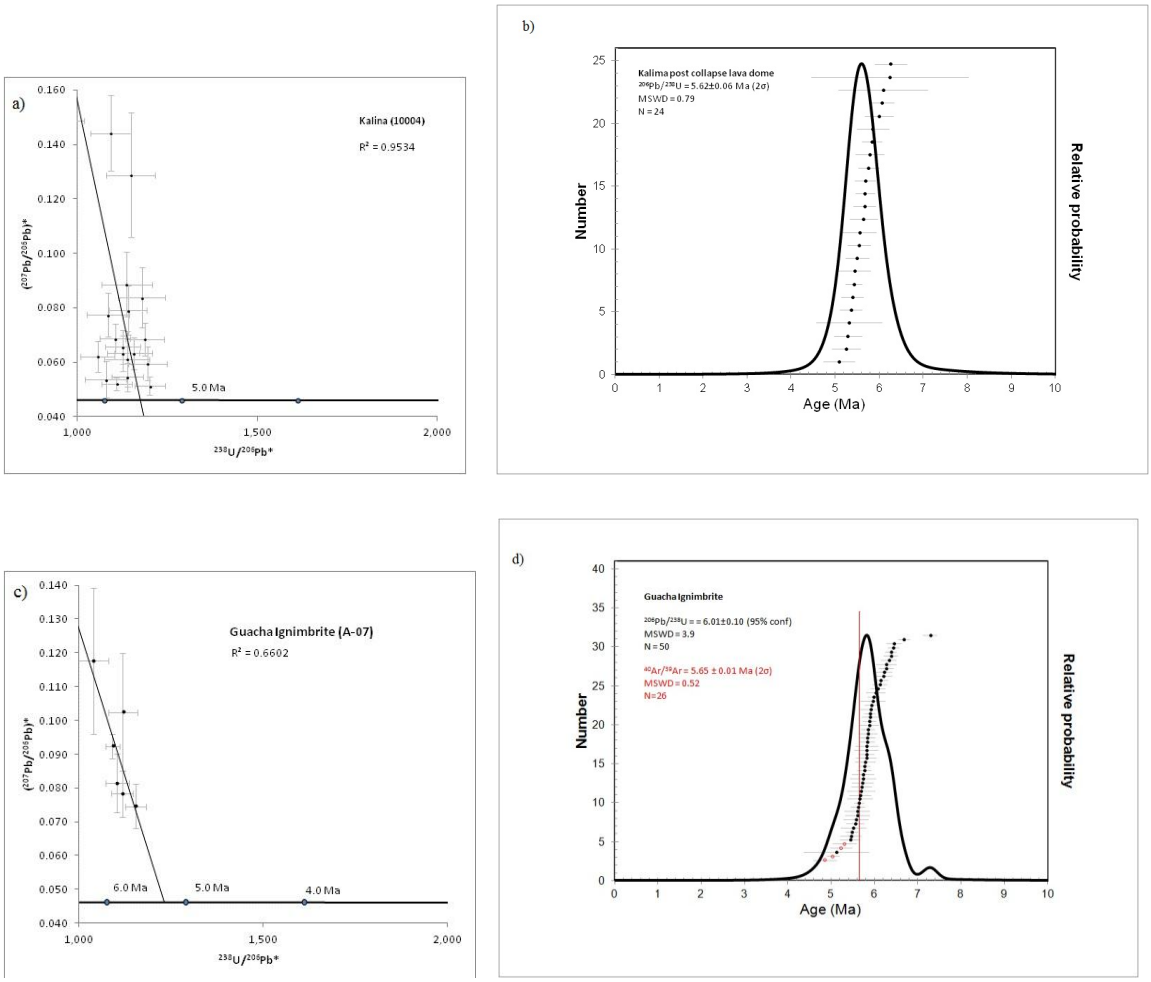

Figure 21 Probability density and Tera Wasserburg concordia plots for the Guacha Ignimbrite and Kalina lavas dome. Red line refers to Ar-Ar age obtained by Salisbury et al., 2010. Line on Tera Wasserburg diagram is obtained by regressing the discordant data points following the method of Baldwin and Ireland (1995) and used for other studies (Schmitt et al., 2003) and was used to obtained $^{207}Pb/^{206}Pb$ ratio (on y axis) which is a proxy (instead of $^{204}Pb/^{206}Pb$) for the common Pb correction. $^{238}U/^{206}Pb$ ages displayed on probability density plots were already corrected by common Pb using the obtained $^{207}Pb/^{206}Pb$ ratio

6.2.2 Tara Ignimbrite

Autocryst ages for the Tara ignimbrite range from 4.44 ± 0.12 to 3.34 ± 0.15 Ma, the latter overlapping within error of the 3.49 ± 0.09 Ar -Ar eruption age (Fig. 23 f). 3 out of 44 zircons report ages younger than the Ar-Ar age (grains 39, 33 and 1, see table 9), which can be interpreted as Pb lost. Estimated weighted U-Pb age yield 3.65 ± 0.06 Ma over 50 single crystals with a MSWD of 3.0. Only one antecryst observed presents a core with an age of 6.27 Ma and a rim that yielded 4.44 Ma (grain 31, Fig. 22). This core age, overlaps with the older autocrysts ages of to the Guacha ignimbrite.

Chajnantor Lavas dome exhibits a weighted U-Pb of 3.59 ± 0.05 Ma from over 25 grains, with a MSWD of 0.84 (Fig. 22b). A younger population of antecrysts yielded "Guacha Ignimbrite" ages of 5.74 and 5.42, meanwhile an older grain (7) yielded an age of 8.87 Ma . The Ar-Ar age for this dome (3.67 ± 0.13 Ma) was determined by Salisbury et al., 2010 using sanidine. As seen for the other units younger zircons overlap with the Ar-Ar age, suggesting that the U-Pb age for the youngest zircon (3.15 Ma ± 0.23 Ma), may be in the range of the eruption of this dome.The autocrysts from the Rio Guacha dome exibit a U-Pb age of 3.54 ±0.04 Ma (Fig. 22d) and a younger zircon yielded an age of 3.07 ± 0.25 Ma, which as in the case of the Chajnantor dome, can be also used as an estimation for the eruption date. An antecrysts population records also two groups of ages that ranging from 5.17 to 6.01 Ma and from 9.3 to 9.97 Ma respectively.

Figure 22 Probability plots and Tera Wasserburg concordia plots for the Tara Ignimbrite, Rio Guacha and Chajnantor Lavas domes. Symbol explanations as in Fig. 22. Straight red line referes to Ar-Ar age obtained from sanidine, meanwhile dashed red line referes to Ar-Ar obtained from biotite both from Salisbury et al., (2010)

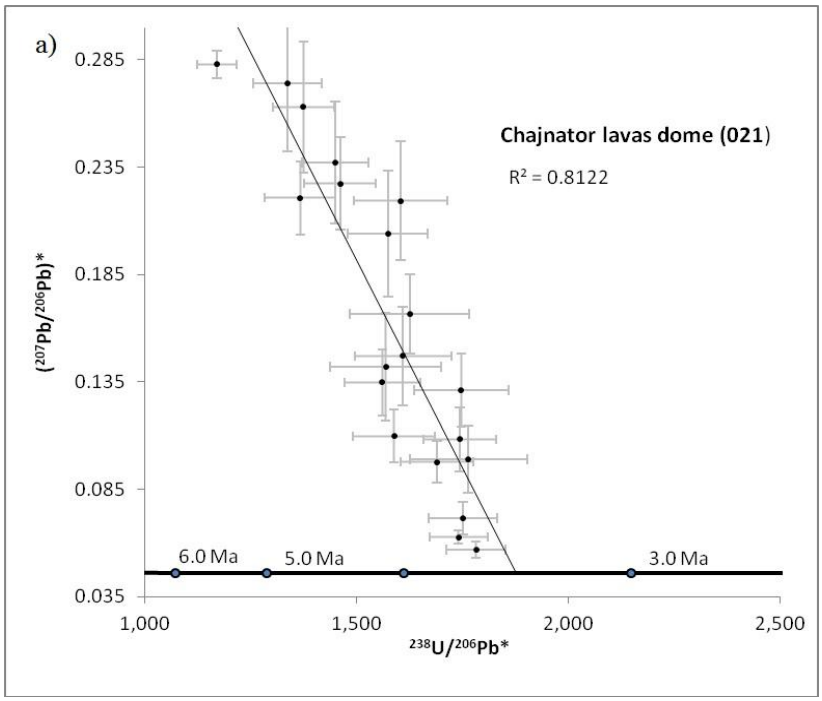
a)
Chajnator lavas dome (021)
R² = 0.8122
6.0 Ma
5.0 Ma
3.0 Ma
(207Pb/206Pb)*
238U/206Pb*
0.285
0.235
0.185
0.135
0.085
0.035
1,000
1,500
2,000
2,500

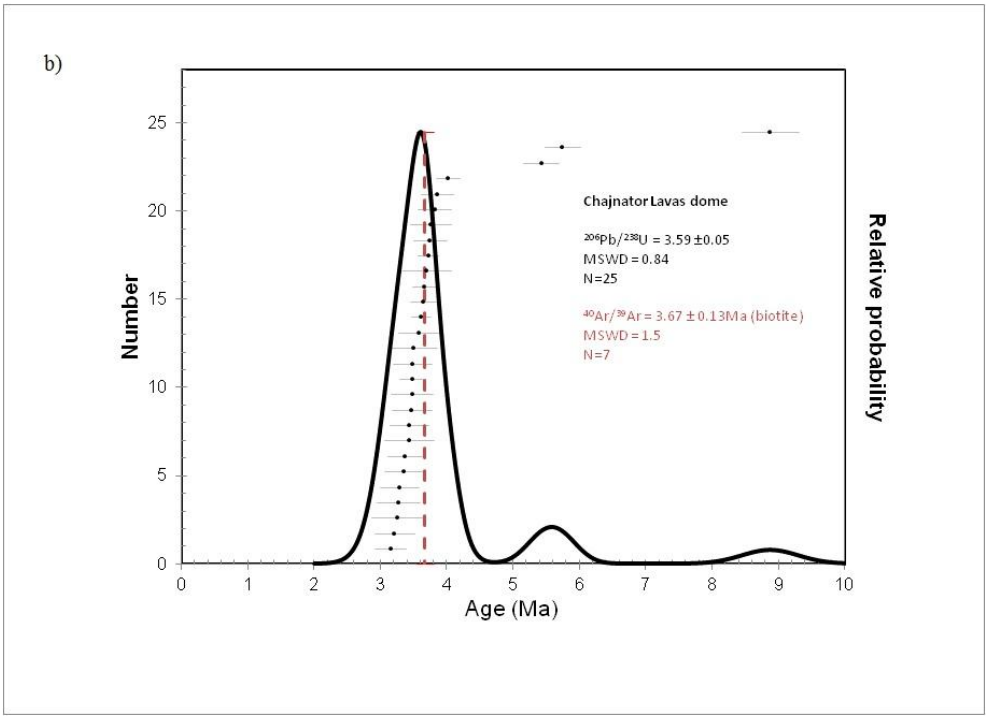
b)
Chajnator Lavas dome
206Pb/238U = 3.59 ±0.05
MSWD = 0.84
N=25
40Ar/39Ar = 3.67 ± 0.13Ma (biotite)
MSWD = 1.5
N=7
Number
Relative probability
Age (Ma)
0
5
10
15
20
25
0
1
2
3
4
5
6
7
8
9
10

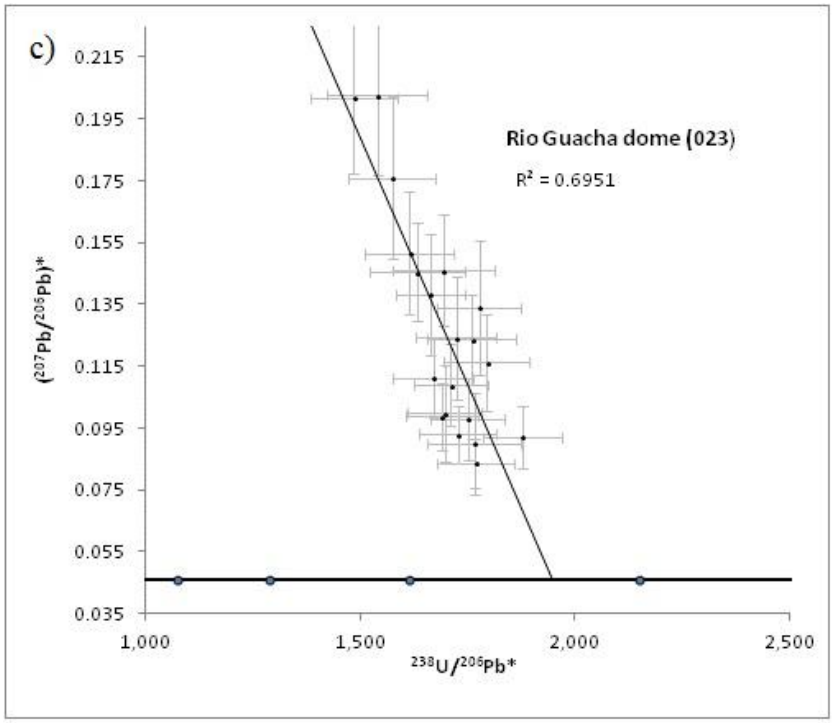
c)
Rio Guacha dome (023)
R² = 0.6951
(207Pb/206Pb)*
238U/206Pb*
0.215
0.195
0.175
0.155
0.135
0.115
0.095
0.075
0.055
0.035
1,000
1,500
2,000
2,500

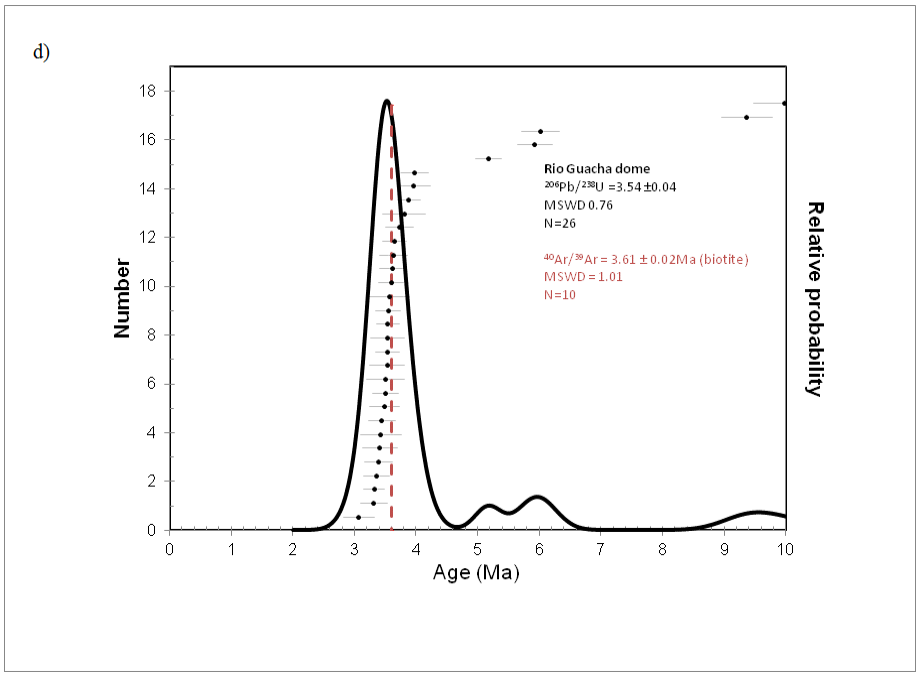
d)
Rio Guacha dome
206Pb/238U =3.54 ±0.04
MSWD 0.76
N=26
40Ar/39Ar = 3.61 ± 0.02Ma (biotite)
MSWD = 1.01
N=10
Number
Relative probability
Age (Ma)

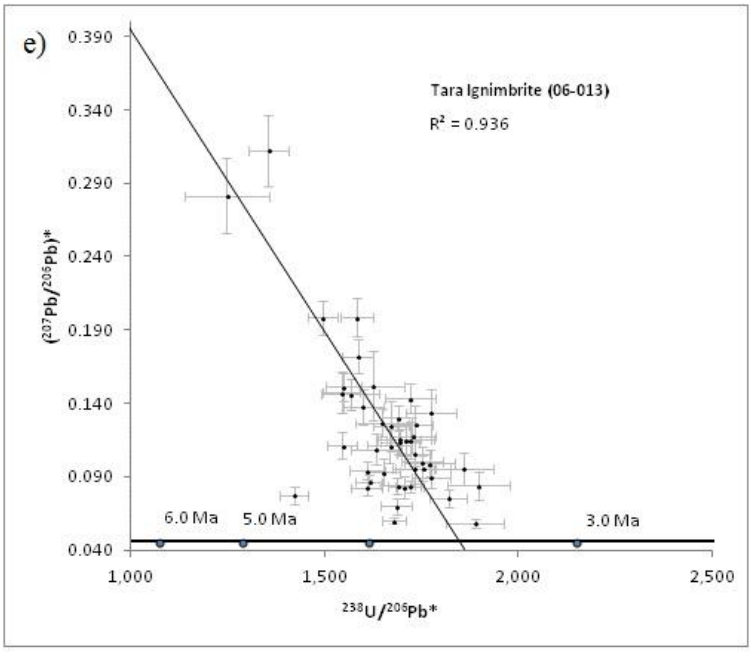
e)
Tara Ignimbrite (06-013)
R² = 0.936
6.0 Ma
5.0 Ma
3.0 Ma
(²³⁷Pb/²⁰⁵Pb)*
²³⁸U/²⁰⁵Pb*
0.390
0.340
0.290
0.240
0.190
0.140
0.090
0.040
1,000
1,500
2,000
2,500

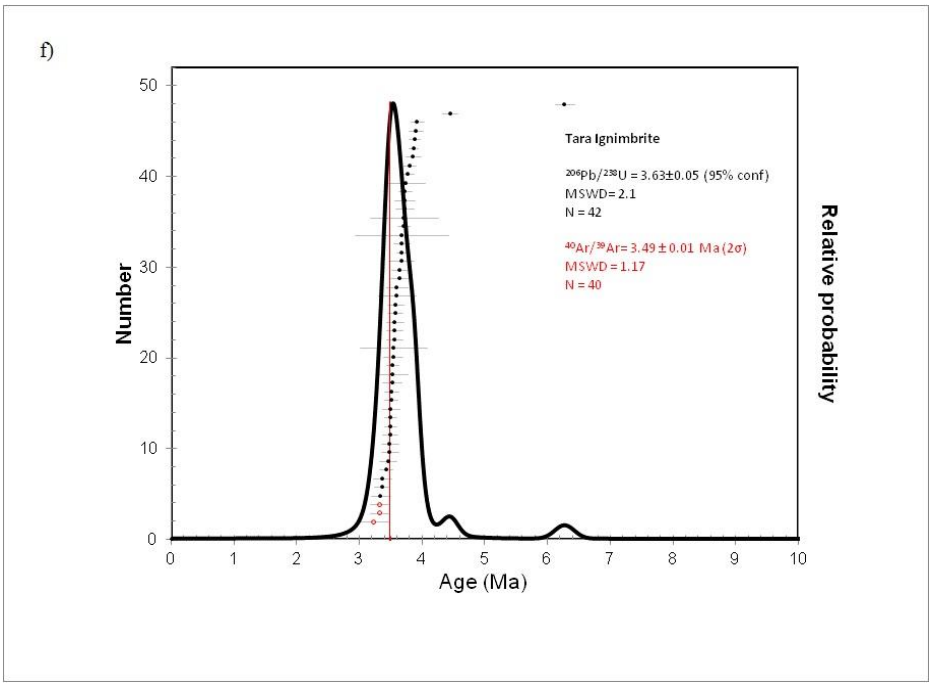
f)
Tara Ignimbrite
²⁰⁶Pb/²³⁸U = 3.63±0.05 (95% conf)
MSWD= 2.1
N = 42
⁴⁰Ar/³⁹Ar= 3.49 ± 0.01 Ma (2σ)
MSWD = 1.17
N = 40
Number
Relative probability
Age (Ma)
50
40
30
20
10
0
0
1
2
3
4
5
6
7
8
9
10

6.2.3 Puripica Chico Ignimbrite

The weighted mean of 47 autocrysts of the Puripica Chico ignimbrite yielded a U-Pb age of 2.09 ± 0.06 Ma along with a high MSWD of 13 (Fig. 23d). This high value could be attributed to the low analytical error determined for the SIMS, protracted range of zircons crystallization ages or more than one single zircon population hidden within the sample. As discussed later it is suggested that more than one single zircon population is hidden within the zircon data of this ignimbrite accounting for the high MSWD value. Low U-Pb errors have been reported in other young ignimbrites of the APVC (Kern J., pers. comm..). Older antecryst in this sample reported an U-Pb age of 4.55.

U-Pb weighted ages for the Totoral dome reported an age of 1.80 ± 0.06 Ma with a MSWD of 1.82. Antecrysts yielded "Tara Ignimbrite ages" of 3.65 and 3.76 Ma along with an older age of 4.35 Ma.

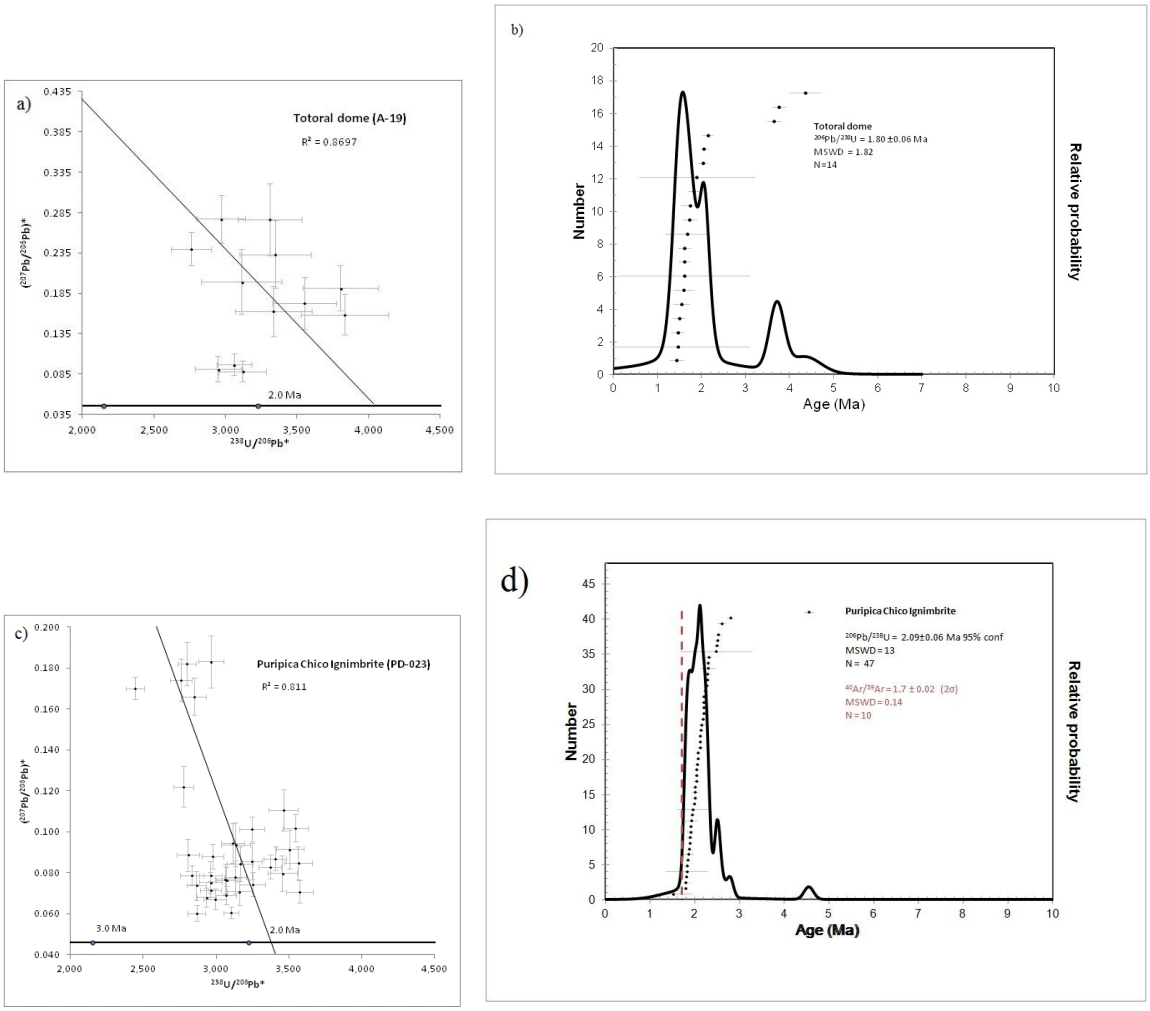

Figure 23 Probability plots and Tera Wasserburg concordia plots for the Puripica Chico Ignimbrite and Totoral lava dome. Symbols are the same as in Figs.21 and 22

Ar-Ar ages from the Negreal andesite (1.52±0.07 Ma) have similar ages to Puripica Chico and Tortoral, confirming that they represent a single magmatic event, representing the youngest phase of activity from the Guacha caldera.

6.3 Summary and discussion

A simplified and general diagram through time is displayed in Fig. 24. Antecrysts were distributed in three populations: population 1) from 9.97 to 8.87 Ma, population 2) from 6.27 to 5.17 Ma and population and 3) from 4.35 to 3.64 Ma. Older antecrysts of the system were recorded by the Rio Guacha and Chajnantor Lavas domes (Figs. 22b, d and Fig. 24d and e). In the Rio Guacha dome ages ranges from 9.97 to 9.36 Ma, while in the Chajnantor Lavas dome the antecrysts ages are younger ~8.87 Ma. The two lava domes and the Tara Ignimbrite also recorded ages that correspond to the Guacha ignimbrite; the Rio Guacha dome exhibits antecrysts with ages that range between 6.01 to 5.17 Ma; the Chajnantor Lavas dome displays ages that ranges between 5.74 to 5.42 Ma and the Tara ignimbrite sampled an antecryst with an age of 6.27 Ma (Figs. 24c, d and e). The third population of antecrysts is recorded by the Totoral dome. The autocryst ages recorded by this dome yielded ages ranging between 4.35 and 3.64 Ma. These range of ages fall within the age range assigned for the Tara Ignimbrite (Figs. 22f and 24g).

Figure 24 Temporal evolution of the Cerro Guacha Caldera. Time goes forward from the bottom up to the top. 3 main autocrysts population were defined (see text for explanations). Colored vertical lines define antecryst populations. Population 1 lies within brown line to the right (9.9-8.8 Ma); population 2 is within gray lines (6.27-5.17 Ma) and population 3 is displayed within the blue line, to the left (3.64-4.35 Ma)Ar-Ar ages are displayed as vertical dotted red line. For detail of the individuals diagrams see Figs. 21-23

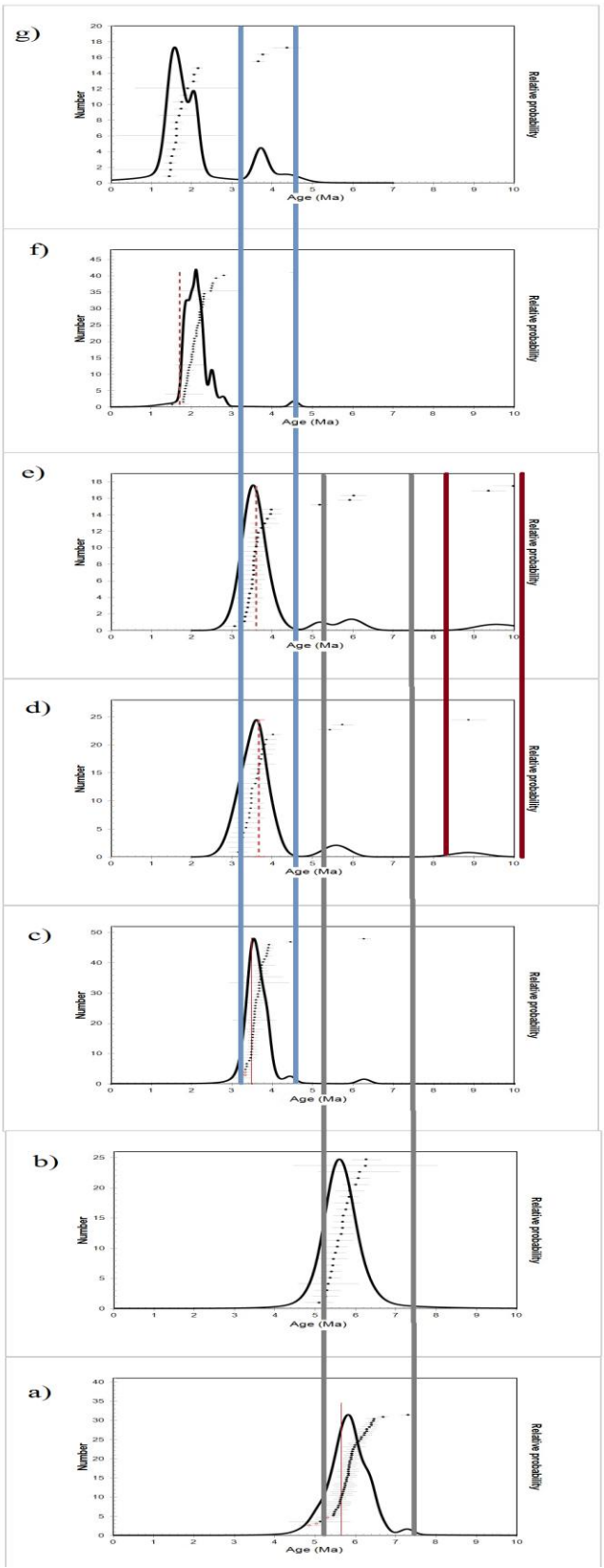
g)
f)
e)
d)
c)
b)
a)
Number
Age (Ma)
Relative probability

6.3.1 Relationship between Ar-Ar ages and U-Pb ages and residence times

The Ar-Ar sanidine weighted mean age determined for the Guacha Ignimbrite is 5.65 ± 0.01 Ma measured from 26 individuals crystals, meanwhile the U-Pb zircon weighted mean age determined here is 6.01 ± 0.1 Ma from 50 individual crytals. The older zircon yielded an age of 7.29 ±0.16 Ma, meanwhile the younger zircon age (counting only U-Pb weighted ages younger than the Ar-Ar age) yielded an age of 5.69 ± 0.29 Ma (crystal A-11-15). Maximum difference between U-Pb and Ar-Ar ages (difference between the older age of the autocryst zircon and the Ar-Ar eruption age) is 1.6 ± 0.16 Ma and is interpreted here as the zircon crystallization range.

Average difference between U-Pb and Ar-Ar yielded 360 ± 200 Ka. The value given by the difference between weighted Ar-Ar and U-Pb ages is 360 ± 100 Ka and is refer to as the minimum residence time.

The Ar-Ar age for the Tara Ignimbrite is 3.49 ± 0.01 Ma over 40 individuals crystals, meanwhile the U-Pb ziron weighted age determined here is 3.65 ± 0.05 Ma over 40 individual crytals. Older and younger zircon ages range from 4.44 ± 0.12 to 3.49 ±0.1 Ma respectively. Zircon cryatallization range is 0.95 ± 0.12 Ma.The average diference between U-Pb and Ar-Ar ages yielded 184 ±0.13 ka and the minimum residence time is 160 ±50.0 ka.

No sanidine Ar-Ar ages are available for the Puripica Chico Ignimbrite, the Ar-Ar age from biotite is 1.7 ±0.02 Ma, which overlaps within error with the youngest U-Pb zircon age (1.52 ± 0.41Ma, crystal 023-PD-16), suggesting that the biotite Ar-Ar age can be used as an eruption age estimation. Older age for this ignimbrite yield 2.79 ± 0.07, yielding a zircon cryatallization range of 1.09± 0.07 Ma. Average difference is 402 ± 70 Ka, meanwhile minimum residence time yielded a value of 390 ± 60 Ka.

6.3.3. Implications for the APVC

The zircon crystallization ranges for the Guacha ignimbrite are 1.64 ± 0.16 Ma, for Tara 0.95 ± 0.12 Ma and Ma 1.09 ± 0.07 Ma for Puripica Chico Ignimbrites been this later value larger than the one for Tara, which cannot be coherent if the volume of the ignimbrites are considered (Puripica Chico Ign vol <10 km^3 , Tara Ign vol ~800 km^3)

The range of residence times estimated for the Cerro Guacha are roughly similar to other sytems within the APVC like the La Pacana or other minor lavas domes. Schmitt et al., 2003 assumed that the Atana and Toconao magmas from La Pacana are consanguineous and estimated an average residence time in the order of ~500 to 750 kyrs. Folkes et al., 2010 described an eruptive recurrence ~50 ka to > 1Ma for the magmas of the Cerro Galan caldera and estimated a time of zircon crystallization <500 ka prior the eruption. Tierney, 2011 estimated a minimum residence time of 275 ka for the Pleistocene lavas that outcrops to the West side of the Pastos Grandes Caldera.

In contrast shorter residence times (less than 100 ka) for large >600 km^3 eruptions were estimated for the Bishop Tuff in the Long Valley Caldera (~100 ka) and the Lava Creek for the Yellowstone caldera (19-57 ka). Residence time studies on in these centers were based on U-Th disequilibrium series (Reid & Coath, 2000, Simon & Reid ,2005) and by difference between Ar-Ar and U-Pb ages (Bindeman et al., 2001; Gansecki et al., 1998 in Costa, 2008). Time required formodeling crust behavior and magma fluxes was done by Annen, (2009) was less than 100 ka for the formation of eruptible magmas. It was also suggested for her study that magma fluxes capable enough to erupt and form a caldera-type eruptions form in a relatively short period of time ~ 40 ky for the case of Taupo New Zealand.

An easy way to unveil hidden population mixed within a whole spectrum is by using the algorithm of Sambridge & Compston, 1994 for multi components mixtures applied to zircon ages. This algorithm uses iterative calculation to determine if more than one single population is hidden behind the dataset. By introducing the number of possible components (in this case the number of suspected populations) this algorithm calculates the weighted ages, their uncertainties (± 1 sigma) and their relative proportions

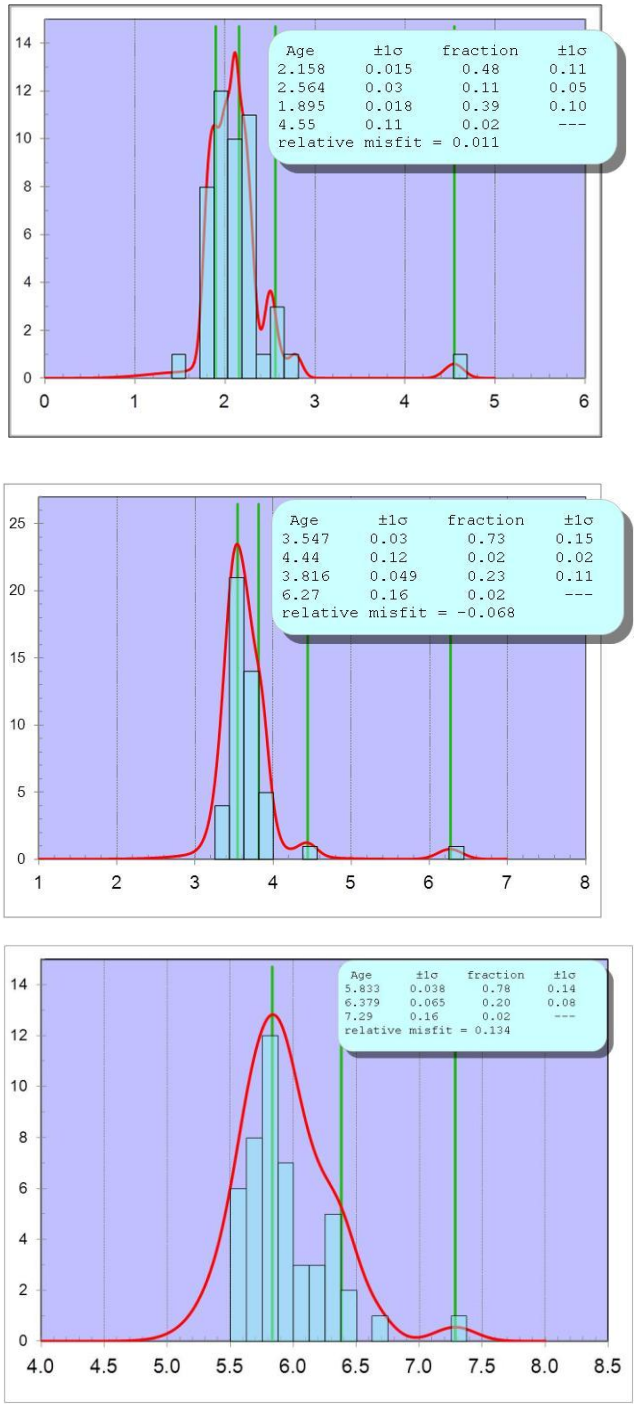

Figure 25 Sambridge & Compston, 1994 method for multi components mixtures applied to zircon ages. a)Puripica Chico; b) Tara Ignimbrite and c) Guacha Ignimbrite. Boxes show ages, ±1 sigma uncertainty, the crystal fraction calculated for each age and the relative misfit. (*) Relative Misfit indicates the degree to which additional components reduces the amount of unexplained scatter in the input data, relative misfit of a single component is 1

For the Guacha Ignimbrite these three ages were unmixed: 7.29 ± 0.16 Ma, 6.38 ± 0.065 and 5.83 ± 0.038. For the Puripica Chico Ignimbrite these four ages were unmixed: 4.55 ± 0.11 Ma, 2.56 ±0.03 Ma, 2.16 ±0.015 and 1.89 ±0.018 Ma.

For the Tara Ignimbrite, the *misfit* (*) yielded a negative value by adding four (or even three) populations, reflecting the fact that the weighted U-Pb age calculated by scaling the U-Pb zircon ages by their assignated errors is correct, and that the outliers (older ages in this case) which do not for part of the coherent age could be rejected

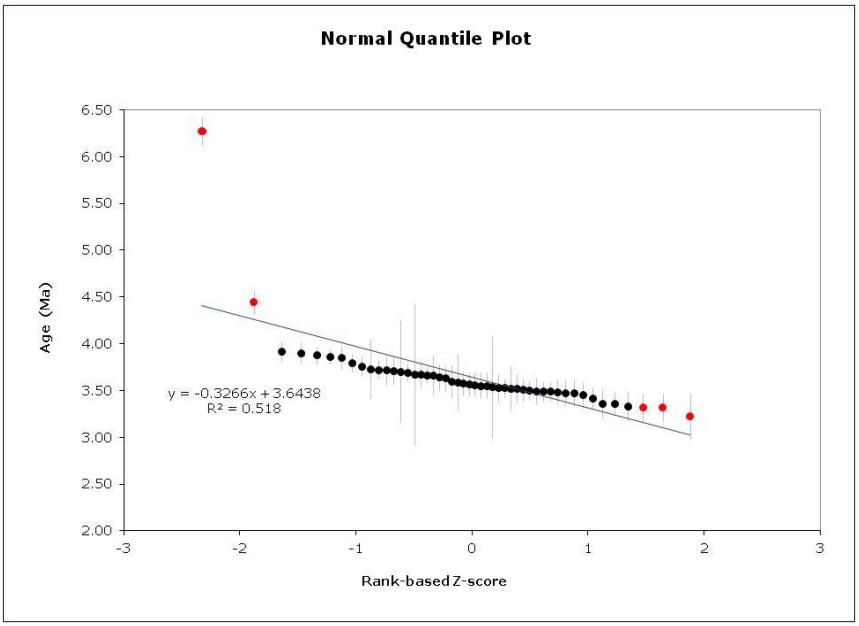

Figure 26 Plot showing rank-based Z score vs. age. Outliers are in red; the older ones are considered here as antecryst, can be part of an older pulse before the ultimate one that generate the Tara Ignimbrite magma chamber; the younger outliers are younger than the Ar-Ar age.

Giving these new calculated ages, the zircon crystallization ages for the Guacha Ignimbrite is 0.49 ±0.16 Ma and ~0.3 ± 0.06 Ma for the Puripica Chico Ignimbrite. If we consider to remove the 4.44 ±0.12 U-Pb age, of the zircon population of the Tara Ignimbrite the zircon crystallization range for this ignimbrite might be 0.43±0.11 Ma.

Even by testing the residence times by this way, the ignimbrites of the Cerro Guacha Caldera still fall within the field of protracted magma residence times (>100 ka), ranging from 650 to 240 ka.

Figure 27 Conceptual model for the evolution of the Cerro Guacha Caldera: a) Onset of a magma chamber following an early pulse of 7.3 Ma with no efusive equivalents within the caldera; 6 km depth of the magma chamber is infered by amphibole geobarometry. Antecryst are showed in black and white correponding the the first pulse between 7.3 to 6.4 Ma; b) Eruption of the Guacha ignimbrite and post trap door collapse as a consequence of mafic recharge; 0.49 ±0.16 Ma corresponds to the range of autocrystic zircon crrytallization calculated using unimx models (autocrysts are symbolized as crystal with filled circle); c) Caldera resurgence is recorded at 5.62 Ma with the eruption of the Kalina lava flow and the Guacha andesite; d) Early pulse previous to the Tara ignimbrite magma chamber onset, early zircon records a magmatic pulse at 4.4 Ma; e) Eruption of the Tara Ignimbrite after mafic recharge; 0.49 ±0.16 Ma corresponds to the range of autocrystic zircon crrytallization calculated if the 4.44 Ma zircon age is considered an antecrystic age (autocrysts are symbolized as unfilled crystals). Collapse of the structure offset Guacha andesite within the inner block of the caldera; f) Second resurgence associated to the Tara ignimbrite with the extrution of the Chajnantor, Rio Guacha and Chajnantor Lavas dome g) 1.5-1.8 Ma Eruption of the of the Puripica Chico Ignimbrite (1.7 Ma); 0.3 ±0.06 Ma corresponds to the range of autocrystic zircon crrytallization calculated using unimx models (autocrysts are symbolized as filled crystals); this eruption is followed by the emplacement of the Totoral Lava dome at (1.8 Ma) at the other rim of the caldera and finally the Negreal andesite (1.5 Ma) whose source probably comes from a different source than the Guacha andesite

6.3.4 Overall Model

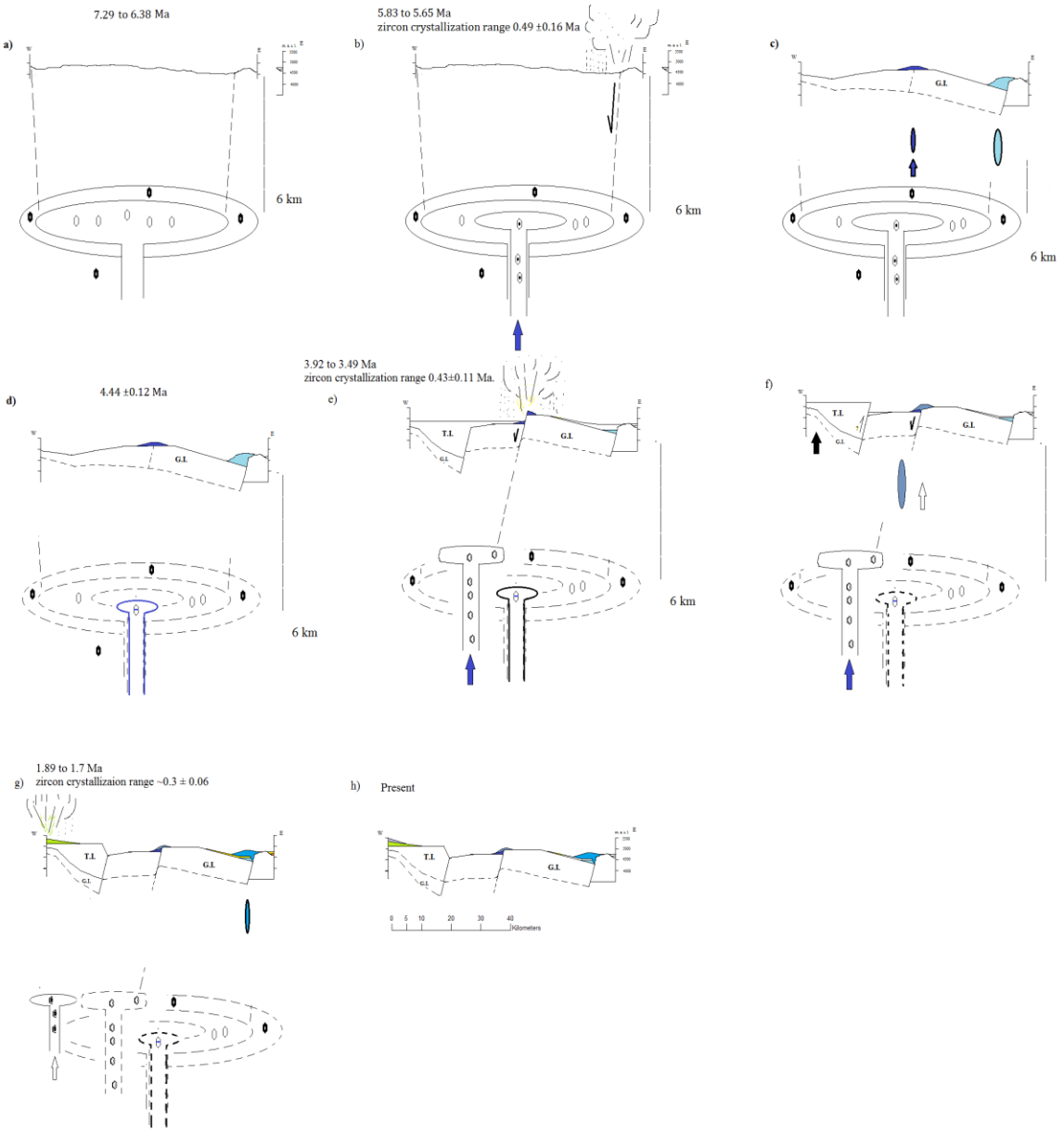

7.0 Conclusions

Three objectives were established to meet the goal of this study:

1) Revise and update the geochronology and stratigraphy of all components of the Guacha caldera
2) Relate the volcanic stratigraphy to the structural elements to constrain the structural development of the caldera
3) Link the volcanological evolution to the magmatic evolution of the system

The following outcomes have been achieved:

17 Ar-Ar ages, 261 new U-Pb ages, and new stratigraphic observations reveal that the first pulse of the caldera is associated to the Guacha Ignimbrite (GIS) at 5.65± 0.01 Ma, along with the eruption of the Guacha andesite and the Kalina post collapse lava dome (5.62 ±0.06 Ma). The Guacha andesite is defined by cross cutting relationships. The second pulse is associated to the Tara Ignimbrite (TIS) at 3.49 ± 0.01Ma, the Chajnantor dome (3.51± 0.02 Ma), the Chjanator Lavas dome (3.67 ± 0.13 Ma) and the Chajnantor Lavas dome (3.67 ± 0.13 Ma) this later with an age slightly older than the other domes and the ignimbrite. The third and last pulse corresponds to the Puripica Chico Ignimbrite (PCTS) at 1.7 ± 0.02Ma, the Negreal andesite (1.57 ± 0.07 Ma) and the Totoral dome (1.8 ± 0.06Ma).

Structural analysis, new U-Pb and Ar-Ar ages keep the chronological order of the units studied, and the association with the main eruptive stages. The resurgent dome of the Guacha Caldera is now understood as a complex nested structure that reflects collapse and resurgence episodic after the eruptions of the Guacha and Tara Ignimbrites. The structural evolution (shown in Fig. 13) is described as follow:

1) 5.65 Ma the Guacha ignimbrite erupted through vents located near the east and north edge of the structural rim defined by an arcuate normal fault that cuts pre caldera units, mostly Cojina lavas. Ages of the Kalina dome (5.62 Ma), location of sedimentary sequences and travertines and arcuate emplacement of younger centers (e.g. Totoral lava dome and Zapaleri volcano) suggest an outer caldera collapse scarp and associated moat

2) Lack of structure to the west suggests the presence of a hinge and a trap door collapse after the eruption.

3) Uplift of the caldera roof due to resurgence generated stress that tilted the intracaldera welded tuff and the Guacha andesite (Fig. 11)

4) 3.49 Ma eruption of the Tara ignimbrite producing a smaller caldera than the Guacha Ignimbrite. Collapse is evidenced by offset of the Guacha resurgent dome and emplacement of lava domes along a distinct arcuate normal fault

5) Second resurgence is a complex nested feature with to separated stages, pre collapse (Chajnator Lavas dome) and post resurgence volcanism associated to emplacement of Chajnantor Dome and Rio Guacha domes

6) The final stage of the Caldera cycle is manifested by the eruption of the Puripica Chico (1.7 Ma) on the western hinged edge of the Guacha caldera followed by the emplacement of the Totoral (1.80 ± 0.06 Ma) and later the Negreal andesite (1.52±0.07 Ma) on the eastern side of the caldera

Geochemistry of the pumices of the Guacha, Tara and Puripica Chico ignimbrites indicates they belong to the high-K series, ranging compositionally from dacite to rhyolites, with andesitic members present as lavas (for the Guacha and Puripica Chico Ignimbrites) and as pumices (for the Tara Ignimbrite).

Trace elements ratios such as Ba vs. Eu /Eu* show larger compositional ranges for the Tara Ignimbrite pumices suggesting less homogeneity of this magma in comparison to the Guacha or Puripica Chico magmas. Modeling Rayleigh fractionation for Ba, Rb and Sr suggests a fractionation of at least 60% of plagioclase, biotite and hornblende to account for the compositional variation between the Guacha andesite and the Chajnantor dome.

Dy/Hb ratio increases with time from the Guacha andesite to the Negreal andesite suggesting that the process of stabilization of garnet owing to crustal thickening that was suggested for other andesites of the Central Volcanic Zone (Mamani, 2010) might be also present in the andesites of the Cerro Guacha Caldera.

U-Pb zircon geochronology indicates zircon was recycled continuously within the caldera. This is seen as U-Pb antecrysts ages that can be divided in: population 1 at the Rio Guacha dome (ranging from 9.97 to 9.36 Ma) and Chajnantor Lavas dome (~8.87 Ma); Population 2 recorded also by these domes as zircons with ages of 6.01 to 5.17 Ma coincident with the preceding Guacha Ignimbrite; and population 3) outside in the eastern caldera rim the Totoral dome recording zircon ages of 4.35 and 3.64 Ma correlated with theTara Ignimbrite.

The zircon crystallization ranges for the Guacha ignimbrite is 1.64 ± 0.16 Ma, for Tara 0.95 ± 0.12 Ma and Ma 1.09 ± 0.07 Ma for Puripica Chico Ignimbrites, however if the older zircon ages of these pumices are considered antecrysts and are filtered out, shortest zircon crystallization ranges can be assignated: 0.49 ±0.16 Ma for the Guacha Ignimbrite, ~0.3 ± 0.06 Ma for the Puripica Chico Ignimbrite and 0.43±0.11 Ma for the Tara Ignimbrite making the Ignimbrites of the Cerro Guacha Caldera fall within the field of protracted magma residence times (>100 Ma) estimated for other centers within the APVC.

The original hypothesis that was to be tested was the Cerro Guacha Caldera is a polycyclic caldera with at least two large super-eruptions that triggered successive confocal collapse and resurgence resulting in the current nested volcano-tectonic depression. Field observations such as the lacustrine sedimentary sequence, the moat of the caldera, the graben like configuration of the Guacha welded tuffs and the U-Pb age of the Kalina lava dome seem to confirm the hypothesis about collapse and resurgence after the eruption of the Guacha Ignimbrite; the Ar-Ar ages of the Rio Guacha and Chajnator domes emplaced along the inner caldera rim that offsets the earlier Guacha andesite also suggest that following the eruption of the Tara Ignimbrite a second episode of resurgence took place in the inner block of the caldera.

References Cited

Almendras, O., Baldellón, E., 1997, Hoja Ollague/San Agustin 5930/6030: Carta Geológica de Bolivia, Esc. 1:100.000, Publicacíon SGM Serie I-CGB-49, Servicio Nacional de Geológica y Mineria.

Baldwin, S., L., and Ireland, T., R., (1995) A tale of two eras: Pliocene-Pleistocene unroofing of Cenozoic and late Archean zircón from active metamorphic core complexes, Solomon Sea, Papua New Guinea, Geology 23, 1023-1026

Christiansen, R., L., 2001, The Quaternary and Pliocene Yellowstone Plateau Volcanic Field of Wyoming, Idaho, and Montana. U.S. Geological Survey. Professional Paper 729-G

Chesner C.A., 2011, The Toba Complex, Quaternary International (2011), doi:10.1016/j.quaint.2011.09025

Coira B., Caffe P., Kay, S.,M., DIaz, A., Ramirez, A., Complejo Volcánico Vilama-Sistema Calderico del Cenozoico Superior en Puna, Jujuy. XIII Congreso Geológico Argentino y III Congreso de Exploración de Hidrocarburos, Actas III: 603-620

de Silva, S. L., 1989a, Altiplano-Puna volcanic complex of the central Andes: Geology v. 17, p. 1102-1106.

de Silva, S. L., 1989b, Geochronology and stratigraphy of the ignimbrites from the 21º30′S to 23º30′S portion of the Central Andes of Northern Chile. Journal of Volcanology and Geothermal Research, v. 37, p. 93-131.

de Silva, S. l. & Francis, P.,W., 1989, Correlation of large volume ignimbrites-two case studies from the Central Andes of N. Chile. Journal of Volcanology and Geothermal Research, 37, 133-149

de Silva, S., L., 1991, Styles of zoning in central Andean ignimbrites; Insight into magma chamber processes, Geological Society of America, Special Paper 265

de Silva, S. l. & Francis, P.,W., 1991, Volcanoes of the Central Andes, Springer-Verlag, Heldelberg, 263 pp.

de Silva, S. L., Zandt G., Trumbull R., Viramonte J. G., Salas G., & Jimenez N., 2006. Large ignimbrite eruptions and volcano-tectonic depressions in the thermomechanical perspective. Geological Society, London, Special Publication, 269, 47-63

de Silva S., L., and Gosnold W. A., 2007, Episodic construction of batholiths: Insight from the spatiotemporal development of an ignimbrite flare-up: Journal of Volcanology and Geothermal Research, v. 167, p. 320-335, doi: 10.1016/j.jvolgeores.2007.07.015

Francis, P.W., & Baker, M.C.W., 1978. Sources of two large-volume ignimbrites in the Central Andes: Some Landsat evidence. J. Volcanol. Geotherm. Res. v.4, p81-87.

Gardeweg, M., Ramirez, C.F., 1987, La Pacana caldera and the Atana ignimbrite: a major ash-flow and resurgent caldera complex in the Andes of northern Chile. Bull. Volcanol. 49, 547-566

Hamilton, W., 1959, Yellowstone Park area, Wyoming: A possible modern lopolith; Geological Society of America Bulletin, v. 70. P. 225-228

Halpern M., 1979, Geological significance of Rb-Sr isotopic data of northern Chile crystalline rocks of Andean orogen between latitudes 23° and 27° South. Geological Society of America Bulletin, v. 89, p. 522-532,

Holland, T.J.B. and Blundy, J.D., 1994. Non-ideal interactions in calcic amphiboles and their bearing on amphibole-plagioclase thermometry. Contributions to Mineralogy and Petrology, 116, 433-447

Isacks, B., L., 1988, Uplift of the central Andean plateau and bending of the Bolivian orocline. Journal of Geophysical Research, 98, p. 3211-3231

James, D., E., 1971, Plate tectonic model for the evolution of the central Andes: Geological Society of America Bulletin, v. 82, p. 332-354

Jimenez, N., Lopez-Velasquez, S., Santiváñez, R., 2009, Evolucion Tectonomagmatica de los Andes Bolivianos, Revista de la Asociacion Geologica Argentina 65 (1): 36-67

Kay., S., M., Coira B., L., Shallowing and steepening subduction zones, continental lithospheric loss, magmatism, and crustal flow under the Central Andean Altiplano-Puna Plateau. Geological Society of America Memoirs, 2009, 204, p. 229-259,

Lindsay, J. M., de Silva, S., Trumbull, R., Emmermann, R., Wemmer, K., 2001. La Pacana caldera, N. Chile: a re-evaluation of the stratigraphy and volcanology of one of the world's largest resurgent calderas. Journal of Volcanology and Geothermal Research, 106(1-2): 145-173

Lindsley, D.H., Spencer, K.J., 1982. Fe–Ti oxide geothermometry:Reducing analyses of coexisting Ti-magnetite (Mt) and ilmenite (Ilm) abstract AGU 1982 Spring Meeting Eos Transactions. American Geophysical Union 63 (18),471.

Lipman, P.W., (1984). The roots of ash-flow calderas in western NorthAmerica: windows into the tops of granitic batholiths. Journal of Geophysical Research 89(B10), 8801-8841.

Lipman, P.W., (2007), Incremental assembly and prolonged consolidation of Cordilleran magma chambers: Evidence from the Southern Rocky Mountain volcanic field. Geosphere; February 2007; v.3; no. 1; p.42-70

Mamani, M., Worner, G., Sempere, T., (2010), Geochemical variations in igneous rocks of the Central Andean orocline (13°S to 18°S): Tracing crustal thickening and magma generation through time and space. Geological Society of America; v. 122; no. ½; p. 162-182

Mobarec, R., et al., (1994) Evolución tectónica y diferenciación magmática de la Caldera de Guacha, sudoeste de Bolivia, Actas VII Congreso Geológico Chileno vol. 1, Universidad de Concepción, Concepción, p. 112–116.

McQuarrie, N., Horton, B., K., Zandt, G., Beck, S., DeCelles, P., G., 2005, Lithosphere evolution of the Andean fold-thrust belt, Bolivia, and the origin of the central Andean plateau, Tectonophysics 399 (2005) p.15-37

Ort M., H., (1993), Eruptive processes and caldera formation in a nested downsag-collapse caldera: Cerro Panizos, central Andes Mountains. Journal of Volcanology And Geothermal Research. Volume: 56. Pages: 221-252

Pacheco, J., Ramirez, V., 1996, Hoja Quetena 6127: Carta Geológica de Bolivia, Esc. 1:100.000, Publicacíon SGM Serie I-CGB-40, Servicio Nacional de Geología y Minería

Pritchard, M. E., and M. Simons (2002), A satellite geodetic survey of large-scale deformation of volcanic centres in the central Andes, Nature, 418, 167–171, doi:10.1038/nature00872.

Pritchard, M. E., and M. Simons (2004a), An InSAR-based survey of volcanic deformation in the central Andes, Geochem. Geophys. Geosyst., 5, Q02002, doi:10.1029/2003GC000610.

Pritchard, M. E., and M. Simons (2004b), An InSAR-based survey of volcanic deformation in the southern Andes, Geophys. Res. Lett., 31, L15610, doi:10.1029/2004GL020545.

Pritchard, M. E., and M. Simons (2004c), Surveying volcanic arcs with satellite interferometry: The central Andes, Kamchatka, and beyond, GSA Today, 14(8), 4 – 9, doi:10.1130/1052-5173(2004)014<4:SVAWSR>2.0.CO;2.

Ridolfi, F., Renzulli, A., Puerini, M., 2010, Stability and chemical equilibrium of amphibole in calc-alkaline magmas: an overview, new thermobarometric formulations and application to subduction-related volcanoes. Contributions Mineral Petrology 160: p. 45-66

Salisbury, M.J., Jicha, B., de Silva, S., Singer, B., Jiménez C., Ort, M., 2011, $^{40}Ar/^{39}Ar$ chronostratigraphy of Altiplano-Puna Volcanic Complex ignimbrites reveals the development of a major magmatic province. Geological Society of America Bulletin, published online on 21 December 2010 as doi: 10.1130/B30280.1

Reutter, K., J., 2001. Le Andi centrali: Elementi di uno orogenesi de margine continentali attivo. Acta Naturalia de Latene Parmense, Parma, Italia 37, 5-37

Schmitt A.K., Grove, M., Harrison, M., Lovera, O., Hulen, J., Walters, M., (2003), The Geysers Cobb Mountains Magma System, California (Part 1): U-Pb zircon ages of volcanic rocks, conditions of zircon crystallization and magma residence times. Geochimica et Cosmochimica Acta, vol. 67, No. 18, pp. 3423-3422

Schmitt A.K., de Silva S., L., Trumbull R., B, Emmermann R., 2001, Magma evolution in the Purico ignimbrite complex, northern Chile: evidence for zoning of a dacitic magma injection of rhyolitic melts following mafic recharge. Contrib Mineral Petrol (2001) 140: 680-700

Self S., Goff F., Gardner J., N., Wright J., V., Kite W., M., 1986, Explosive Rhyolitic Volcanism in the Jemez Mountains: Vent Locations, Caldera Development and Relation to Regional Structure. Journal of Geophysical Research, Vol. 91, No. B2, p. 1779-1798

Smith, R.L., Bailey, R.A., 1968. Resurgent cauldrons. Geol. Soc. Am. Mem. 116, 613-662

Soler, M.M., Caffe, P.J., Coira, B.L., Onoe, A.T., Kay, S., Mahlburg, Geology of the Vilama caldera: a new interpretation of a large-scale explosiveevent in the Central Andean plateau during the Upper Miocene, Journal of Volcanology and Geothermal Research (2007), doi: 10.1016/j.jvolgeores.2007.04.002

Steven, T.A., and Lipman, P.W., 1976, Calderas of the San Juan Volcanic Field, Southwestern Colorado: U.S. Geological Survey Professional Paper 958, 35 p.

Van Bemmelen, R.W., 1939, The volcano-tectonic origin of Lake Toba (North Sumatra). De Ingenieur in Nederlandsch Indie 6-9, 126-140

Appendix A Thin sections petrographic descriptions
Guacha Ignimbrite System

B06-085 (dacite pumice)

Fractured phenocrysts of euhedral to subhedral plagioclase An_{13-30} with no sieving structure, anhedral quartz (1.6%), imbricated sub-anhedral biotite (2.8%), subhedral hornblende (1.5%), euhedral-subhedral Fe-Ti oxides (1.3%), glass (46.0%) and vesicles 38.2%

B06-030 (dacite crystal-rich pumice, phenocrysts 46%)

Fractured phenocrysts of subhedral plagioclase An_{12-30} (8.7%) with no sieving structure, coarse anhedral quartz (20.0%), flexed subhedral biotite with inclusions of quartz (13.25%), subhedral hornblende (2.0%), subhedral Fe-Ti oxides (1.75%) and glass (54.2%)

A-13 Guacha Andesite

Phenocrysts of subhedral and sieved plagioclase An_{26-32} to An16-24 (25%) some with reaction rims, cumulates and phenocryts of subhedral opx (5.5%) most with opx reaction rims, Fe-Ti oxides (1.75%) surrounded by devitrified glass (68%) made up of plagioclase, Fe-Ti oxides

A-04 Kalina post collapse dome

Coarse grain foliated dacite with fractured phenocryst of rounded euhedral to anhedral quartz (20.0%) + euhedral plagioclase An_{24-16} to An_{13-30} (21.25%) with inclusions of biotite + euhedral sanidine (0.25%)+ euhedral hornblende with inclusions of biotite and plagioclase (0.25%)+ subhedral biotite (11.5%) with inclusions of plagioclase + rombic sphene (0.25%) + euhedral Fe-Ti oxides (2.5%) with quartz inclusions + zircon (0.25%). Glass (43.75%) perlitic partially devitrified (spherulites)

5.2.2 Tara Ignimbrite System

BO6-013 (rhyolite pumice)

Phenocrysts of subhedral plagioclase An_{12-30} (3.5%), subhedral flakes of biotite (2.25%), anhedral to subhedral quartz (3.0 %), apatite (0.25%), vesicles (37.0%) and glass (54.0) made up of quartz and feldspar.

B06-027 (dacite pumice)

Fractured phenocrysts of subhedral plagioclase An_{13-30} (13.75%), euhedral to suhedral hornblende (2.25%), subhedral biotite (1.25%), subhedral clinopyroxene (1.0%), anhedral Fe-Ti oxides (0.75%), vesicles (33.5%) and glass (47.5%)

B06-023 (Rio Guacha dome)

Porphyrytic coarse grain rock with phenocrysts of euhedral to subhedral plagioclase An_{12-26} (17.25%), some with sieve texture, subhedral biotite (4.75%) with inclusions of quartz, subhedral to euhedral hornblende (1.75%), euhedral to subhedral clinopyroxene (1.5%) embedded in a devitrified glass with spherulites (73.25%). Xenoliths of sandstones and gabbros (?) were also observed (1.5%)

B06-024 (Chajnator dome)

Porphyrytic rock made up of phenocrysts of suhedral to anhedral quartz (5.0%), suhedral plagioclase An_{18-10} (1.75%), suhedral sanidine (4.5%), suhedral biotite (1.0%), Fe-Ti oxides (0.75%) and glass (87.0%)

5.2.3 Puripica Chico Totoral System

BO6-073 (crystal rich dacite pumice)

Phenocrysts of suhedral plagioclase An_{13-30} (37.5%), euhdral to subhedral biotite (6.25), suhedral hornblende (0.25%), euhdral to suhedral Fe-Ti oxides (3.25%), vesicles (10.25%) and glass (39%)

A-05 Dark inclusion on Puripica Chico Ignimbrite

Welded tuff inclusion with fragmented phenocrysts of plagioclase (5.5%) +quarttz (3.5%) + sandstone xenoliths (14.5%) + biotite (10.0%) pyroxenes (?) + apatite in a welded glassy fluidal altered glass.

A-01 Negreal del Totoral

The rock is aphanitic with an interbedded layer of richer in Fe-Ti oxides. Porphyritic texture shows sieved plagioclase An_{12-26} to An_{13-27} (22.5%), clinopyroxene (8.3%), amphibole (0.1%) and Fe-Ti oxides (2.0%). Phenocrysts in a microcrystalline matrix (67.1%) made of plagioclase (75%) and Fe-Ti oxides (25%)

A-19 Totoral Dome

Porphyrytic crystal rich rock made up of subhedral and sieved plagioclase An_{13-30} (27.5%)+ subhedral clinopyroxene (6.5%)+ subhedral biotite (5.0%)+Fe-Ti oxides (2.0%) on a devitrified glass with spherulites (58.25%)

Appendix B XRF-ICP whole rock analysis

System	Guacha Ignimbrite Sytem									
Unit	Guacha	Guacha	Guacha	Guacha	Guacha	Guacha	Guacha	Guacha	Guacha-andesite	Kalina dome
Rock Unit	pumice	pumice	pumice	pumice	pumice	pumice	pumice	pumice	lava	lava
Sample	CHIC-96h-3B	BOL11*	B06-085*	B06-007*	B06-030*	A-07*	A-08*	A-10*	A-13	A-04
SiO2	71.44	65.55	67.05	71.30	68.40	69.80	66.18	68.91	61.02	65.88
TiO2	0.42	0.65	0.58	0.32	0.45	0.38	0.78	0.55	1.11	0.70
Al2O3	13.79	16.69	16.05	15.00	16.10	15.63	15.10	15.74	17.64	16.96
Fe2O3	1.84	4.28	3.72	2.10	2.90	2.78	4.13	2.96	5.39	3.74
MnO	0.06	0.07	0.06	0.08	0.05	0.05	0.07	0.05	0.09	0.05
MgO	0.46	1.88	1.71	0.81	1.40	0.97	1.68	1.12	2.64	1.45
CaO	1.76	4.20	4.05	3.01	3.58	3.11	4.19	3.57	6.73	3.80
Na2O	2.28	2.80	2.64	2.76	3.13	2.57	3.26	2.74	2.95	2.94
K2O	5.39	3.70	4.01	4.50	3.84	4.51	4.43	4.23	2.22	4.29
P2O5	0.10	0.18	0.13	0.09	0.12	0.18	0.20	0.12	0.22	0.18
CO2	0.11									
H2O	2.34									
Total	100.00	100.00	100.00	99.97	99.97	100.00	100.00	100.00	100.00	100.00
Ba	383.53	634.41	539.00	435.00	551.00	548.86	573.00	540.16	560.15	590.74
Cr	<10		87.00	71.00	75.00	11.90	7.60	8.00	33.20	13.20
Ni	<10		45.00	36.00	39.00	7.00	4.00	2.80	8.70	5.70
Rb	271.30	168.20	230.00	200.00	189.00	182.17	182.52	189.99	89.98	203.35
Sr	122.45	321.79	333.00	262.00	305.00	257.40	249.37	287.25	372.94	290.16
V	37.66		79.60	43.80	63.30	59.40	102.20	60.60	172.90	82.20
Y	21.20	20.41	18.00	17.00	18.00	17.85	27.57	18.58	28.74	19.44
Zn	58.58		66.40	51.20	64.60	55.30	74.90	68.40	87.70	84.70
Zr	134.43	156.01	153.00	115.00	145.00	144.66	194.12	167.24	198.48	184.55
Nb	13.19	12.33	11.90	11.90	12.00	11.85	15.00	12.05	13.14	15.00
Th		18.76	19.00	23.00	22.00	24.92	19.97	22.17	10.72	20.82
U		5.13	5.10	7.80	5.90	7.65	6.01	6.22	2.42	7.08
Sn										
Pb		8.23	33.00	27.00	24.00	32.73	17.23	24.80	11.65	23.58

System	Guacha Ignimbrite Sytem									
Unit	Guacha	Guacha	Guacha	Guacha	Guacha	Guacha	Guacha	Guacha	Guacha-andesite	Kalina dome
Rock Unit	pumice	pumice	pumice	pumice	pumice	pumice	pumice	pumice	lava	lava
Sample	CHIC-96h-3B	BOL11*	B06-085*	B06-007*	B06-030*	A-07*	A-08*	A-10*	A-13	A-04
La		40.83	45.10	35.60	39.30	48.95	43.47	38.97	34.24	40.77
Ce		82.34	86.80	70.70	75.40	93.72	89.64	79.59	67.97	82.01
Pr		9.24	9.70	7.90	8.50	10.06	10.67	9.43	8.66	9.68
Nd		33.24	33.80	27.50	29.60	33.69	39.92	34.70	33.83	35.61
Sm		6.25	6.10	5.20	5.50	5.75	8.16	6.66	7.09	7.15
Eu		1.19	1.20	0.90	1.10	1.01	1.34	1.17	1.53	1.38
Gd		4.92	4.60	4.00	4.20	4.27	6.71	5.01	6.33	5.54
Tb		0.74	0.70	0.60	0.60	0.61	1.04	0.72	1.00	0.78
Dy		4.05	3.80	3.30	3.40	3.40	5.82	3.85	5.76	4.14
Ho		0.77	0.70	0.60	0.60	0.65	1.06	0.69	1.12	0.73
Er		1.97	1.90	1.70	1.70	1.71	2.63	1.68	2.87	1.76
Tm		0.28	0.30	0.30	0.30	0.25	0.36	0.24	0.39	0.25
Yb		1.78	1.70	1.70	1.50	1.64	2.16	1.49	2.38	1.48
Lu		0.27	0.30	0.30	0.30	0.25	0.32	0.23	0.37	0.23
Li										
Sc		11.86	9.80	5.80	8.30	6.43	11.15	6.73	18.33	8.26
Co										
Cu			5.10	4.90	5.20	3.80	8.40	6.50	11.70	4.40
Ga			19.40	16.70	18.90	19.10	17.80	19.30	20.30	20.80
Cs		15.45	23.00	28.00	26.00	13.73	14.09	20.94	5.02	15.00
Hf		4.51	4.70	3.80	4.60	4.63	5.59	4.95	5.35	5.28
Ta		1.17	1.20	1.50	1.30	1.38	1.49	1.30	0.96	1.46

System	Tara Ignimbrite System									
Unit	Tara	Tara	Tara	Tara	Tara	Tara	Río Guacha Dome	Chajnantor Lavas	Chajnantor Dome	Tara
Rock Unit	pumice	pumice	pumice	pumice	pumice	pumice	Lava	Lava	Lava	tuff
Sample	BOL10	88037.00	BOL15	BOL19	B06-013	B06-027	B06-023	BOL21	B06-024	CHIC-96h-6
SiO2	76.68	74.44	66.12	68.76	72.60	66.60	65.70	64.43	77.10	67.94
TiO2	0.12	0.27	0.71	0.56	0.37	0.76	0.86	0.92	0.08	0.51
Al2O3	13.17	14.01	16.78	16.34	14.50	15.90	16.50	16.98	12.80	15.90
Fe2O3	0.89	1.21	4.29	2.85	2.10	3.80	4.40	4.79	0.70	2.79
MnO	0.05	0.03	0.06	0.06	0.05	0.07	0.06	0.08	0.07	0.03
MgO	0.37	0.39	1.96	1.35	0.56	1.26	1.66	1.64	0.07	0.88
CaO	0.95	1.77	3.12	2.94	2.31	4.25	4.54	4.80	0.70	3.00
Na2O	2.29	2.52	2.38	2.58	3.09	3.52	3.37	3.52	3.36	3.45
K2O	5.47	5.27	4.37	4.36	4.36	3.69	2.76	2.63	5.08	3.83
P2O5	0.02	0.07	0.21	0.19	0.08	0.18	0.20	0.22	0.01	0.12
CO2										0.08
H2O										1.47
Total	100.00	100.00	100.00	100.00	100.02	100.03	100.05	100.00	99.97	100.00
Ba	270.40	867.11	634.16	645.93	806.00	760.00	671.00	709.56	87.00	615.82
Cr	3.00				125.00	91.00	87.00		48.00	10.30
Ni	0.00				66.00	46.00	43.00		21.00	<10
Rb	245.14	251.09	192.00	189.96	173.00	152.00	186.00	129.77	383.00	153.75
Sr	66.23	180.11	271.99	324.64	236.00	353.00	347.00	369.19	26.00	263.71
V	3.60				31.80	73.50	102.50		1.80	53.68
Y	27.92	22.71	18.33	19.63	22.00	28.00	29.00	28.24	46.00	24.75
Zn	33.90				58.20	79.30	102.70		29.00	53.58
Zr	82.11	138.31	171.94	152.43	172.00	269.00	288.00	316.12	67.00	176.03
Nb	13.42	14.40	12.40	12.67	14.40	15.80	17.00	16.14	26.80	14.98
Th	26.52	25.05	15.99	16.23	22.00	16.00	16.00	14.41	30.00	
U	9.70	8.62	5.02	5.91	5.10	3.80	4.90	3.95	17.00	
Sn										
Pb	27.51	27.10	16.05	17.46	23.00	36.00	23.00	26.60	27.00	

System	Tara Ignimbrite System									
Unit	Tara	Tara	Tara	Tara	Tara	Tara	Río Guacha Dome	Chajnantor Lavas	Chajnantor Dome	Tara
Rock Unit	pumice	pumice	pumice	pumice	pumice	pumice	Lava	Lava	Lava	tuff
Sample	BOL10	88037.00	BOL15	BOL19	B06-013	B06-027	B06-023	BOL21	B06-024	CHIC-96h-6
La	26.99	49.60	41.64	41.07	66.50	45.70	43.00	49.19	21.00	
Ce	54.85	100.82	82.39	80.80	124.90	90.70	87.00	97.33	47.90	
Pr	6.78	10.94	9.54	9.30	13.40	10.60	10.40	11.37	6.20	
Nd	26.03	38.09	35.04	33.76	44.60	39.20	39.00	42.38	23.80	
Sm	6.04	6.94	6.83	6.39	7.00	7.60	7.80	8.14	6.90	
Eu	0.69	1.07	1.34	1.19	1.30	1.60	1.60	1.77	0.40	
Gd	5.26	5.12	5.13	4.92	5.20	6.40	6.60	6.72	7.60	
Tb	0.89	0.79	0.75	0.73	0.80	1.00	1.00	1.02	1.40	
Dy	5.22	4.42	3.90	3.93	4.30	5.60	5.90	5.70	8.30	
Ho	1.01	0.84	0.70	0.74	0.80	1.10	1.10	1.09	1.60	
Er	2.64	2.19	1.75	1.90	2.20	2.80	2.90	2.77	4.30	
Tm	0.40	0.32	0.25	0.28	0.30	0.40	0.40	0.40	0.60	
Yb	2.53	2.03	1.54	1.70	2.00	2.50	2.50	2.40	4.00	
Lu	0.38	0.32	0.23	0.25	0.30	0.40	0.40	0.37	0.60	
Li										
Sc	4.13	4.91	10.59	9.09	4.70	11.30	13.10	13.76	5.00	
Co										
Cu	2.30				12.90	5.30	4.50		0.70	
Ga	16.00				16.90	18.80	20.00		16.90	
Cs	15.28	15.30	9.77	14.77	9.00	22.00	26.00	12.98	34.00	
Hf	3.38	4.53	4.76	4.35	5.40	7.40	7.80	7.80	3.40	
Ta	1.76	1.64	1.03	1.26	1.30	1.20	1.50	1.24	4.20	

Tara Ignimbrite System

Unit	Tara	Tara	Tara	Tara	Tara	Tara	Tara	Tara	Tara
Rock Unit	tuff	tuff	pumice	pumice	pumice	pumice	pumice	pumice	pumice
Sample	TARA-96h-32A	CHIC-96h-9	QUIS-96h-7	TARA-96h-1	TARA-96h-2	TARA-96h-34	CHIC-96h-3A	CHIC-96h-7	TARA-96h-
SiO2	71.28	68.26	68.84	69.05	68.64	70.28	68.79	68.40	72.36
TiO2	0.32	0.38	0.52	0.51	0.54	0.32	0.40	0.52	0.26
Al2O3	14.52	14.13	14.27	14.90	15.54	14.49	15.08	15.01	13.62
Fe2O3	2.04	3.67	3.21	1.99	2.01	1.92	2.15	2.52	1.67
MnO	0.08	0.04	0.08	0.05	0.04	0.07	0.05	0.05	0.05
MgO	0.37	0.84	1.10	0.84	0.77	0.44	1.04	0.70	0.42
CaO	1.72	2.47	2.78	2.50	2.76	1.72	2.90	2.59	1.75
Na2O	4.40	2.57	3.21	2.99	3.07	3.63	2.28	2.26	2.46
K2O	3.60	3.56	3.89	3.99	4.43	4.31	4.49	3.96	5.11
P2O5	0.07	0.08	0.14	0.12	0.13	0.08	0.12	0.10	0.07
CO2	0.03	0.06	0.11	0.13	0.06	0.08	0.07	0.11	0.11
H2O	1.56	3.92	1.85	2.93	2.02	2.66	2.64	3.76	2.13
Total	100.00	100.00	100.00	100.00	100.00	100.00	100.00	100.00	100.00
Ba	643.72	630.10	626.15	637.97	829.88	650.63	464.91	821.23	494.57
Cr	<10	<10	<10	<10	<10	<10	11.85	<10	<10
Ni	<10	<10	<10	<10	<10	<10	<10	<10	<10
Rb	186.66	181.05	198.41	206.39	199.47	196.70	220.34	160.77	250.83
Sr	206.68	227.03	213.76	234.90	259.31	207.30	246.77	232.20	138.19
V	5.01	37.72	64.50	36.10	29.53	<10	37.90	46.99	14.71
Y	31.20	15.90	21.46	19.70	29.43	33.44	15.38	22.37	19.08
Zn	61.78	57.33	56.84	62.57	65.99	64.21	45.55	64.28	50.00
Zr	247.29	166.88	171.71	208.90	221.99	249.68	135.99	195.85	141.99
Nb	21.82	12.35	15.48	15.48	14.72	19.42	10.99	13.86	12.30
Th									
U									
Sn									
Pb									

	Tara Ignimbrite System							
Unit	Tara	Tara	Tara	Tara	Tara	Tara	Tara	Tara
Rock Unit	pumice	pumice	pumice	pumice	pumice	pumice	pumice	pumice
Sample	TARA-96h-24	TARA-96h-29a	TARA-96h-29b	TARA-96h-13	TARA-96h-27	TARA-96h-28	TARA-96h-18	TARA-96h-19
SiO2	72.35	61.79	68.18	69.47	71.28	73.08	72.32	74.08
TiO2	0.28	1.09	0.56	0.45	0.33	0.22	0.27	0.21
Al2O3	13.45	16.07	14.61	14.70	14.11	13.48	13.55	13.19
Fe2O3	1.88	5.88	3.25	2.52	2.05	1.50	1.53	1.11
MnO	0.05	0.10	0.07	0.06	0.05	0.05	0.04	0.05
MgO	0.42	1.76	0.90	0.70	0.52	0.34	0.39	0.27
CaO	1.60	4.64	2.85	2.57	1.84	1.39	1.61	1.28
Na2O	2.66	3.31	2.97	2.67	2.67	2.73	2.44	2.70
K2O	4.87	3.10	4.24	4.30	4.79	5.03	4.96	4.98
P2O5	0.07	0.39	0.17	0.09	0.08	0.05	0.07	0.05
CO2	0.13	0.09	0.09	0.07	0.12	0.04	0.18	0.05
H2O	2.25	1.77	2.10	2.41	2.15	2.09	2.65	2.03
Total	100.00	100.00	100.00	100.00	100.00	100.00	100.00	100.00
Ba	423.01	635.38	597.53	758.17	604.76	302.65	441.49	286.36
Cr	<10	<10	<10	<10	<10	<10	20.61	<10
Ni	<10	<10	<10	<10	<10	<10	14.52	<10
Rb	251.59	114.89	193.14	182.34	229.73	263.52	266.01	294.78
Sr	131.93	347.00	230.88	230.61	168.79	108.89	138.41	95.46
V	15.67	71.50	34.73	50.83	20.92	11.25	22.53	<10
Y	21.14	30.59	25.98	19.94	22.02	22.58	17.82	24.11
Zn	53.81	103.72	72.17	60.49	56.55	48.67	54.88	46.95
Zr	152.05	224.44	192.67	196.90	178.84	129.35	142.04	123.08
Nb	13.82	16.36	14.94	12.15	13.76	14.78	13.99	16.25
Th				19.00		29.00		24.00
U				5.10		9.00		10.00
Sn				4.90		3.20		4.20
Pb				28.00		23.00		28.00

	Tara Ignimbrite System							
Unit	Tara	Tara	Tara	Tara	Tara	Tara	Tara	Tara
Rock Unit	pumice	pumice	pumice	pumice	pumice	pumice	pumice	pumice
Sample	TARA-96h-24	TARA-96h-29a	TARA-96h-29b	TARA-96h-13	TARA-96h-27	TARA-96h-28	TARA-96h-18	TARA-96h-19
La				53.00		36.00		30.00
Ce				101.00		64.00		47.00
Pr				12.00		9.50		6.60
Nd				38.00		32.00		24.00
Sm				6.50		6.70		5.90
Eu				1.20		0.82		0.72
Gd				5.10		5.50		5.40
Tb				0.76		0.86		0.87
Dy				4.00		4.60		4.80
Ho				0.79		0.81		0.88
Er				2.10		2.10		2.40
Tm				0.32		0.33		0.35
Yb				2.10		2.10		2.30
Lu				0.35		0.33		0.36
Li				42.00		28.00		23.00
Sc				5.90		4.50		4.40
Co				3.20		0.94		0.89
Cu				5.10		3.10		6.80
Ga				19.00		18.00		17.00
Cs				9.80		18.00		33.00
Hf				3.00		1.90		1.90
Ta				1.30		2.20		2.50

	Tara Ignimbrite System		Puripicar Chico Totoral System						
Unit	Tara	Tara	Tara	Totoral	Totoral	Negreal	Negreal	Puripicar Chico	Puripicar Chico
Rock Unit	pumice	pumice	pumice	lava	lava	lava	lava	pumice	pumice
Sample	CHIC-96h-10	TARA-96h-33	TARA-96h-6b	009BOL*	A-19*	10BOL*	A-01*	BOL23P*	B06-073*
SiO2	71.10	71.11	72.26	65.36	65.16	62.55	62.18	67.48	67.30
TiO2	0.45	0.51	0.21	1.00	1.01	1.09	1.15	0.62	0.63
Al2O3	13.92	13.89	13.49	16.34	16.10	16.72	16.62	15.66	15.50
Fe2O3	1.97	1.93	1.84	4.98	5.10	5.66	5.95	3.93	3.80
MnO	0.06	0.06	0.06	0.07	0.07	0.07	0.08	0.07	0.07
MgO	0.51	0.49	0.46	1.85	1.99	2.68	2.86	1.57	1.67
CaO	1.89	1.85	1.76	4.00	4.15	5.30	5.12	3.79	3.89
Na2O	2.42	2.38	2.27	2.50	2.51	2.41	2.66	3.02	3.09
K2O	5.13	5.22	5.17	3.67	3.69	3.25	3.12	3.70	3.90
P2O5	0.10	0.10	0.10	0.24	0.22	0.28	0.28	0.16	0.14
CO2	0.10	0.11	0.11						
H2O	2.34	2.34	2.28						
Total	100.00	100.00	100.00	100.00	100.00	100.00	100.00	100.00	99.99
Ba	427.49	412.83	398.18	576.10	554.59	603.42	609.25	492.68	481.00
Cr	<10	<10	10.30		15.80		34.90		90.70
Ni	<10	<10	<10		4.90		7.10		65.00
Rb	257.32	261.98	266.64	183.91	180.47	152.02	153.35	175.75	217.00
Sr	140.70	134.61	128.53	275.47	272.68	351.36	348.02	275.62	278.00
V	37.66	37.64	37.68		123.80		151.90		18.70
Y	21.64	21.49	21.35	24.10	24.11	20.60	20.03	18.54	20.00
Zn	58.89	58.79	58.68		100.30		120.00		
Zr	144.75	141.31	137.87	210.68	208.36	253.94	260.34	134.46	138.00
Nb	13.56	13.43	13.31	17.95	17.80	14.29	14.28	12.66	13.50
Th				21.43	20.51	24.05	24.68	23.04	23.00
U				6.30	6.17	4.35	3.82	8.55	8.10
Sn									
Pb				22.28	21.60	18.53	18.01	25.16	10.00

	Tara Ignimbrite System		Puripicar Chico Totoral System						
Unit	Tara	Tara	Tara	Totoral	Totoral	Negreal	Negreal	Puripicar Chico	Puripicar Chico
Rock Unit	pumice	pumice	pumice	lava	lava	lava	lava	pumice	pumice
Sample	CHIC-96h-10	TARA-96h-33	TARA-96h-6b	009BOL*	A-19*	10BOL*	A-01*	BOL23P*	B06-073*
La				49.78	48.44	56.77	58.83	35.37	32.80
Ce				102.11	99.43	121.93	126.82	65.61	64.90
Pr				12.22	11.86	14.98	15.84	7.74	7.50
Nd				45.60	44.46	56.04	59.46	27.75	27.70
Sm				8.93	8.89	9.88	10.31	5.35	5.60
Eu				1.56	1.57	1.61	1.64	1.09	1.10
Gd				6.95	6.91	6.72	6.83	4.34	4.60
Tb				1.02	1.00	0.91	0.91	0.66	0.70
Dy				5.25	5.21	4.64	4.59	3.72	3.90
Ho				0.91	0.92	0.78	0.78	0.69	0.70
Er				2.24	2.17	1.85	1.81	1.79	1.90
Tm				0.30	0.29	0.25	0.24	0.26	0.30
Yb				1.75	1.75	1.43	1.42	1.61	1.70
Lu				0.26	0.26	0.21	0.20	0.26	0.30
Li									
Sc				9.68	10.57	11.02	12.06	8.07	8.70
Co									
Cu					5.40		7.00		66.90
Ga					21.70		21.10		20.30
Cs				12.19	11.60	5.70	4.39	12.66	15.00
Hf				5.90	5.92	6.66	6.96	4.08	4.30
Ta				1.68	1.65	1.07	1.00	1.39	1.50

Appendix C Ar-Ar analysis

36Ar(a)	37Ar(ca)	38Ar(cl)	39Ar(k)	40Ar(r)	Age ± 2σ (Ma)	40Ar(r) (%)	39Ar(k) (%)	K/Ca ± 2σ
0.000330	0.003075	0.000211	0.010519	0.006074	1.51 ± 2.68	5.86	1.21	1.471 ± 0.045
0.000435	0.006644	0.000473	0.029107	0.017260	1.55 ± 0.75	11.82	3.34	1.884 ± 0.050
0.000501	0.020649	0.001105	0.068359	0.038801	1.48 ± 0.27	20.76	7.84	1.424 ± 0.037
0.000866	0.073784	0.002568	0.181541	0.106508	1.53 ± 0.09	29.36	20.83	1.058 ± 0.025
0.000565	0.071912	0.002004	0.138279	0.080158	1.52 ± 0.12	32.42	15.87	0.827 ± 0.019
0.000377	0.052429	0.001289	0.084707	0.049650	1.53 ± 0.10	30.82	9.72	0.695 ± 0.016
0.000381	0.048798	0.001230	0.078968	0.046718	1.55 ± 0.11	29.32	9.06	0.696 ± 0.016
0.000401	0.043459	0.001049	0.072775	0.043671	1.57 ± 0.10	26.91	8.35	0.720 ± 0.017
0.000521	0.047000	0.001285	0.083597	0.049365	1.54 ± 0.13	24.27	9.59	0.765 ± 0.018
0.000391	0.037994	0.001135	0.072580	0.043626	1.57 ± 0.33	27.40	8.33	0.821 ± 0.019
0.000285	0.025902	0.000779	0.051026	0.030298	1.55 ± 0.33	26.42	5.86	0.847 ± 0.020
0.005054	0.431646	0.013129	0.871456	0.512130				

Results	40(r)/39(k) ± 2σ	Age ± 2σ (Ma)	MSWD	39Ar(k) (%,n)	K/Ca ± 2σ
Weighted Plateau	0.5891 ± 0.0158 ± 2.68%	1.54 ± 0.04 ± 2.90%	0.08	100.00 11	0.826 ± 0.136
		External Error ± 0.05	2.23	Statistical T Ratio	
		Analytical Error ± 0.04	1.0000	Error Magnification	
Total Fusion Age	0.5877 ± 0.0253 ± 4.31%	1.54 ± 0.07 ± 4.44%		11	0.868 ± 0.007
		External Error ± 0.07			
		Analytical Error ± 0.07			

12C1414.AGE >>> 10001 >>> DE SILVA PROJECT

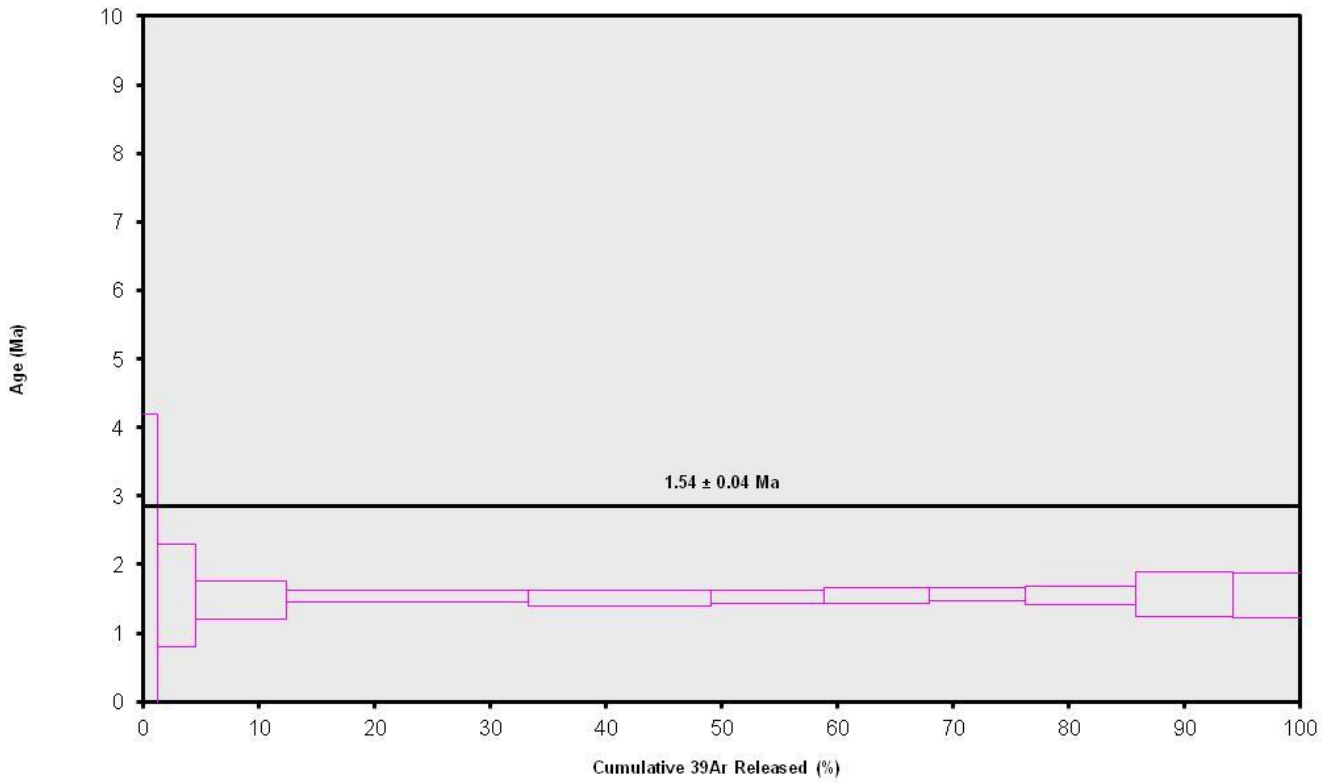

Ar-Ages in Ma

WEIGHTED PLATEAU
1.54 ± 0.04
TOTAL FUSION
1.54 ± 0.07
NORMAL ISOCHRON
1.52 ± 0.22
INVERSE ISOCHRON
1.52 ± 0.22

MSWD
0.08

Sample Info

groundmass
Bolivia
jfk

IRR = OSU1A12
J = 0.0014496 ± 0.0000080

Appendix D Zircon U-Pb SIMS analyses

Purpica Chico Ignimbrite	238U/ 206Pb	238U/ 206Pb 1 s.e.	207Pb/ 206Pb	207Pb/ 206Pb 1 s.e.	Correlation of TW Concordia Ellipses	204Pb/ 206Pb	204Pb/ 206Pb 1 s.e.	% 206Pb*	206Pb/ 238U age [Ma]	206Pb/ 238U age [Ma] 1 s.e.	U ppm	U/ Th	UO/U
07-BOL-023-PD@27.ais	1416.23	31.49	0.06	0.01	-0.04	0.00	0.00	97.81	4.55	0.11	879.57	4.34	7.84
07-BOL-023-PD@51.ais	2333.72	58.27	0.06	0.00	-0.19	0.00	0.00	97.64	2.79	0.07	1026.94	3.85	7.93
07BOL-023-PD@9.ais	2311.60	60.92	0.13	0.02	-0.47	0.01	0.00	89.86	2.60	0.09	1147.46	4.01	7.83
07-BOL-023-PD@20.ais	50.66	3.85	0.81	0.00	-0.01	0.05	0.00	1.95	2.57	13.65	1265.95	3.19	8.02
07BOL-023-PD@15.ais	2540.65	59.00	0.08	0.01	0.16	0.01	0.00	95.85	2.53	0.06	955.66	3.35	7.93
07-BOL-023-PD@32.ais	2639.22	63.04	0.06	0.00	-0.02	0.00	0.00	98.77	2.50	0.06	2514.13	2.58	7.79
07-BOL-023-PD@25.ais	2577.98	57.75	0.08	0.01	0.40	0.01	0.00	95.87	2.49	0.06	1056.56	3.27	8.01
07-BOL-023-PD@48.ais	499.50	18.89	0.68	0.02	-0.29	0.05	0.00	18.36	2.47	0.80	661.12	4.87	7.65
07-BOL-023-PD@44.ais	2442.60	63.24	0.17	0.01	-0.23	0.01	0.00	84.15	2.31	0.07	1481.63	2.90	7.89
07-BOL-023-PD@21.ais	2865.33	61.82	0.06	0.00	-0.07	0.00	0.00	98.19	2.29	0.05	1947.62	1.93	7.90
07-BOL-023-PD@45.ais	2317.50	106.34	0.21	0.02	-0.44	0.01	0.00	78.62	2.29	0.16	434.70	5.30	7.87
07BOL-023-PD@14.ais	2834.47	79.14	0.08	0.00	0.03	0.01	0.00	95.81	2.28	0.06	1644.92	4.59	7.76
07-BOL-023-PD@33.ais	2806.62	77.67	0.09	0.01	-0.12	0.01	0.00	94.55	2.27	0.07	862.36	4.20	8.01
07-BOL-023-PD@36.ais	2864.51	66.71	0.07	0.01	0.24	0.00	0.00	96.46	2.26	0.06	1114.14	3.02	7.76
07-BOL-023-PD@19.ais	2933.41	63.76	0.07	0.00	0.14	0.00	0.00	97.19	2.23	0.05	1804.32	3.25	7.78
07-BOL-023-PD@39.ais	2961.21	70.24	0.07	0.00	-0.33	0.00	0.00	96.74	2.20	0.05	1534.77	2.66	7.84
07-BOL-023-PD@49.ais	2773.93	69.10	0.12	0.01	-0.15	0.01	0.00	90.30	2.19	0.07	1005.10	4.05	7.73
07BOL-023-PD@12.ais	2992.22	76.91	0.07	0.01	-0.06	0.00	0.00	97.32	2.19	0.06	1286.13	3.20	7.89
07-BOL-023-PD@26.ais	2961.21	78.04	0.08	0.01	-0.03	0.00	0.00	96.26	2.19	0.06	1212.45	3.37	7.76
07BOL-023-PD@5.ais	2961.21	77.34	0.08	0.01	-0.01	0.01	0.00	95.82	2.18	0.06	1054.71	2.87	8.05
07-BOL-023-PD@42.ais	2977.08	75.78	0.09	0.01	0.00	0.01	0.00	94.64	2.14	0.06	845.88	3.71	7.90
07-BOL-023-PD@29.ais	3067.48	72.36	0.07	0.00	0.22	0.00	0.00	97.07	2.13	0.05	1432.39	3.27	7.76
07BOL-023-PD@4.ais	3060.91	66.71	0.08	0.01	0.27	0.01	0.00	96.06	2.12	0.05	1177.46	3.16	8.05
07-BOL-023-PD@46.ais	3103.66	50.38	0.06	0.00	0.05	0.00	0.00	98.15	2.12	0.03	2880.69	1.61	8.09
07-BOL-023-PD@31.ais	3071.25	72.07	0.08	0.01	0.25	0.00	0.00	96.13	2.11	0.05	947.52	3.39	7.78
07-BOL-023-PD@24.ais	3159.56	84.65	0.07	0.01	0.02	0.01	0.00	96.84	2.07	0.06	1332.23	3.80	7.77

Purpica Chico Ignimbrite	238U/ 206Pb	238U/ 206Pb 1 s.e.	207Pb/ 206Pb	207Pb/ 206Pb 1 s.e.	Correlation of TW Concordia Ellipses	204Pb/ 206Pb	204Pb/ 206Pb 1 s.e.	% 206Pb*	206Pb/ 238U age [Ma]	206Pb/ 238U age [Ma] 1 s.e.	U ppm	U/ Th	UO/U
07-BOL-023-PD@30.ais	3129.89	74.35	0.08	0.01	0.15	0.00	0.00	95.92	2.07	0.05	1123.03	3.54	7.78
07BOL-023-PD@1.ais	2758.62	73.28	0.17	0.01	-0.27	0.01	0.00	83.64	2.04	0.07	1537.91	2.62	7.78
07BOL-023-PD@11.ais	3112.36	80.50	0.09	0.01	-0.03	0.00	0.00	93.81	2.04	0.06	661.67	4.36	7.99
07-BOL-023-PD@18.ais	3163.56	89.07	0.08	0.01	0.05	0.00	0.00	95.11	2.03	0.06	737.02	3.13	7.80
07-BOL-023-PD@52.ais	3133.81	98.11	0.09	0.01	0.54	0.01	0.00	93.92	2.03	0.07	867.36	4.16	7.88
07BOL-023-PD@3.ais	3249.92	87.77	0.07	0.01	0.12	0.00	0.00	96.38	2.00	0.06	1300.20	2.75	7.76
07-BOL-023-PD@35.ais	2850.63	81.02	0.17	0.01	0.38	0.01	0.00	84.66	2.00	0.07	1233.55	2.23	7.39
07-BOL-023-PD@38.ais	2798.77	61.80	0.18	0.01	0.02	0.01	0.00	82.61	2.00	0.06	1169.12	3.33	7.96
07-BOL-023-PD@40.ais	3243.59	73.54	0.09	0.01	-0.06	0.00	0.00	94.95	1.98	0.05	1050.64	3.36	7.94
07BOL-023-PD@2.ais	1394.70	89.09	0.51	0.02	0.04	0.04	0.00	40.61	1.96	0.35	1400.91	1.68	7.76
07BOL-023-PD@10.ais	3245.70	86.49	0.10	0.01	0.11	0.00	0.00	92.94	1.94	0.06	1167.46	3.09	7.80
07-BOL-023-PD@34.ais	2291.48	70.36	0.32	0.03	-0.21	0.02	0.01	64.80	1.92	0.13	531.71	4.14	7.90
07-BOL-023-PD@28.ais	3369.27	77.99	0.08	0.01	0.18	0.01	0.00	95.29	1.91	0.05	1198.19	2.34	7.84
07-BOL-023-PD@17.ais	2572.68	76.78	0.27	0.01	0.09	0.03	0.01	71.99	1.90	0.09	910.86	3.12	7.83
07-BOL-023-PD@41.ais	2965.60	86.63	0.18	0.01	-0.17	0.01	0.00	82.48	1.89	0.07	1064.89	3.40	7.88
07BOL-023-PD@8.ais	3405.99	77.26	0.09	0.01	0.17	0.01	0.00	94.77	1.89	0.04	1199.49	3.13	7.81
07-BOL-023-PD@23.ais	3454.23	99.51	0.08	0.01	-0.17	0.01	0.00	95.70	1.87	0.06	978.07	2.36	7.84
07-BOL-023-PD@37.ais	3005.71	128.29	0.19	0.02	-0.43	0.01	0.00	81.98	1.85	0.11	791.08	3.02	7.79
07BOL-023-PD@13.ais	3572.70	90.12	0.07	0.01	0.07	0.00	0.00	96.85	1.84	0.05	1440.35	3.47	7.81
07BOL-023-PD@7.ais	3505.08	95.09	0.09	0.01	-0.24	0.01	0.00	94.20	1.83	0.06	768.49	3.68	7.82
07-BOL-023-PD@50.ais	1415.03	100.92	0.53	0.03	-0.30	0.04	0.00	37.75	1.81	0.47	947.89	3.56	7.88
07BOL-023-PD@6.ais	3563.79	95.76	0.08	0.01	0.04	0.00	0.00	95.05	1.81	0.05	1100.99	3.21	7.86
07-BOL-023-PD@43.ais	3461.41	101.12	0.11	0.01	0.42	0.01	0.00	91.77	1.80	0.06	894.20	2.51	7.67
07-BOL-023-PD@47.ais	3543.59	87.27	0.10	0.01	-0.18	0.00	0.00	92.88	1.78	0.05	988.43	3.06	8.03
07-BOL-023-PD@16.ais	572.41	13.96	0.73	0.02	0.10	0.04	0.01	12.59	1.52	0.41	404.89	4.47	7.86

Guacha Ignimbrite	238U/ 206Pb	238U/ 206Pb 1 s.e.	207Pb/ 206Pb	207Pb/ 206Pb 1 s.e.	Correlation of TW Concordia Ellipses	204Pb/ 206Pb	204Pb/ 206Pb 1 s.e.	% 206Pb*	206Pb/ 238U age [Ma]	206Pb/ 238U age [Ma] 1 s.e.	U ppm	U/ Th	UO/U
ARIBOL 10007@38.ais	12.00	0.31	0.06	0.00	0.68	0.00	0.00	99.44	513.14	12.70	300.84	2.06	8.03
ARIBOL 10007@26.ais	887.31	19.45	0.05	0.00	0.23	0.00	0.00	98.90	7.29	0.16	891.42	11.05	8.00
ARIBOL 10007@33.ais	962.46	18.06	0.06	0.00	0.28	0.00	0.00	98.25	6.68	0.13	580.21	4.53	8.10
ARIBOL 10007@7.ais	956.94	21.70	0.09	0.01	0.10	0.00	0.00	94.49	6.44	0.16	243.27	1.92	7.79
ARIBOL 10007@18.ais	1005.43	20.62	0.05	0.00	0.02	0.00	0.00	98.98	6.43	0.13	797.19	2.63	7.87
ARIBOL 10007@31.ais	1005.33	18.60	0.06	0.01	-0.06	0.00	0.00	98.18	6.37	0.13	714.80	1.79	7.95
ARIBOL 10007@30.ais	997.01	25.15	0.07	0.01	0.27	n.d.	n.d.	97.21	6.37	0.17	323.06	2.53	7.76
ARIBOL 10007@34.ais	1009.29	28.11	0.06	0.01	0.67	0.00	0.00	97.62	6.32	0.18	586.51	2.86	7.90
ARIBOL 10007@37.ais	995.02	33.96	0.08	0.01	-0.28	0.00	0.00	95.37	6.26	0.23	318.25	2.57	7.85
ARIBOL 10007@13.ais	1006.44	26.03	0.07	0.01	0.17	0.00	0.00	96.35	6.26	0.17	408.04	2.95	7.79
ARIBOL 10007@21.ais	1005.03	27.58	0.08	0.01	0.20	0.00	0.00	95.61	6.22	0.18	288.81	2.32	7.89
ARIBOL 10007@19.ais	1042.75	33.38	0.05	0.01	0.45	0.01	0.00	98.97	6.21	0.20	440.06	2.93	7.70
ARIBOL 10007@20.ais	1031.03	24.87	0.07	0.01	0.29	0.01	0.00	96.87	6.14	0.16	425.81	2.57	7.89
ARIBOL 10007@36.ais	1043.41	26.67	0.06	0.01	0.63	n.d.	n.d.	97.68	6.12	0.17	414.89	2.70	7.95
ARIBOL 10007@4.ais	1044.06	28.12	0.07	0.01	-0.06	0.00	0.00	96.93	6.07	0.17	318.25	2.09	7.82
ARIBOL 10007@15.ais	1048.11	35.48	0.07	0.01	-0.08	n.d.	n.d.	96.44	6.02	0.22	265.48	3.00	8.11
ARIBOL 10007@17.ais	1068.83	22.05	0.07	0.01	0.02	n.d.	n.d.	97.56	5.97	0.13	414.15	3.28	8.04
ARIBOL 10007@10.ais	1066.21	26.83	0.07	0.01	0.14	0.00	0.00	96.74	5.93	0.16	549.29	2.06	7.74
ARIBOL 10007@2.ais	1075.96	21.07	0.07	0.01	0.06	0.00	0.00	96.91	5.90	0.12	333.24	2.97	7.98
ARIBOL 10007@3.ais	1043.95	31.50	0.09	0.01	0.13	0.00	0.00	93.98	5.89	0.20	222.16	3.24	7.98
ARIBOL 10007@9.ais	1090.99	28.92	0.06	0.00	-0.03	0.00	0.00	98.03	5.88	0.16	547.81	2.34	7.89
ARIBOL 10007@28.ais	1051.41	33.83	0.09	0.01	-0.32	0.00	0.00	94.33	5.87	0.22	275.11	3.14	7.94
ARIBOL 10007@32.ais	1057.53	25.39	0.09	0.01	0.23	0.00	0.00	94.63	5.85	0.16	502.27	1.91	8.06
ARIBOL 10007@12.ais	1105.71	32.89	0.06	0.00	0.30	0.00	0.00	98.67	5.83	0.18	684.44	1.79	7.86
ARIBOL 10007@35.ais	1084.72	30.24	0.07	0.01	0.48	0.00	0.00	96.52	5.82	0.17	495.23	2.70	7.87
ARIBOL 10007@29.ais	1090.99	31.78	0.07	0.01	0.01	0.00	0.00	96.70	5.81	0.18	564.10	3.67	8.10

Guacha Ignimbrite	238U/ 206Pb	238U/ 206Pb 1 s.e.	207Pb/ 206Pb	207Pb/ 206Pb 1 s.e.	Correlation of TW Concordia Ellipses	204Pb/ 206Pb	204Pb/ 206Pb 1 s.e.	% 206Pb*	206Pb/ 238U age [Ma]	206Pb/ 238U age [Ma] 1 s.e.	U ppm	U/ Th	UO/U
ARIBOL 10007@27.ais	1120.32	24.98	0.06	0.01	0.46	0.00	0.00	98.73	5.77	0.14	666.48	2.34	8.10
ARIBOL 10007@11.ais	1100.11	26.99	0.07	0.01	-0.09	0.01	0.00	96.83	5.76	0.16	354.72	2.23	8.15
ARIBOL 10007@25.ais	1038.10	40.74	0.12	0.02	-0.07	0.00	0.00	90.86	5.73	0.29	145.28	2.75	7.86
ARIBOL 10007@16.ais	1104.00	31.08	0.08	0.01	-0.31	0.01	0.00	95.49	5.66	0.18	314.54	2.95	8.03
ARIBOL 10007@6.ais	1091.46	20.25	0.09	0.00	0.01	0.00	0.00	94.09	5.64	0.11	844.03	1.96	8.05
ARIBOL 10007@1.ais	1117.69	29.36	0.08	0.01	0.11	0.00	0.00	95.89	5.61	0.16	251.60	1.81	8.07
ARIBOL 10007@8.ais	1153.93	27.56	0.07	0.01	-0.10	0.00	0.00	96.37	5.47	0.14	331.21	2.18	8.14
ARIBOL 10007@14.ais	1119.57	39.11	0.10	0.02	0.22	0.01	0.01	92.80	5.43	0.23	200.69	2.18	7.87
ARIBOL 10007@23.ais	1258.18	185.21	0.06	0.00	0.12	0.00	0.00	98.15	5.12	0.76	589.10	2.76	8.43
ARIBOL 10007@24.ais	1223.54	32.34	0.09	0.01	0.13	0.01	0.01	94.13	5.04	0.15	191.80	2.19	8.45
Tara Ignimbrite													
BOL-06-013@32.ais	1013.58	24.35	0.07	0.01	0.50	0.00	0.00	97.19	6.27	0.16	444.14	2.80	7.85
BOL-06-013@31.ais	1420.66	36.93	0.08	0.01	-0.11	0.01	0.00	96.01	4.44	0.12	398.96	2.47	7.87
BOL-06-013@27.ais	1607.98	41.63	0.08	0.01	0.37	0.01	0.00	95.31	3.92	0.11	552.07	4.38	7.77
BOL-06-013@5.ais	1546.07	38.48	0.11	0.01	0.15	0.01	0.00	91.67	3.90	0.11	541.70	1.76	7.52
BOL-06-013@36.ais	1614.73	34.16	0.09	0.00	-0.03	0.00	0.00	94.80	3.88	0.09	1629.74	3.57	7.83
BOL-06-013@45.ais	1678.98	31.57	0.06	0.00	-0.05	0.00	0.00	98.21	3.86	0.07	2467.84	3.48	7.77
BOL-06-013@8.ais	1610.05	47.44	0.09	0.01	-0.16	0.01	0.00	93.84	3.85	0.12	565.22	3.91	7.63
BOL-06-013@47.ais	1685.77	39.79	0.07	0.01	0.25	0.00	0.00	96.97	3.80	0.09	739.43	3.07	7.69
BOL-06-013@20.ais	1652.07	42.30	0.09	0.01	-0.23	0.01	0.00	94.00	3.76	0.11	507.45	3.54	7.71
BOL-06-013@50.ais	643.09	15.38	0.54	0.01	0.00	0.04	0.01	36.37	3.73	0.32	332.87	2.35	7.83
BOL-06-013@21.ais	1687.48	43.57	0.08	0.01	-0.39	0.01	0.00	95.17	3.73	0.10	422.66	2.89	7.75
BOL-06-013@48.ais	1631.06	65.18	0.11	0.01	0.42	0.01	0.00	92.01	3.72	0.16	369.90	2.23	7.29
BOL-06-013@10.ais	1543.45	48.12	0.15	0.01	0.26	0.02	0.01	87.08	3.71	0.15	236.05	1.70	7.72
BOL-06-013@35.ais	1247.19	109.20	0.28	0.03	-0.39	0.05	0.01	69.92	3.71	0.54	412.85	3.43	7.45
BOL-06-013@25.ais	1705.32	41.30	0.08	0.01	0.13	0.01	0.00	95.30	3.70	0.10	356.94	3.59	7.68

Tara Ignimbrite	238U/ 206Pb	238U/ 206Pb 1 s.e.	207Pb/ 206Pb	207Pb/ 206Pb 1 s.e.	Correlation of TW Concordia Ellipses	204Pb/ 206Pb	204Pb/ 206Pb 1 s.e.	% 206Pb*	206Pb/ 238U age [Ma]	206Pb/ 238U age [Ma] 1 s.e.	U ppm	U/ Th	UO/U
BOL-06-013@28.ais	912.41	73.84	0.43	0.03	-0.24	0.04	0.01	50.65	3.67	0.75	280.29	4.25	7.96
BOL-06-013@17.ais	1548.47	45.32	0.15	0.01	0.00	0.01	0.00	86.53	3.67	0.13	502.64	1.39	7.94
BOL-06-013@7.ais	1719.10	36.94	0.08	0.00	0.16	0.00	0.00	95.22	3.67	0.08	1203.74	4.68	7.66
BOL-06-013@6.ais	1567.15	74.42	0.15	0.01	-0.06	0.02	0.01	87.19	3.66	0.21	236.97	1.69	7.67
BOL-06-013@40.ais	1599.23	51.15	0.14	0.01	0.46	0.02	0.01	88.31	3.64	0.14	239.19	1.96	7.79
BOL-06-013@29.ais	1668.61	57.63	0.11	0.01	0.40	0.02	0.01	91.70	3.63	0.14	257.34	3.21	7.92
BOL-06-013@2.ais	1648.26	69.01	0.13	0.01	0.05	0.02	0.01	89.68	3.60	0.17	243.27	2.74	7.75
BOL-06-013@12.ais	646.83	14.48	0.55	0.01	0.03	0.04	0.01	35.18	3.59	0.30	397.67	2.37	7.60
BOL-06-013@26.ais	1731.90	55.79	0.10	0.01	0.69	0.00	0.00	93.68	3.57	0.13	319.73	2.54	7.82
BOL-06-013@16.ais	1693.48	49.33	0.11	0.01	0.15	0.00	0.00	91.37	3.57	0.12	373.79	2.68	7.71
BOL-06-013@19.ais	1495.44	38.91	0.20	0.01	-0.08	0.02	0.01	80.53	3.56	0.13	353.61	3.39	7.66
BOL-06-013@14.ais	1692.05	54.97	0.12	0.01	-0.26	0.02	0.01	91.10	3.55	0.14	351.02	2.16	7.71
BOL-06-013@9.ais	1670.56	47.16	0.12	0.02	0.11	0.02	0.01	89.94	3.55	0.13	348.05	2.13	7.73
BOL-06-013@42.ais	911.58	43.38	0.45	0.03	-0.44	0.02	0.00	48.72	3.54	0.54	313.43	3.26	7.69
BOL-06-013@37.ais	1752.54	70.34	0.10	0.01	0.22	0.01	0.01	93.68	3.53	0.15	291.40	2.46	7.92
BOL-06-013@11.ais	1731.30	43.16	0.11	0.01	-0.08	0.01	0.00	92.36	3.53	0.10	472.83	2.61	7.72
BOL-06-013@15.ais	1625.22	81.35	0.15	0.02	-0.35	0.02	0.01	86.46	3.52	0.24	242.53	3.53	7.92
BOL-06-013@22.ais	1708.82	63.95	0.12	0.01	0.11	0.03	0.01	91.15	3.52	0.15	261.04	1.97	7.89
BOL-06-013@38.ais	1751.01	52.43	0.10	0.01	0.44	0.01	0.00	93.08	3.51	0.12	459.50	2.03	7.82
BOL-06-013@23.ais	1774.31	48.80	0.09	0.01	0.48	0.01	0.00	94.41	3.50	0.10	476.35	1.45	7.78
BOL-06-013@46.ais	1720.87	59.52	0.12	0.01	0.39	0.00	0.00	91.18	3.50	0.14	216.42	1.99	7.75
BOL-06-013@43.ais	1818.84	49.29	0.08	0.01	0.25	0.01	0.00	96.22	3.49	0.10	555.22	1.96	7.94
BOL-06-013@4.ais	1689.47	41.10	0.13	0.01	0.24	0.01	0.00	89.24	3.49	0.10	538.74	2.28	7.65
BOL-06-013@49.ais	1585.04	41.96	0.17	0.01	0.04	0.02	0.01	83.94	3.49	0.12	351.94	1.57	7.71
BOL-06-013@41.ais	1771.17	64.62	0.10	0.01	0.42	0.02	0.01	93.19	3.48	0.14	330.84	2.25	7.97
BOL-06-013@24.ais	1726.52	58.43	0.12	0.01	0.13	0.01	0.00	90.83	3.48	0.14	256.04	2.28	7.66

Tara Ignimbrite	238U/ 206Pb	238U/ 206Pb 1 s.e.	207Pb/ 206Pb	207Pb/ 206Pb 1 s.e.	Correlation of TW Concordia Ellipses	204Pb/ 206Pb	204Pb/ 206Pb 1 s.e.	% 206Pb*	206Pb/ 238U age [Ma]	206Pb/ 238U age [Ma] 1 s.e.	U ppm	U/ Th	UO/U
BOL-06-013@34.ais	1888.57	74.54	0.06	0.00	-0.22	0.00	0.00	98.41	3.45	0.14	1412.95	4.02	7.94
BOL-06-013@13.ais	1733.40	46.27	0.13	0.01	0.46	0.01	0.00	89.77	3.42	0.11	351.94	1.87	7.89
BOL-06-013@3.ais	1719.39	64.74	0.14	0.01	-0.02	0.03	0.01	87.54	3.36	0.15	330.84	1.81	7.83
BOL-06-013@30.ais	1583.53	41.63	0.20	0.01	0.16	0.03	0.01	80.51	3.36	0.12	379.90	1.94	7.93
BOL-06-013@44.ais	1858.39	78.05	0.10	0.01	0.65	0.02	0.01	93.70	3.34	0.15	375.82	2.25	7.39
BOL-06-013@39.ais	1896.09	79.81	0.08	0.01	0.17	0.02	0.01	95.17	3.32	0.15	400.82	2.26	7.33
BOL-06-013@33.ais	1354.28	51.90	0.31	0.02	-0.09	0.04	0.01	65.91	3.22	0.24	324.73	2.11	7.74
BOL-06-013@18_1.ais	73.05	2.26	0.81	0.01	-0.03	0.05	0.00	2.40	2.19	3.96	246.41	1.47	7.76

Kalina lava dome	238U/206Pb	238U/206Pb	207Pb*/ 206Pb*	207Pb*/ 206Pb*	Correlation of TW Concordia Ellipses	% 206Pb*	206/238 age [Ma]	±1s [Ma]	U ppm	UO/U
		1 s.e.		1 s.e.				1 s.e.		
2012_3_18Mar\ SDS10_004@1.ais	1149.0	67.2	0.1287	0.0229	0.44	89.4	5.09	0.36	130	8.7
2012_3_18Mar\ SDS10_004@3.ais	1201.8	41.6	0.0512	0.0034	0.02	99.4	5.42	0.19	2415	8.9
2012_3_18Mar\ SDS10_004@4.ais	1109.6	42.5	0.0521	0.0023	-0.01	99.2	5.83	0.22	2935	8.7
2012_3_18Mar\ SDS10_004@5.ais	1140.9	51.8	0.0791	0.0091	0.11	95.8	5.50	0.26	265	8.9
2012_3_18Mar\ SDS10_004@6.ais	1188.1	52.9	0.0684	0.0059	0.09	97.2	5.36	0.25	510	8.8
2012_3_18Mar\ SDS10_004@7.ais	1092.4	56.0	0.1442	0.0139	-0.02	87.5	5.25	0.32	192	8.7
2012_3_18Mar\ SDS10_004@8.ais	1195.6	54.3	0.0594	0.0062	0.14	98.3	5.39	0.25	608	8.8
2012_3_18Mar\ SDS10_004@9.ais	585.8	30.2	0.4571	0.0241	-0.13	47.4	5.32	0.75	371	8.7
2012_3_18Mar\ SDS10_004@10.ais	1127.1	44.6	0.0632	0.0066	0.09	97.8	5.68	0.23	1056	8.7
2012_3_18Mar\ SDS10_004@11.ais	1179.1	65.2	0.0837	0.0111	0.03	95.2	5.29	0.31	206	8.9
2012_3_18Mar\ SDS10_004@12.ais	1056.3	46.3	0.0621	0.0056	0.12	98.0	6.06	0.27	627	8.6
2012_3_18Mar\ SDS10_004@13.ais	1126.6	49.1	0.0656	0.0062	0.12	97.5	5.66	0.25	484	8.7
2012_3_18Mar\ SDS10_004@14.ais	1138.7	63.0	0.0611	0.0103	0.43	98.1	5.65	0.32	365	8.8
2012_3_18Mar\ SDS10_004@15.ais	328.6	13.6	0.5889	0.0059	-0.02	30.6	6.09	1.01	1437	8.7
2012_3_18Mar\ SDS10_004@16.ais	1079.8	57.8	0.0536	0.0066	0.34	99.0	6.00	0.32	413	8.6
2012_3_18Mar\ SDS10_004@17.ais	1137.3	70.2	0.0886	0.0118	-0.41	94.6	5.44	0.37	219	8.7
2012_3_18Mar\ SDS10_004@18.ais	1156.3	52.9	0.0633	0.0058	0.23	97.8	5.54	0.26	534	8.7
2012_3_18Mar\ SDS10_004@19.ais	1104.9	43.2	0.0687	0.0053	-0.12	97.1	5.76	0.23	642	8.7
2012_3_18Mar\ SDS10_004@2.ais	1139.0	44.0	0.0546	0.0052	0.12	98.9	5.68	0.22	1171	8.6
2012_3_18Mar\ SDS10_004@20.ais	727.8	27.4	0.3452	0.0082	-0.06	61.8	5.55	0.38	849	8.7
2012_3_18Mar\ SDS10_004@21.ais	900.1	42.4	0.1542	0.0110	-0.21	86.2	6.26	0.36	1456	8.6
2012_3_18Mar\ SDS10_004@22.ais	969.0	50.9	0.1488	0.0066	-0.13	86.9	5.86	0.36	491	8.6
2012_3_18Mar\ SDS10_004@23.ais	414.8	36.8	0.5182	0.0182	-0.18	39.6	6.24	1.79	955	8.4
2012_3_18Mar\ SDS10_004@24.ais	1085.1	58.3	0.0773	0.0081	0.14	96.0	5.79	0.32	349	8.7

Guacha Ignimbrite	238U/206Pb	238U/206Pb	207Pb*/ 206Pb*	207Pb*/ 206Pb*	Correlation of TW Concordia Ellipses	% 206Pb*	206/238 age [Ma]	±1s [Ma]	U ppm	UO/U
		1 s.e.		1 s.e.				1 s.e.		
2012_3_18Mar\ SDS10_011@1.ais	1093.7	44.7	0.0555	0.0036	0.14	98.8	5.90	0.24	1237	8.6
2012_3_18Mar\ SDS10_011@10.ais	1208.6	53.3	0.0744	0.0136	0.09	96.4	5.23	0.25	296	8.8
2012_3_18Mar\ SDS10_011@11.ais	1168.0	44.2	0.0526	0.0034	0.03	99.2	5.55	0.21	1503	8.7
2012_3_18Mar\ SDS10_011@12.ais	1152.1	57.9	0.0698	0.0094	0.16	97.0	5.51	0.29	303	8.9
2012_3_18Mar\ SDS10_011@13.ais	1109.1	44.3	0.0609	0.0077	-0.01	98.1	5.78	0.24	763	8.8
2012_3_18Mar\ SDS10_011@14.ais	1115.7	42.3	0.0485	0.0031	0.08	99.7	5.85	0.22	2186	8.8
2012_3_18Mar\ SDS10_011@15.ais	1115.7	62.1	0.0700	0.0089	0.28	97.0	5.69	0.33	253	8.7
2012_3_18Mar\ SDS10_011@16.ais	1136.9	55.1	0.0725	0.0061	-0.11	96.6	5.56	0.28	702	8.8
2012_3_18Mar\ SDS10_011@17.ais	1110.0	43.7	0.0720	0.0059	-0.10	96.7	5.70	0.23	1488	8.7
2012_3_18Mar\ SDS10_011@18.ais	1115.7	46.9	0.0640	0.0049	0.06	97.7	5.73	0.25	677	8.6
2012_3_18Mar\ SDS10_011@19.ais	1077.6	49.0	0.1079	0.0144	0.02	92.1	5.60	0.29	249	8.7
2012_3_18Mar\ SDS10_011@2.ais	1098.7	47.6	0.0646	0.0087	0.25	97.6	5.81	0.26	673	8.7
2012_3_18Mar\ SDS10_011@20.ais	1015.8	40.3	0.1228	0.0128	-0.13	90.2	5.81	0.27	655	8.7
2012_3_18Mar\ SDS10_011@3.ais	1046.9	46.5	0.0824	0.0110	0.27	95.4	5.96	0.28	575	8.6
2012_3_18Mar\ SDS10_011@4.ais	1137.4	48.0	0.0510	0.0035	-0.04	99.4	5.72	0.24	1166	8.7
2012_3_18Mar\ SDS10_011@5.ais	1118.4	56.2	0.0730	0.0067	0.14	96.6	5.65	0.29	587	8.7
2012_3_18Mar\ SDS10_011@6.ais	1167.5	58.3	0.0903	0.0094	0.15	94.4	5.30	0.28	404	8.9
2012_3_18Mar\ SDS10_011@7.ais	1173.7	50.6	0.0647	0.0100	0.22	97.6	5.45	0.25	472	8.7
2012_3_18Mar\ SDS10_011@8.ais	1116.9	43.7	0.0535	0.0040	-0.02	99.1	5.80	0.23	1549	8.7
2012_3_18Mar\ SDS10_011@9.ais	1124.4	55.1	0.0761	0.0104	0.14	96.2	5.60	0.29	247	8.9
Totoral lava dome										
2012_3_18Mar\ SDS10_019@1.ais	1772.4	75.1	0.0647	0.0069	0.06	97.6	3.65	0.16	944	8.8
2012_3_18Mar\ SDS10_019@2.ais	1711.7	70.3	0.0674	0.0047	0.06	97.3	3.76	0.16	1187	8.6
2012_3_18Mar\ SDS10_019@3.ais	3113.3	281.1	0.1992	0.0402	0.32	80.4	1.74	0.21	181	8.6
2012_3_18Mar\ SDS10_019@4.ais	856.9	41.5	0.6632	0.0217	0.00	21.1	1.68	0.51	620	8.6
2012_3_18Mar\ SDS10_019@5.ais	2758.6	139.3	0.2402	0.0203	0.37	75.2	1.83	0.13	466	8.8
2012_3_18Mar\ SDS10_019@6.ais	2968.2	169.2	0.2773	0.0296	0.20	70.4	1.61	0.15	277	8.8
2012_3_18Mar\ SDS10_019@7.ais	3551.1	223.2	0.1729	0.0322	0.01	83.8	1.61	0.14	323	8.7
2012_3_18Mar\ SDS10_019@8.ais	3309.1	221.2	0.2768	0.0446	0.37	70.5	1.44	0.16	183	8.7

Totoral lava dome	238U/206Pb	238U/206Pb	207Pb*/ 206Pb*	207Pb*/ 206Pb*	Correlation of TW Concordia Ellipses	% 206Pb*	206/238 age [Ma]	±1s [Ma]	U ppm	UO/U
		1 s.e.		1 s.e.				1 s.e.		
2012_3_18Mar\ SDS10_019@10.ais	437.8	33.7	0.7473	0.0200	0.08	10.3	1.61	1.49	476	8.6
2012_3_18Mar\ SDS10_019@11.ais	1317.3	87.5	0.1449	0.0206	-0.06	87.4	4.35	0.35	119	9.0
2012_3_18Mar\ SDS10_019@12.ais	636.5	58.3	0.6877	0.0174	-0.12	18.0	1.89	1.31	1223	8.5
2012_3_18Mar\ SDS10_019@13.ais	1934.2	101.8	0.4756	0.0296	-0.16	45.1	1.60	0.25	377	8.7
2012_3_18Mar\ SDS10_019@14.ais	3119.2	165.4	0.0882	0.0126	0.02	94.6	2.04	0.11	429	8.7
2012_3_18Mar\ SDS10_019@15.ais	2948.1	160.8	0.0912	0.0153	0.20	94.2	2.14	0.13	426	8.6
2012_3_18Mar\ SDS10_019@16.ais	3802.3	266.0	0.1913	0.0279	0.08	81.4	1.46	0.13	203	8.7
2012_3_18Mar\ SDS10_019@17.ais	3334.4	269.1	0.1628	0.0308	0.61	85.1	1.73	0.17	174	8.7
2012_3_18Mar\ SDS10_019@18.ais	3060.0	122.7	0.0968	0.0130	0.21	93.5	2.06	0.09	526	8.7
2012_3_18Mar\ SDS10_019@19.ais	3345.6	249.6	0.2335	0.0414	-0.33	76.0	1.55	0.19	272	8.5
2012_3_18Mar\ SDS10_019@20.ais	318.3	18.3	0.7751	0.0124	-0.01	6.8	1.46	1.63	536	8.6
Chajnantor Lavas dome										
2012_3_19Mar\ SDS11_021@1.ais	1690.3	86.6	0.0978	0.0097	0.22	93.4	3.65	0.20	489	8.5
2012_3_19Mar\ SDS11_021@3.ais	1374.8	72.4	0.2629	0.0306	-0.14	72.3	3.48	0.32	168	8.5
2012_3_19Mar\ SDS11_021@4.ais	1449.7	78.4	0.2371	0.0283	-0.05	75.6	3.43	0.29	229	8.5
2012_3_19Mar\ SDS11_021@5.ais	1561.3	89.5	0.1348	0.0153	-0.30	88.7	3.75	0.26	292	8.5
2012_3_19Mar\ SDS11_021@7.ais	711.7	33.3	0.0668	0.0054	0.19	97.4	8.87	0.43	820	8.5
2012_3_19Mar\ SDS11_021@8.ais	1763.7	138.4	0.0991	0.0156	0.23	93.2	3.49	0.29	289	8.6
2012_3_19Mar\ SDS11_021@9CORE.ais	1610.6	115.9	0.2068	0.0308	0.12	79.5	3.27	0.33	181	8.6
2012_3_19Mar\ SDS11_021@10.ais	1536.3	111.6	0.2391	0.0377	-0.13	75.3	3.25	0.38	115	8.6
2012_3_19Mar\ SDS11_021@11.ais	1721.8	91.6	0.1874	0.0252	-0.04	81.9	3.15	0.23	249	8.7
2012_3_19Mar\ SDS11_021@12.ais	1574.8	94.2	0.2040	0.0294	0.10	79.8	3.35	0.29	144	8.5
2012_3_19Mar\ SDS11_021@13CORE.ais	1367.6	83.6	0.2207	0.0171	0.10	77.7	3.75	0.31	331	8.5
2012_3_19Mar\ SDS11_021@14.ais	1170.5	47.4	0.2828	0.0064	0.05	69.7	3.85	0.24	4242	8.5
2012_3_19Mar\ SDS11_021@15.ais	1751.6	81.6	0.0715	0.0076	-0.19	96.8	3.66	0.18	851	8.5
2012_3_19Mar\ SDS11_021@16.ais	1626.0	140.7	0.1667	0.0185	-0.34	84.6	3.43	0.37	218	8.6
2012_3_19Mar\ SDS11_021@17.ais	1585.8	69.9	0.0648	0.0052	0.01	97.6	4.02	0.18	3069	8.4
2012_3_19Mar\ SDS11_021@18CORE.ais	1782.2	70.2	0.0569	0.0039	-0.02	98.6	3.62	0.14	4547	8.6
2012_3_19Mar\ SDS11_021@19.ais	1588.6	96.7	0.1097	0.0123	0.01	91.9	3.82	0.26	323	8.4

Chajnantor Lavas dome	238U/206Pb	238U/206Pb	207Pb*/ 206Pb*	207Pb*/ 206Pb*	Correlation of TW Concordia Ellipses	% 206Pb*	206/238 age [Ma]	±1s [Ma]	U ppm	UO/U
		1 s.e.		1 s.e.				1 s.e.		
2012_3_19Mar\ SDS11_021@21.ais	1126.4	52.1	0.0564	0.0067	0.05	98.7	5.74	0.27	812	8.5
2012_3_19Mar\ SDS11_021@22.ais	1337.3	80.3	0.2740	0.0316	0.01	70.9	3.50	0.35	238	8.4
2012_3_19Mar\ SDS11_021@23.ais	1609.5	113.7	0.1470	0.0228	0.37	87.1	3.57	0.30	233	8.5
2012_3_19Mar\ SDS11_021@24.ais	1743.7	86.0	0.1082	0.0148	-0.19	92.1	3.48	0.20	511	8.6
2012_3_19Mar\ SDS11_021@25.ais	1747.3	111.1	0.1311	0.0171	-0.35	89.1	3.37	0.25	334	8.5
2012_3_19Mar\ SDS11_021@26.ais	1569.1	130.5	0.1421	0.0251	-0.38	87.7	3.69	0.38	221	8.3
2012_3_19Mar\ SDS11_021@27.ais	1462.2	84.5	0.2273	0.0215	-0.32	76.8	3.47	0.30	345	8.6
2012_3_19Mar\ SDS11_021@28.ais	1740.6	68.8	0.0628	0.0031	0.02	97.9	3.72	0.15	3197	8.6
2012_3_19Mar\ SDS11_021@29.ais	1692.0	115.4	0.1715	0.0266	-0.06	84.0	3.28	0.29	232	8.6
2012_3_19Mar\ SDS11_021@2CORE.ais	1604.6	109.7	0.2193	0.0277	0.50	77.9	3.21	0.30	153	8.8
Rio Guacha dome										
2012_3_19Mar\ SDS11_023@1.ais	1077.6	50.4	0.0659	0.0080	-0.18	97.5	5.92	0.29	723	8.5
2012_3_19Mar\ SDS11_023@2CORE.ais	1036.5	50.0	0.0824	0.0095	0.36	95.4	6.01	0.31	397	8.5
2012_3_19Mar\ SDS11_023@3.ais	1664.2	81.4	0.1382	0.0198	0.13	88.2	3.50	0.21	321	8.6
2012_3_19Mar\ SDS11_023@4.ais	1760.3	105.3	0.1905	0.0239	-0.15	81.5	3.07	0.25	408	8.5
2012_3_19Mar\ SDS11_023@5.ais	1670.0	95.1	0.1112	0.0130	0.15	91.7	3.62	0.23	389	8.5
2012_3_19Mar\ SDS11_023@6.ais	1541.1	116.8	0.2026	0.0260	0.44	80.0	3.42	0.34	176	8.5
2012_3_19Mar\ SDS11_023@7.ais	1750.4	86.7	0.0979	0.0134	-0.22	93.4	3.52	0.19	435	8.6
2012_3_19Mar\ SDS11_023@8.ais	661.4	28.0	0.0825	0.0064	-0.03	95.4	9.36	0.42	392	8.6
2012_3_19Mar\ SDS11_023@9.ais	622.7	29.5	0.0797	0.0094	0.08	95.7	9.97	0.50	257	8.5
2012_3_19Mar\ SDS11_023@10.ais	1410.2	90.3	0.1914	0.0346	0.16	81.4	3.80	0.35	102	8.5
2012_3_19Mar\ SDS11_023@11.ais	1631.6	88.4	0.1061	0.0134	0.09	92.3	3.72	0.22	372	8.3
2012_3_19Mar\ SDS11_023@12.ais	1632.9	112.0	0.1454	0.0158	-0.17	87.3	3.52	0.29	226	8.5
2012_3_19Mar\ SDS11_023@13.ais	1673.4	79.8	0.0610	0.0060	0.04	98.1	3.87	0.19	1404	8.4
2012_3_19Mar\ SDS11_023@14.ais	1690.0	84.5	0.0988	0.0108	-0.03	93.3	3.64	0.20	435	8.5
2012_3_19Mar\ SDS11_023@15.ais	1760.6	102.6	0.1237	0.0145	-0.02	90.1	3.38	0.23	280	8.5
2012_3_19Mar\ SDS11_023@16.ais	1698.1	85.6	0.0998	0.0156	-0.21	93.1	3.61	0.21	385	8.5
2012_3_19Mar\ SDS11_023@17.ais	1765.8	110.7	0.0900	0.0163	-0.02	94.4	3.49	0.24	454	8.5
2012_3_19Mar\ SDS11_023@18CORE.ais	1556.9	99.1	0.0895	0.0109	-0.26	94.5	3.96	0.27	271	8.4